

Molecular Circuits of Biological Oscillators

by

Zhengda Li

A dissertation submitted in partial fulfillment
of the requirements for the degree of
Doctor of Philosophy
(Bioinformatics)
in the University of Michigan
2019

Doctoral Committee:

Assistant Professor Qiong Yang, Chair
Associate Professor Laura Buttitta
Professor Daniel Barclay Forger
Associate Professor David K Lubensky
Professor Santiago David Schnell

Zhengda Li

lzd@umich.edu

ORCID iD: 0000-0002-9960-4394

© Zhengda Li 2019

Acknowledgements

My life as a graduate student is both challenging and rewarding. I've been deeply attracted by the mysteries of nature when I was a kid, but only after I entered graduate school did I start to do real scientific research, and the help from people around me is indispensable for my progress. I'd like to thank my mentor Qiong Yang. In the beginning of my graduate study, with all the curiosity and passion, I barely know anytime about how scientific research works, and it is with her hands-on help did I learn how to pursue ideas and questions. She is not only a scientific advisor, but also a friend, who gives me enormous help when I just started to live in this new country. Biological research is teamwork, the help from current and previous lab members, Meng Sun, Shiyuan Wang, Ye Guan, Minjun Jin, Xuwen Liu, Patrick Barnes, Jesse Cisneros Solis, Daniel Khain, has been critical for the progression of my project. Meng Sun designed and built the microfluidic devices in the oscillator tunability project. Ye Guan and Shiyuan Wang taught me techniques to make the *Xenopus* egg extract and helped my experiments on various occasions. I also want to thank other lab members, Owen Puls, Chun-Yen Sung, Usha Kadiyala, Bowen Lian, for their ideas and comments for my project. I want to thank my collaborators Laura Buttitta, Dan Sun, Alexander Pearson, and Ajai Pulianmackal at the University of Michigan and Ran Kafri at the University of Toronto for having provided me invaluable experiences of working on a variety of experimental systems. I also want to thank the people who have given me critical advice and learning opportunities, including Andrea Pobocik, Vasiliy Chernyshev, Wenying Shou, Shawn Chen, Wallace Marshall, Oleg Igoshin, Xinqing Ding, and many more. In addition, I want to thank my committee members, Daniel Forger, David

Lubensky, Laura Buttitta, and Santiago Schnell for having provided me critical advice and help to keep my Ph.D. on track. In the end, I want to thank my family. My parents have been extremely supportive of my pursuits in academic. Education by my parents enlightened me to pursue truth and kindness in both work and life. My girlfriend Shixuan Liu, has given me invaluable support both in academics and in life. Without them, I would never achieve as much as I do today.

Table of Contents

Acknowledgements	ii
List of Figures	vi
List of Tables	viii
Abstract	ix
Chapter 1 Introduction.....	1
1.1. Biological oscillators drive important biological process	1
1.2. Theoretical and experimental research on specific oscillators	5
1.3. Efforts to rebuild biological oscillators.....	9
1.3.1. Theoretical efforts in building simple models that support oscillations	9
1.3.2. Pioneering works of creating simple <i>de novo</i> synthetic oscillators.....	10
1.3.3. Recent efforts in making more complicated synthetic oscillators.....	14
1.3.4. Investigating biological oscillator in the cell-free system	16
1.4. New questions and challenges in the investigation of biological oscillators.....	19
Chapter 2 Systematic analysis of the molecular network structures of biological oscillators.....	21
2.1. Method for systematic enumeration of all network motifs that support oscillations	22
2.2. Incoherent inputs increase the robustness of biological oscillators	26
2.2.1. Definition of oscillator robustness	28
2.2.2. Establishing a complete map of oscillatory networks	29
2.2.3. Oscillatory cores set the basic levels of robustness.....	30
2.2.4. Incoherent inputs enhance the overall robustness of an oscillatory network.....	33
2.2.5. Incoherent inputs increase robustness in real biological networks	42
2.3. Positive feedback increases the tunability of biological oscillators.....	46
2.3.1. Method to calculate oscillator tunability	47
2.3.2. Positive feedback increases the average frequency range of oscillators.....	49

2.3.3. Analysis on the waveform of biology oscillators.....	51
2.4. Conclusion.....	54
Chapter 3 Investigating network circuits of cell cycle oscillator using cell-free <i>Xenopus</i> extract droplets	57
3.1. Droplets of <i>Xenopus</i> egg extracts reliably drive the periodic progression of multiple mitotic events	58
3.2. Oscillation duration of <i>Xenopus</i> extract is effectively tuned by wee1 inhibitors.	63
3.3. Cell cycle frequency can be effectively tuned with cyclin B1 mRNAs and is sensitive to droplet size	65
3.4. Energy depletion model recapitulates dynamics of the oscillator	68
3.5. Building artificial cells with a uniform size	71
3.6. Disruption of positive feedback reduces the tunability of cell cycle oscillators.....	75
3.7. Cell cycle oscillation shows a pulsatile waveform	78
3.8. Conclusion.....	80
Chapter 4 Discussions	82
Appendix	86
1. Derivation of the enzymatic reaction models.....	86
2. Models for real-world biological oscillators.....	87
3. A stochastic model of the embryonic cell cycle including energy effect.....	88
Bibliography.....	95

List of Figures

Figure 1 Biological oscillators are diverse and complicated.	4
Figure 2 Examples of synthetic oscillators.	12
Figure 3 Building oscillator atlas of all 3-node network.	31
Figure 4 Effect of oscillatory cores on oscillator robustness.....	32
Figure 5 Comparison of the robustness of a few example topologies	35
Figure 6 Analyzing the effect of one-edge motifs on network robustness	36
Figure 7 Analyzing the effect of two-edge motifs on network robustness.....	39
Figure 8 Effect of incoherent input is different on different parameters	41
Figure 9 Comparing to a single input, incoherent (coherent) inputs increase (decrease) the nullcline range of a node.	42
Figure 10 Two examples of the real biological oscillator	45
Figure 11 Pipeline to investigate oscillator tunability	48
Figure 12 Relationship between parameter tuning range and oscillator property tuning range.....	50
Figure 13 Statistical analysis to find the motif that is responsible for high oscillator tunability.	50
Figure 14 Analysis of tunability distribution of single oscillators.....	53
Figure 15 Relationship between peak time and oscillation period.....	56
Figure 16 Making cell-free cell cycle extract from <i>Xenopus</i> eggs.....	61

Figure 17 <i>Xenopus</i> extract cell cycle oscillator reliably drives the periodic progression of multiple mitotic events.....	62
Figure 18 wee1 inhibitor could increase the cell cycle oscillation number and sustaining time.	63
Figure 19 Effect of external cyclinB concentration and droplet size on cell cycle number and period.	67
Figure 20 Energy depletion model of cell cycle.....	70
Figure 21 Droplet microfluidic platform.	73
Figure 22 Image processing pipeline for automatic droplet analysis.....	74
Figure 23. Investigation of the effect of the wee1 inhibitor on cell cycle tunability in response to cyclin B mRNAs.	77
Figure 24 Pulsatile waveform of the cell cycle oscillations	80
FigureA 1 Incoherent inputs improve the robustness of biological oscillators in network enumeration.	92
FigureA 2 Role of some network motifs in oscillators with more than 3 nodes.	93
FigureA 3 .Supplemental analysis on cell cycle model	94

List of Tables

Table 1 Parameter ranges in random parameter search	25
TableA 1 Parameter ranges in the cell cycle model, related to STAR Methods: Models for real-world biological oscillators.....	89
TableA 2 Reaction rates and stoichiometry of the cell cycle two-ODE model.....	90
TableA 3 Reaction rates in the model considering ATP.....	91

Abstract

A variety of biological systems, including the circadian clock, heartbeat, and cell cycle, display rhythmic oscillating activities. Early genetic studies have identified central genes required for these biological oscillators and have mapped out the underlying molecular interaction networks. While these biological oscillators have distinct functions and utilize different genes and proteins, the central network architectures of the oscillators are highly conserved. This suggests that network structure is key in determining the properties of biological oscillators. In my graduate study, I investigated the fundamental design principles shared among biological oscillators. I first systematically analyzed the network structures of biological oscillators in a theoretical framework. This work identified novel network structures that affect robustness (resistance to environmental perturbations) and tunability (ability to change frequency), both are key properties of oscillator functions. To further study the function of these newly identified network structures, I have developed an artificial cell system that reconstitutes robust cell cycle oscillations in cell-free droplets. Importantly, this system is amenable to high-throughput single-droplet analysis and precise control of various experimental manipulations. I have further used this system to test predictions from my computational works and explored the mechanisms of cell cycle regulation. Combining both theoretical and experimental work on the biological oscillators, my Ph.D. study identified novel mechanisms that fine-tune biological oscillators. These discoveries provide valuable insights to understand biological oscillator functions and may inspire a new understanding of diseases caused by deficiencies in biological oscillators.

Chapter 1 Introduction

Oscillations are ubiquitous among biological systems and play major roles in maintaining life. From primitive single-celled bacteria to the most sophisticated organisms like a human, oscillatory signals and behaviors have been observed in a broad spectrum of biological processes such as neuron firing, signal transduction, heartbeats, cell cycles, and circadian rhythms (Figure 1A). These biological oscillators are vital for living systems. They ensure the correct timing of critical biological events and code important physiological and biochemical information according to the environment. Consequently, defects in these oscillators can cause a variety of diseases from insomnia to cancer, and it is of great significance to elucidate the fundamental design principles of biological oscillators. Although theories on oscillators have been developed for centuries in physics and mathematics, systematic analysis of biological oscillator remains underexplored. Biological oscillators differ from physical oscillators in variety and complexity, study thereof facing challenges both theoretically and experimentally. In this chapter, I will briefly discuss the history of the research on biological oscillators. Some of the paragraphs and figure 1-2 are adapted from my previously published review (Li and Yang, 2018).

1.1. Biological oscillators drive important biological process

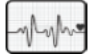



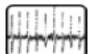



Biological oscillators are extremely diverse in their dynamic properties and compositions. From sub-second neural spikes, to daily circadian rhythms, to annual reproduction in plants and animals, the periods of biological oscillators span orders of magnitudes. The molecular machineries that drive these events are also drastically different. According to the differences in

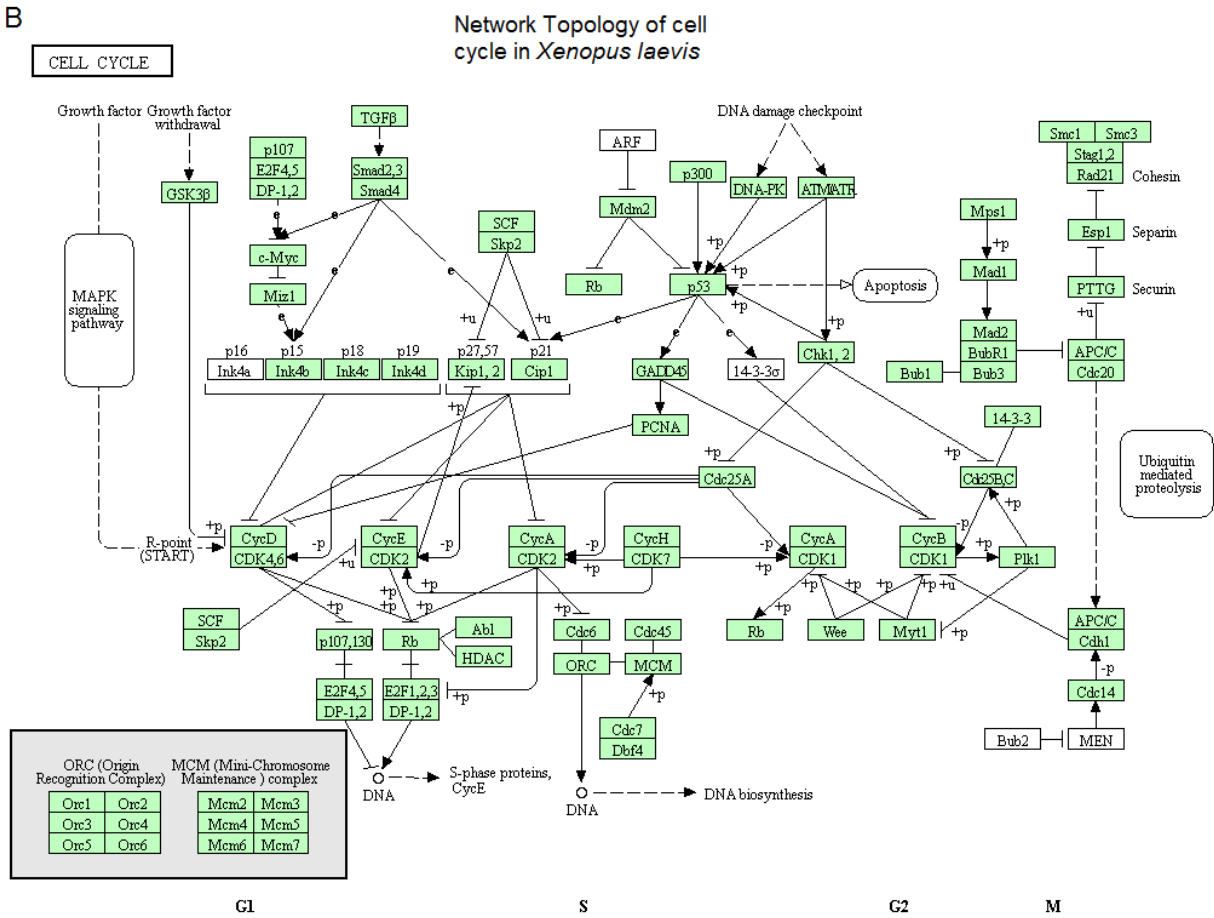
the types of molecular machinery, intracellular oscillators can be categorized into three types (Li and Yang, 2018): 1) cytoplasmic oscillators, in particular, glycolytic oscillators, are formed by proteins and small molecule metabolites that mainly interact within the cytoplasm; 2) Ionic oscillators, such as action potentials in neural and cardiac pacemaker cells, are formed by regulatory ion channels on the membrane; 3) genetic oscillators, such as the circadian rhythm and segmentation clock, involve transcription and translation of genes that regulate each other inside organisms.

These oscillators also perform diverse biological functions (Figure 1A). Most oscillators function as an endogenous pacemaker to generate regularity in time and/or space. For example, circadian clocks, which exist in a vast range of organisms on earth generate endogenous cycles in the organisms to adapt to the natural periodicity of the earth's day-night cycles, by orchestrating their intrinsic gene expressions with a period of approximately 24 hours (Bell-Pedersen et al., 2005; Dunlap, 1999; Gallego and Virshup, 2007). Heartbeat (Brown et al., 1979), respiration (Paydarfar and Eldridge, 1987), and the cell cycle (Hartwell and Kastan, 1994; Kastan and Bartek, 2004; McDonald and El-Deiry, 2000), can also be classified in this category. Pacemaker oscillators also play a role in the spatial organization of development. Through an excitable medium, a local oscillatory signal may trigger waves that propagate over a large distance much faster than through pure diffusion (Gelens et al., 2014). Examples of trigger waves include polar regeneration in *Acetabularia* (Novak and Bentrup, 1972), cAMP waves in the aggregation and differentiation of *Dictyostelium discoideum* (Gerisch, 1968), and mitotic waves recently reconstituted in *Xenopus* cell-free extracts (Chang and Ferrell Jr, 2013). Alternatively, in multidimensional or metamer systems, the phase differences among cell-autonomous periodic events in cells as a function of their spatial locations, resulted in another type of wave, called the

phase wave. These may be exemplified by pattern formation of hypostome in *Hydra* (Goodwin and Cohen, 1969) and periodic tissue morphogenesis of vertebrates such as somitogenesis (Benazeraf and Pourquie, 2013; Oates et al., 2012). Other than the pacemakers, oscillators also function to code biological information by generating frequency-modulated signals to regulate downstream gene expression levels and cellular fate decisions (Isomura and Kageyama, 2014). Examples of these information oscillators include frequency coding of neurons (Ainsworth et al., 2012) and a number of signal transduction pathways with oscillatory dynamics, such as NF- κ B (Nelson et al., 2004), p53 (Purvis et al., 2012), p38 (Tomida et al., 2015), Ca²⁺ signaling (Cai et al., 2008). These oscillators are generally also flexible in tuning their frequencies in response to upstream signals.

A

Oscillators	Period	Oscillator type	Function
 Cardiomyocytes calcium spike	~1s	Membrane oscillators	Endogenous pacemaker
 Xenopus embryo cell cycle (early stage)	10min~24h	Cytoplasmic oscillators	Endogenous pacemaker
 Zebrafish Segmentation clock	25min (zebrafish) 90min(chicks) 2h(mice)	Genetic oscillators	Endogenous pacemaker
 Mammal circadian clock	24h	Genetic oscillators	Endogenous pacemaker
 Action potential	0.001s~10s	Membrane oscillators	Signal processing and transduction
 p38 oscillation	~60min	Cytoplasmic oscillators	Signal processing and transduction
 NF- κ B spike	~100min	Genetic oscillators	Signal processing and transduction
 p53 oscillation	~6h	Genetic oscillators	Signal processing and transduction



04110 11/15/18
(c) Kanehisa Laboratories

Figure 1 Biological oscillators are diverse and complicated.

(A) Examples of biological oscillators and their network structures. From top to bottom: calcium spikes in cardiomyocytes(Cai et al., 2008; Salazar et al., 2008), embryonic cell cycles in *Xenopus*(Murray and Kirschner, 1989), segmentation clock in Zebrafish(Oates et al., 2012), and circadian clock in Mammals(Bell-Pedersen et al., 2005), action potential in neuron(Ainsworth et al., 2012), p38 oscillations in HeLa cells(Tomida et al., 2015), NF-κB spikes in fibroblasts(Nelson et al., 2004), p53 oscillation in human cell lines(Purvis et al., 2012). (B) The cell cycle pathway diagram of *Xenopus laevis* adopted from Kyoto Encyclopedia of Genes and Genomes (KEGG) database. Highlighting the complexity of the system

Biological oscillators are highly complicated. When we look at a biological oscillator, the functional behavior may be obvious and simple, but the underlying oscillatory machinery usually involves complicated temporal and spatial interactions of tens to hundreds of molecules. Studies over the past decades have made major progress in identifying key genes, proteins, and

metabolites that are involved in the rhythmic phenomena. However, important information regarding the detailed molecular interactions in most oscillators remain largely incomplete, and the spatial and temporal information of the oscillatory molecules are usually unknown. An example molecular network from the cell cycle pathway in KEGG is shown in Figure 1B. This network contains hundreds of interacting molecules with different spatial and temporal information. To fully understand such a complicated system would require simplification and abstraction of the system.

1.2. Theoretical and experimental research on specific oscillators

Given their high complexity and broad diversity, it may be difficult to define and investigate general biological oscillators. Previous researchers in the field have made pioneering progress to characterize various specific molecular mechanisms driving some oscillations. In the mid-20th century, breakthroughs were made to characterize the molecular mechanism of neural spikes. Using giant nerve fibers of *Loligo*, Alan Hodgkin and Andrew Huxley carried out a series of measurements of the nerve cell membrane ionic current under a ‘voltage clamp’ (Hodgkin and Huxley, 1952a, b, c; Hodgkin et al., 1952; Hodgkin and Katz, 1949). Under certain conditions, the nervous system exhibits an oscillatory behavior, with electrical pulses repeatedly generated in response to a stimulus. To interpret their findings, they developed a set of ordinary differential equations (ODEs) (Hodgkin and Huxley, 1952d) that include multiple voltage-dependent currents of ion (e.g. potassium and sodium) channels, known as the Hodgkin-Huxley model. The model marks the starting point for theoretical biophysics of action potential. Further research on other species including humans (Buchthal et al., 1954) showed striking similarities with regard to the mechanism of action potentials, suggesting that the action potential oscillatory mechanisms are highly conserved.

In addition to neural spikes, another key biological oscillator, the cell cycle, also showed significant conservation among species. Initial research on the cell cycle was conducted in different systems with different approaches. In yeast, *cdc* mutant strains enabled identification of genes responsible for cell division (Hartwell, 1971; Hartwell et al., 1974; Hartwell et al., 1970; Hartwell et al., 1973). Using *Xenopus* egg extract, proteins supporting cell cycle progression were found and named M-Phase-promoting factor (MPF)(Masui and Markert, 1971; Smith and Ecker, 1971). MPF was later purified and tested (Lohka et al., 1988). Soon thereafter, it becomes clear that part of the MPF and Cdc2 were homologs (Gautier et al., 1988), which unified the cell cycle research across species.

However, not all biological oscillators are conserved among species. Circadian clocks, for example, are fundamentally different between cyanobacteria and mammals. The former mainly involves protein phosphorylation while the latter is a genetic oscillator (Bell-Pedersen et al., 2005; Rust et al., 2007). However, both can oscillate reliably and show some sort of temperature compensation (the period of oscillation is resistant to temperature changes). It is interesting to ask why for similar functions, some oscillators are highly conserved while the others are not? Is the conservation among certain biological oscillators simply a trapped local optimum (a convenient solution randomly found) during evolution or is there a limited number of globally optimal solutions to achieve certain functions? The answer to these questions may allow for a unified understanding of the design principles of all biological oscillators. However, given the complexity and variety of biological oscillators, abstraction or simplification is needed to address this question, and the most straightforward method is to build simplified biophysical models.

As in the research on neural spikes, theoretical modeling has been used extensively to explain the mechanisms of various biological oscillators. About a decade after the first

publication of the Hodgkin-Huxley model, researchers reported the observations of oscillations in the metabolic pathway of glycolysis, demonstrated by the repetitive fluctuations of concentrations of intermediate metabolites. This time, the oscillations were not observed in the membrane of a giant cell, but in a whole cell suspension (Ghosh and Chance, 1964) and a cytosolic cell-free system (Chance et al., 1965) of yeast cells *Saccharomyces carlsbergensis*. Although these early metabolic assays only captured damped sinusoidal oscillations, theoretical work describing six reaction equations using ODE models for phosphofructokinase and the associated glycolytic intermediates predicted the existence of self-sustained limit-cycle behaviors in glycolytic oscillations (Higgins, 1964). Such limit-cycle oscillations were soon observed in a later experiment (Pye and Chance, 1966). Other metabolic oscillations have also been observed in cAMP synthesis (Gerisch et al., 1975) and peroxidase-oxidase reactions (Olsen and Degn, 1978). These pioneering works demonstrate the power of applying theories to understand biological systems and guide new biological discoveries.

The first theoretic genetic oscillator was proposed by Brian Goodwin back in 1963 (Goodwin, 1965), shortly after the development of the operon model for the control of gene regulation by Francois Jacob and Jacques Monod (Jacob et al., 1960). This classical Goodwin oscillator contains only a single gene whose product represses itself after a sufficient delay, allowing for periodic gene expression to occur. Remarkably, this theoretically predicted limit cycle oscillations in a genetic circuit, even before any real genetic oscillator was discovered experimentally. The experimental investigations of genetic oscillators lagged until the development of genetic engineering techniques in modern molecular biology and the rapidly growing popularity of luminescence and fluorescence microscopy techniques.

One of the most characterized genetic oscillators is the circadian clock, which has been found in all eukaryotes and some prokaryotes such as cyanobacteria. Circadian clocks endogenously drive cell-autonomous oscillations roughly once per day, so that organisms maintain the ability to anticipate the time of day. Studies on circadian clocks have been performed on various organisms (*Synechococcus* (Liu et al., 1995), *Neurospora* (Crosthwaite et al., 1997), *Drosophila* (Hamblen et al., 1998), mouse (Antoch et al., 1997) and *Arabidopsis* (Goldbeter, 2002)). These studies successfully combined experimental measurements and mathematical modeling to enable understanding of how each of these biological oscillators functions in great quantitative details. Following these studies, similar quantitative approaches have been applied to the discovery and characterization of many more oscillators.

Major progress has been made in understanding relevant components and functions of biological oscillators. However, challenges for further quantitative analysis of these oscillators in living systems are obvious. For one, the core architecture of an oscillator is often embedded in a significantly more complicated network and usually interferes with other pathways or couples with other oscillators (Bieler et al., 2014; Feillet et al., 2015; Yang et al., 2010). It is therefore difficult to isolate the central oscillator circuitry for investigation. Another obstacle is the limited capability of specifically dissecting or permutating feedback loops since most proteins have multiple functions in a cell. Two different approaches have been used to address these problems, one is to use tools from synthetic biology to create well-defined *de novo* oscillatory circuitry in a system amenable to detailed analysis and accurate control, the other is to extract the backbone of biological oscillators in an isolated and well-controlled cell-free system for extensive screening and systematic analysis. In the following sections, I will briefly review reported studies that used the two approaches to investigate biological oscillators.

1.3. Efforts to rebuild biological oscillators.

1.3.1. Theoretical efforts in building simple models that support oscillations.

Ever since the early discoveries of biological oscillations, theorists have started pursuing the answers to the question of what conditions can support oscillations. Their approaches are to build the simplest possible models that capture fundamental mechanisms of various oscillatory systems. Following the discovery of metabolic oscillations, Ilya Prigogine investigated three biochemical oscillators of distinct catalytic properties in physicochemical terms and argued that all these biochemical oscillations are not different than non-equilibrium spatial and temporal self-organization as dissipative structures in chemical systems (Prigogine et al., 1969). This view provides a conceptual framework that supported later research aimed at unifying all biological oscillators (Goldbeter, 2002).

Throughout the years, efforts have been made in simplifying existing detailed models, the complexity of which may obscure the fundamental design principles underlying the core architecture of an oscillator. In contrast to complicated models, a model with only the most essential components is more accessible to experimental validation as it requires fewer parameters to measure to build an accurate model. The original Hodgkin-Huxley studies of the action potential (Hodgkin and Huxley, 1952d) described in a detailed manner the voltage-current relationship based on experimental observations, which required more than twenty parameters. It was simplified in the FitzHugh-Nagumo (FHN) model (Fitzhugh, 1961) and later in the Morris-Lecar model (Morris and Lecar, 1981), where two differential equations describe the system as coupled positive and negative feedback loops. Importantly, despite the simplifications, these models capture the main dynamic responses, and by adding diffusion, the FHN model generates trigger wave propagations as seen in axons (Gelens et al., 2014).

Simple models have also helped postulate the fundamental requirements for designing an oscillator. Since the design of the Goodwin oscillator (Goodwin, 1965), the inhibitory feedback loop and a source of delay in this feedback have been postulated as two required elements for limit cycle oscillations (Friesen and Block, 1984). However, a single time-delayed negative feedback loop could not explain the noise-resistance behavior in circadian rhythms. The activator-repressor oscillator was thus proposed by Barkai and Leibler (Barkai and Leibler, 2000). As the name suggested, their model consisted of a two-component gene circuit that contains both an activator and a repressor. In addition to the negative feedback loop formed by the activator activating its own repressor, the activator can also auto-activate itself resulting in a self-positive feedback loop. Remarkably, it turns out such a ‘design principle’, i.e., the coupled positive and negative feedback loops, is commonly found in biological oscillators. In a 2008 review article, Novak and Tyson extensively discussed the general requirements for biochemical oscillations (Novak and Tyson, 2008). Besides the negative feedback and the time delay, sufficient nonlinearity and properly balanced timescales of opposing chemical reactions are also reported to be indispensable. In addition, the positive feedback is helpful to amplify and delay the negative-feedback signal, which makes the oscillator more robust. A computational study has suggested that adding positive feedback may increase the robustness and frequency range of the system (Tsai et al., 2008). Altogether, these computational studies have provided key theoretical bases for creating robust synthetic oscillators.

1.3.2. Pioneering works of creating simple *de novo* synthetic oscillators

With the development of the genetic engineering tools, creating a *de novo* designed oscillator in real biological systems became possible. A list of well-known synthetic oscillators has been summarized in Figure 2 and will be described in more details below.

In 2000, Elowitz and Leibler, in a landmark study in synthetic biology, constructed the first genetic oscillator in *Escherichia coli* cells, named the repressilator (Elowitz and Leibler, 2000). In this oscillator, three negative transcriptional regulators, TetR, λ cI and LacI, repress each other to form a delayed negative feedback loop. A green fluorescence protein GFP under the control of TetR promoter was used to report the oscillatory behavior of the system, confirming that single negative feedback is sufficient for generating oscillations. However, it was not robust, with only 40% of the cells oscillate. Based on this work, many new oscillators have been proposed aiming for improved performance.


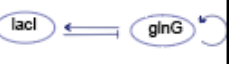
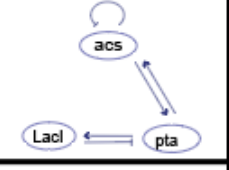
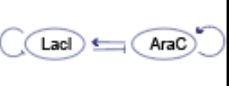


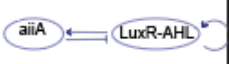
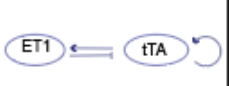

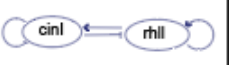

Molecular network description	Organism	Period	Year
	E. coli	~150min	Elowitz and Leibler, 2000 Niederholtmeyer et al. 2015 Potvin-Trottier et al. 2016
	E. coli	10h~20h	Atkinson et al. 2003
	E. coli	45min~3h	Fung et al. 2005
	E. coli	13min~100min	Stricker et al. 2008 Mondragón-Palomino et al. 2011 Hussain et al. 2014 Butzin et al. 2016
	Mamalian cell line (CHO K1)	2h~8h	Tigges et al. 2009
	E. coli	~50min	Dies et al. 2010
	E. coli population	52min~90 min	Danino et al. 2010
	Mamalian cell line (CHO K1)	26h	Tigges et al. 2010
	Mamalian cell line (MCF7)	~6h	Toettcher et al. 2010
	E. coli population	100min~250min	Chen et al. 2015
	E. coli extract	2h~20h	Niederholtmeyer et al. 2015

Figure 2 Examples of synthetic oscillators.

For each synthetic oscillator, the information such as its molecular network structure, the organism that the oscillator is built in, and the period, has been listed

In 2003, Atkinson et al. constructed for the first time the activator-repressor genetic oscillator (Atkinson et al., 2003), reminiscent of the theoretical clock of Barkai and Leibler (Barkai and Leibler, 2000). Turbidostat cell cultures of *E. coli* containing this oscillator achieved synchronized oscillations. However, the oscillations became damped over time, possibly due to a loss of synchrony. Further development of a synthetic oscillator in bacteria was made by Stricker et al. (Stricker et al., 2008). Besides negative feedback formed by *araC* and *lacI*, *araC* also activates itself and *lacI* inhibits itself. This time, the oscillator was tested in microfluidic devices using single-cell fluorescence microscopy. Unlike ensemble measurements, the ability to track single cells relieves the requirement of synchronization. Single-cell data has shown that the period of this oscillator can be as short as 13 min and the oscillation is self-sustained and robust.

The first metabolic circuit using glycolytic flux to generate oscillations was designed in *E. coli* by Fung et al, called the metabolator (Fung et al., 2005). Like all genetic oscillators at the time, this synthetic metabolic oscillator was designed in bacteria cells. The first synthetic oscillator in mammalian cells was reported by Tigges et al. in 2009 (Tigges et al., 2009). Using auto-regulated sense-antisense transcription control, they built a molecular network that resembles the typical activator-repressor circuit, where tetracycline-dependent transactivator (tTA) functions as an activator and pristinamycin-dependent transactivator (PIT) a repressor. Further development of this system has led to an oscillator with a frequency comparable to that of a circadian clock (Tigges et al., 2010). These pioneering studies of synthetic oscillators play an important role in testing the minimal design principles postulated by theoretical studies. The simple synthetic oscillators have also paved the way for more complicated designs.

1.3.3. Recent efforts in making more complicated synthetic oscillators

At present, while new designs continue to expand the list of synthetic oscillators, the focus of the field has shifted from making new circuits to improving the existing oscillators with new functions or applications. This section reviews four types of efforts in recent studies that expand the features and functions of previously established synthetic oscillators.

First, a series of studies have modified oscillator circuits to allow control of the oscillator dynamics properties. By modifying the aforementioned synthetic oscillator with coupled positive- and negative-feedback loops (Stricker et al., 2008), Mondragon-Palomino et al. have built an oscillator that can be entrained by external periodic signals (Mondragon-Palomino et al., 2011). Butzin et al. (Butzin et al., 2016) further demonstrated that such synthetic oscillators can also be entrained by aperiodic signals, similar to the entrainment of cells in our body by the noisy natural signals. Modifying the same dual-feedback oscillator (Stricker et al., 2008) through a single amino acid mutation to its core repressor, Hussain et al. have built an oscillator with temperature compensation (Hussain et al., 2014). The temperature compensation, i.e. keeping a constant period over a range of temperatures, is an essential property of the circadian clock. In addition, Potvin-Trottier et al. focused on noise resistance and built an improved version of the repressilator that can lead to synchrony in bacteria without coupling (Potvin-Trottier et al., 2016).

Second, a number of interesting papers have explored methods to program population-level dynamics and emergent collective behaviors. Using quorum sensing to couple individual genetic oscillators, Danino et al. were able to construct synchronized oscillations at the colony level. In microfluidics devices, they demonstrated a variety of spatiotemporal waves propagating across cellular populations (Danino et al., 2010). This work was further developed by Prindle et

al. by coupling 12,000 such quorum-sensing synchronized colonies, called ‘biopixels’, in a macroscopic array, through gas-phase redox signaling. The ability to synchronize a large scale of colonies across the entire array enabled the construction of a low-cost biosensor that can detect heavy metals like arsenic via modulation of the frequency (Prindle et al., 2011). Chen et al. further extended the monoclonal system to create a synthetic microbial consortium containing two distinct cell types. The ‘activator’ cells and ‘repressor’ cells expressed orthogonal cell-signaling molecules and can only oscillate when both strains were present (Chen et al., 2015b). They also showed that certain network topologies of the two-strain circuit exhibited more robust oscillations than others. A recent study has developed a more complicated synthetic microbial community through multiplexed quorum sensing circuits (Scott and Hasty, 2016). Although all above-mentioned studies have utilized quorum sensing as a key design to produce population-level dynamics, Marguet et al. were able to construct oscillations in bacterial populations that required no quorum-sensing genes or promoters. Instead, the oscillations arise through the unexpected interplay of the host cell and the density-dependent plasmid amplification that established population-level negative feedback. This study highlighted the importance of considering ‘hidden interactions’ between the synthetic circuits and the pre-existing metabolic and regulatory networks in complex host cells (Marguet et al., 2010).

Third, a few studies explored integrating synthetic components into natural biological oscillators to modulate endogenous oscillator behaviors. By adding MTF1 in the p53 signaling pathway, Toettcher et al. constructed an oscillatory system that is tunable in frequency (Toettcher et al., 2010). In another study, Dies et al. linked the cell division cycle to a dual-feedback oscillator (Stricker et al., 2008) in *E. coli*, by driving the *hda* and *dnaN* genes that inhibit the initiation of chromosomal replication, under the oscillator. In this engineered system,

they observed the entrainment between the synthetic oscillator and the cell cycle (Dies et al., 2016).

Finally, studies have started to introduce synthetic circuits into organisms to enable a new function or application. A recent study has reconstructed the cyanobacterial KaiABC oscillator in *E. coli*, making this endogenously non-circadian bacterium perform circadian rhythms (Chen et al., 2015a). This demonstrated that a circadian oscillator is transplantable to a heterologous organism. Moreover, another study engineered a bacterium capable of synchronous lysis at a threshold population density (Din et al., 2016). Introducing the lysis strain in combination with chemotherapy, the study showcased the potential of using synthetic oscillators in clinical applications.

1.3.4. Investigating biological oscillator in the cell-free system

The previous sections described efforts in making *de novo* synthetic oscillators in live bacteria and cell lines, but these synthetic oscillators often lack similarity with real biological oscillations. On the other hand, real biological oscillators have been reconstituted *in vitro* in well-defined cell-free systems for decades. Comparing to live cells, a cell-free system has several unique advantages. First, a cell-free system usually contains only the most essential components in a test tube, which reduces potential interferences from the complex intracellular and extracellular environment. Second, it is convenient to introduce recombinant plasmids, mRNAs, proteins, as well as small molecules and drugs into the cell-free system, to precisely tune its oscillatory reactions, without worrying about the cytotoxicity, delivery efficiency, cross-talks, etc. Because of such flexibility and specificity of introducing molecules, it is more efficient and less time-consuming to design and test a functional circuit in cell-free systems than in living systems. Remarkably, it makes dissection of the circuits much easier, allowing one to obtain the

steady state response function of each dissected reaction, parameters of which are crucial to building models.

Previously, such cell-free assays have made major contributions to the initial discovery and characterization of central mitotic regulators. Extracts prepared from eggs of *Xenopus laevis* enabled the first purification and in vitro kinase activity characterization of the maturation-promoting factor (MPF), later known as the protein complex cyclin B1-Cdk1 (Lohka et al., 1988; Murray, 1991). Clam oocyte extracts allowed for the first discovery of anaphase-promoting complex or cyclosome (APC/C) (Sudakin et al., 1995), functioning as an E3 ubiquitin ligase that is critical to control cell cycle progression. The activation of cyclin B1-Cdk1 drives mitotic entry and activates APC/C-Cdc20, which in turn marks cyclin B1 for degradation and deactivates Cdk1, resulting in mitotic exit, and thereby completing a core negative feedback loop. Studies making use of cycloheximide-treated interphase *Xenopus* egg extracts have shown that when adding APC-resistant cyclin mutants into the extracts, the extracts approach a steady state of Cdk1 activity rather than oscillating (Murray, 1991). This confirms the essential role of the negative-feedback loop in mitotic oscillations.

In theory, negative feedback alone can generate oscillations. However, additional positive feedback loops through the regulations of Wee1 and Cdc25 are evolutionarily conserved (Kumagai and Dunphy, 1992; Mueller et al., 1995). Compromising the positive feedback loops will suppress oscillations in *Xenopus* egg extracts (Pomerening et al., 2005), suggesting that these are essential for sustained embryonic cell cycle oscillations. Together, these studies have identified the core architecture of the cell cycle as interlinked positive and negative feedback loops, one of the aforementioned commonly occurring motifs.

In addition to discovering the core architecture, cell-free assays have been combined with theory to study the function of the interconnected feedback loops. Tyson and Novak (Novak and Tyson, 1993b) and Thron (Thron, 1996) first proposed that the Cdk1/Cdc25/Wee1 system functions as a bistable trigger for mitosis. This hypothesis was then examined with quantitative measurements using the *Xenopus* cell-free systems, showing that both Wee1 and Cdc25 respond to Cdk1 in an ultrasensitive (i.e. highly non-linear) manner (Kim and Ferrell, 2007; Pomerening et al., 2005; Pomerening et al., 2003). In a rate balance analysis (Ferrell, 2008), this mirror-image, two-loop structure composed of Cdk1, Cdc25, and Wee1 with ultrasensitive responses makes it substantially easier to generate a bistable response than otherwise. The bistability is a key consequence of positive feedback that delays the negative-feedback signal and prevents the system from entering a stable steady state (Novak and Tyson, 2008). Indeed, this hypothesis has been supported by experimental evidence that short-circuiting positive feedback in cell-free cycling *Xenopus* extracts makes the cell cycle oscillations damped (Pomerening et al., 2005).

Further studies, by integrating real-time fluorescence assays into the cell-free system, have revealed the core negative feedback system to operate as a time-delayed, digital switch, with a time lag of ~15 min between Cdk1 and APC/C-Cdc20 activation and a tremendously high degree of ultrasensitivity (Ferrell et al., 2011; Yang and Ferrell, 2013b). A simple, analytically tractable model has been developed to show how the attributes of time delay and ultrasensitivity contribute to the generation of robust, clock-like oscillations. The studies also postulated that multisite phosphorylation of APC may explain how the ultrasensitivity and the time delay are generated.

Altogether, these studies have demonstrated that cell-free extracts are amenable to quantitative biochemical and synthetic approaches. By reconstituting and analyzing mitotic

cycles in cell-free extracts, they have identified the key mechanisms for the mitotic oscillations: negative feedback, sufficient time delay, sufficient ‘nonlinearity’ of the reaction kinetics, positive feedback, all consistent with the general requirements for biochemical oscillations (Novak and Tyson, 2008).

1.4. New questions and challenges in the investigation of biological oscillators.

In this chapter, we reviewed the previous research on biological oscillators, especially the efforts to rebuild a functional biological oscillatory system. Our understanding of biological oscillators has progressed extensively over the past years. Decades ago, research on specific oscillators mostly focused on identifying various genes and proteins responsible for the process. At the same time, theorists and synthetic biologists mostly used highly abstract models, focusing on fundamental physical questions. These different approaches left a gap between the abstract oscillatory system in theory and the complicated real biological oscillators. Nowadays, with development of the high-throughput experimental methods and computational tools, theorists and experimentalists are brought closer, yet challenges remain. On the one hand, while the research on oscillation conditions are profoundly explored, the investigation of detailed properties of the oscillators are far from complete. On the other hand, while the high-throughput method is widely used in synthetic oscillators, applications in real biological oscillators are rare. In my Ph.D. study, I established a pipeline to systematically analyze the properties of oscillators with realistic models and tested my discoveries with experiments in automated high-throughput systems. Using this platform, I investigated two important properties of an oscillator: robustness (resistance to environmental perturbations) and tunability (ability to change frequency). In both studies, I focused on the role of network circuits topology, starting with a computational

simulation of abstract networks, and progressing to test these predictions and discoveries in cell-free *Xenopus* extract which recapitulate cell cycle properties.

Chapter 2 Systematic analysis of the molecular network structures of biological oscillators

Biological oscillators drive essential physiological and developmental processes in all forms of life that range from bacteria to vertebrates. These biological oscillators span a wide range of periods and molecular forms. Despite the complexity and diversity of these oscillators, their central network architectures are highly conserved (Bell-Pedersen et al., 2005; Cross et al., 2011), suggesting that network topology is key in determining the properties of biological oscillations.

Previous studies have focused on the core topologies of oscillators to understand the systems-level characteristics such as periodicity and robustness (Castillo-Hair et al., 2015; Lomnitz and Savageau, 2014; Nguyen, 2012; Novak and Tyson, 2008; Woods et al., 2016). In principle, a single negative feedback loop is required and sufficient to generate self-sustained oscillations (Friesen and Block, 1984; Lomnitz and Savageau, 2014; Novak and Tyson, 2008). However, known biological oscillators are organized into more complex network structures. Some of the additional structures, such as positive feedback loops, are not required for generating oscillations but are evolutionarily conserved, which raises the question of what functional role they may play. I hypothesize that the auxiliary network structures are functional, and they may regulate the oscillator properties such as robustness and tunability. Biological oscillators function in a noisy and fluctuating environment. Depending on the functions served, some biological oscillators are required to cycle with the same rate under different environment while others change certain oscillator features to adapt to the environment. For example, the

circadian clock keeps an almost constant period despite different temperatures (Bell-Pedersen et al., 2005), but heartbeat raises or drops according to the physiological conditions (Brown et al., 1979). Different oscillator performs different roles in the biological system, so different topologies are likely selected to optimize its performance for its function (Milo et al., 2004; Milo et al., 2002).

In this chapter, I will examine the relationship between network structures and oscillator properties. First, I will introduce a computational pipeline for oscillatory network enumeration. Second, I will describe a published work on oscillator robustness (Li et al., 2017). Specifically, I have systematically simulated all 3-node oscillators to study the effects of network motifs on oscillator robustness and tunability. I have identified several interesting network structures including coherent/incoherent inputs which significantly affect the oscillator robustness. Some of the paragraphs and figures in this chapter are adapted from my previous publications (Li et al., 2017). Last, I will discuss an exploration on oscillator tunability. Using network enumeration and simulation, I have verified the role of positive feedbacks on increasing network frequency range, and further revealed possible link between oscillatory circuits and their waveforms.

2.1. Method for systematic enumeration of all network motifs that support oscillations

Protein and genetic networks are highly complicated in biological systems. However, if we decompose giant networks into three or four node subnetworks, which we call network motifs, we could find that the distribution of a network motif in biological networks is vastly different from that in randomly generated networks (Milo et al., 2002). In addition, certain motifs are enriched in biological networks with similar functions (Milo et al., 2002). This result suggests that network motifs may be building blocks for specific biological function and are selected during evolution (Milo et al., 2004).

To further our understanding of the design principle of biological networks, the role of network motifs has been intensely investigated, and the motifs that are responsible for adaptation (Ma et al., 2009), switch response (Shah and Sarkar, 2011), polarity (Ma et al., 2006), and many more have been identified. However, oscillators perform some of the most important biological functions, yet a systematic enumeration of motifs that support oscillation hasn't been performed. The main challenge facing oscillator enumeration is that an oscillatory system keeps changing over time, different from previous functions, where the system will end up in a steady state. This means that analyzing oscillators requires more computational power and post-processing of simulation data to achieve unbiased motif investigation. Here, I addressed this problem by building a computational pipeline to systematically enumerate topologies that are responsible for oscillations.

To map out the entire design space of enzymatic networks capable of robust oscillations, I enumerated and analyzed all 3,325 unique topologies containing no more than three nodes. This approach is computationally plausible and allowed for an exhaustive analysis of all possible network configurations. Previous research has suggested that many biological oscillators are centered on three-node negative feedback loops (Gene, mRNA, Protein), and large networks can be decomposed into smaller networks (Han et al., 2004; Milo et al., 2004; Milo et al., 2002). In our study, each topology can be represented by a 3X3 matrix. Each edge can be assigned to value 0 (no interaction), 1 (positive interaction) or -1 (negative interaction). This gives a total of $3^9 = 19683$ networks. After removing all isometric equivalents by comparing networks in all possible permutations, the number becomes 3410. I then remove the networks with isolated nodes (only accepting input, giving output, or completely isolated), and the number of networks reduces to 3325. These include 2 one-node networks, 39 two-node networks, and 3284 three-

node networks. However, the research is not restricted to 3-node networks. While we enumerated all topologies with no more than three nodes, networks with more than 3-node are also generated and tested. The role of incoherent inputs we revealed from three-node networks was shown applicable in four-node and five-node networks (Figure 7D-G) and is likely generalizable to larger networks.

In the analysis, I restricted the networks to be a protein system and assumed that each node represents a specific protein. Many biological oscillators, including the cell cycle and the circadian clock of cyanobacteria, are enzymatic protein systems (Golden and Canales, 2003). I then used a protein interaction model to describe the networks. For each specific network, the interaction function may play a significant role in its dynamics, so I tested two different models. In both models, each variable corresponds to a node in the network, the value of which indicates the activity level of the protein that the node represents. Each node has both active and inactive forms, and these two forms can transform into each other at a basal rate. The interaction between any two nodes is enzymatic. In the first model, I used a previously established equation (Eq. 1) to describe the protein interactions (Tsai et al., 2008), which can be derived from mass action kinetics (Appendix 1). In the second model, I tested another equation using Michaelis-Menten kinetics to model the interaction (Eq. 2). The detailed functions are shown below, and the derivation is listed in Appendix 1.

Equations for protein-protein interactions in the model: Let the activity of a protein on node i be A_i , the interaction type from node j to i be δ_{ji} and the interaction strength k_{ji} .

$$\delta_{ji} = \begin{cases} 1 & \text{positive interaction} \\ 0 & \text{no interaction} \\ -1 & \text{negative interaction} \end{cases}$$

The ODE for node A can be represented as follows:

$$\frac{dA_i}{dt} = k_{act}(1 - A_i) - k_{inh}A_i + \sum_j k_{ji} \frac{\delta_{ji}(\delta_{ji} + 1)}{2} A_i \frac{A_j^n}{K^n + A_j^n} - \sum_j k_{ji} \frac{\delta_{ji}(\delta_{ji} - 1)}{2} (1 - A_i) \frac{A_j^n}{K^n + A_j^n} \quad [\text{Eq 1}]$$

For a Michaelis-Menten kinetics model:

$$\frac{dA_i}{dt} = k_{act}(1 - A_i) - k_{inh}A_i + \sum_j k_{ji} \frac{\delta_{ji}(\delta_{ji} + 1)}{2} A_j \frac{(1 - A_i)^n}{K^n + (1 - A_i)^n} - \sum_j k_{ji} \frac{\delta_{ji}(\delta_{ji} - 1)}{2} A_j \frac{A_i^n}{K^n + A_i^n} \quad [\text{Eq 2}]$$

Using this model, each topology was simulated independently with a collection of 1,000,000 parameter sets randomly sampled within a pre-defined parameter space that is considered to be biologically relevant, as shown in Table 1. The parameter range selections are consistent with a study that used the same model (Tsai et al., 2008). I have mainly used logarithmic sampling in the study, and most parameters have a range of 4 in log10-space. Linear sampling was also used to verify that the sampling method won't affect the result.

Table 1 Parameter ranges in random parameter search

Parameters	Value Range (logarithmic)	Value Range (linear)
k_{act}, k_{inh}	$10^{-3} \sim 10^1$	0~10
k_{ij}	$10^{-1} \sim 10^3$	0~1000
n	$10^0 \sim 10^1$	1~10
K	$10^{-3} \sim 10^1$	0~10

For each randomly sampled parameter, a simulation was repeated five times with different initial conditions. Hence, we analyzed a total of approximately three billion dynamical systems (3,325x1,000,000 parameter sets), each having five replicates. For the simulation, we used the Dormand–Prince method in Boost library to simulate the equation (with relative error 10^{-6} and absolute error 10^{-8}). Each system was simulated from $t=0$ to $t=2000$ in arbitrary units,

which was long enough to detect most of the oscillations. During the simulation, if a system reaches steady states, then it is not an oscillator. We monitored the recurrence of the states of nodes. Without loss of generality, the peak of a specific node is selected as a reference. Let the time at peak i be t_i , and the values of all nodes are (x_i, y_i, z_i) . If at least N consecutive ($N=7$ in our simulation) peaks that satisfy $d((x_i, y_i, z_i), (x_{i+1}, y_{i+1}, z_{i+1})) < \varepsilon$ are found, and if the system

satisfies: 1). Stable amplitude: $\frac{std(x_i)}{mean(x_i)} < \sigma$, $\sigma = 10^{-2}$, and 2). Stable period:

$\frac{std(t_{i+1} - t_i)}{mean(t_{i+1} - t_i)} < \delta$, $\delta = 10^{-2}$, then we consider this system a limit cycle oscillator.

The detected oscillators are then subjected to time-series analysis, and properties like period, amplitude, phase difference between variables will be calculated for further analysis.

Specifically, in my Ph.D. study, I focused on two oscillator properties, robustness (Section 2.2) and tunability (Section 2.3).

2.2. Incoherent inputs increase the robustness of biological oscillators

Robustness means the ability of a system to function reliably under different perturbations or environment. Although robustness is clearly important in biological systems, the mathematical definition of robustness could be controversial. In my study, I have defined ‘robustness’ as the likelihood of maintaining self-sustained oscillations under a perturbation in the parameter space.

How is oscillator robustness affected by network structures? Previous studies on several biological oscillators such as the cell cycle have shown that adding a self-positive feedback loop, in which a node can activate itself, to a core oscillatory circuit can increase the oscillator’s robustness, while adding a self-negative feedback loop to the same core cannot

(Ananthasubramaniam and Herzel, 2014; Gerard et al., 2012; Tsai et al., 2008). However, whether positive feedback is necessary or sufficient to increase robustness has remained controversial. A recent study using synthetic circuits (Chen et al., 2015b), has shown that adding a negative feedback loop to an oscillator could also increase its robustness. In addition, while both Wee1 and Cdc25 form positive feedbacks in embryonic cell cycles, only the one from Cdc25 is critical for the robustness of the oscillation period (Tsai et al., 2014a). Moreover, a recent study on the p53 oscillation dynamics (Moore et al., 2015) demonstrated that only one out of the three microRNA-mediated positive feedbacks increases the robustness of the oscillator. Taken together, these studies, each focusing on a specific biological oscillator, have failed to yield a converging conclusion. Importantly, it also demonstrates the difficulty to identify generalizable mechanisms by analyzing only a subset of oscillators. To obtain a more complete picture beyond any subset of chosen systems, a comprehensive mapping from the entire topology space to the function space is necessary.

To this end, I have systematically analyzed the robustness of all oscillatory topologies with no more than three nodes to search for the structures that are most significantly associated with high oscillation robustness. In agreement with previous work (Castillo-Hair et al., 2015; Goldbeter, 2002; Novak and Tyson, 2008), I found that certain core network topologies are essential for robust oscillations. However, I also found that local modifications on a node of the network have a significant impact on the global network robustness. Specifically, I identified local motifs such that nodes receiving incoherent inputs (both positive and negative inputs) significantly increase the robustness of the network, while nodes with coherent inputs (only positive or negative inputs) decrease the robustness. The effect can be general as it is conserved in networks with higher node numbers and in various real biological oscillators whose models

and parameters are experimentally supported. Nullcline analyses demonstrate that incoherent or coherent inputs differentially influence the robustness by extending or narrowing a node's span of steady states. Additionally, I found that incoherent inputs are enriched in almost all known natural and synthetic oscillators, suggesting that incoherent inputs may be a generalizable design principle that promotes oscillatory robustness.

2.2.1. Definition of oscillator robustness

In general, 'robustness' in this study was defined using a mathematical representation, $R_{a,p}^s = \int_p \psi(p) D_a^s(p) dp$, proposed by Hiroaki Kitano (Kitano, 2007), where the robustness (R) of a system (s) depends on function (a) under a set of perturbations (P). Since the system is random and it is difficult to identify the real parameter distribution in general, we assumed the equal probability of perturbations of all parameters, which gives $\psi(p)$ the value $1/N$, where N is the total number of parameters. $D_a^s(p)$ is an evaluation function that determines to what degree the system still maintains function under a perturbation (p). In our system, since the only property of interest is whether a system is oscillating or not, $D_a^s(p)$ is set to 1 if the system maintains sustained oscillations, and otherwise 0. This definition is equivalent to the Q value, defined as the number of sampled parameters sets that yield sustained oscillations (Ma et al., 2009; Tsai et al., 2008). A topology is more robust if there is a larger parameter volume to support oscillations. It also means that under environmental perturbations on the parameters, a system having a higher Q value is more likely to remain oscillatory.

However, the Q value has some problems. Firstly, the random sampling size is limited, and the parameter-set range is finite, both of which may result in a Q value that is skewed by the dimension of a system (i.e. network complexity). For different purposes, studies have used

different approaches, such as unscaled percentage of parameter sets (Ma et al., 2009; Tsai et al., 2008), or the probability distribution of the parameters based on Bayesian statistics (Woods et al., 2016), to restore the measure of robustness to some degree, so that it is less sensitive to dimension. In our study, to reconcile the dependence of robustness on network complexity (number of edges), we performed a normalization for the networks with the same complexity and used the rank percentage of the Q value of each network as a robustness measurement. This way we avoided a direct comparison of the Q values among networks with different complexity. Secondly, the $1/N$ value is set based on an arbitrary parameter sampling scheme, that is, if we change the parameter sampling method, we also change the probability of perturbation. To avoid this problem, I analyzed detailed distribution after identifying potential topology that increases the robustness, and showed that the parameters that support oscillations in non-robust oscillators are a subset of parameters that support oscillation in robust oscillators (Figure 8).

2.2.2. Establishing a complete map of oscillatory networks

This analysis generated a comprehensive atlas of 1,420 oscillators from which we can define a hierarchy of network complexity. Any two topologies are connected as a pair if both topologies contain the same number of nodes and if one topology can produce another topology by adding one edge. Two topologies with different numbers of nodes can be connected if one topology can produce another topology by adding at least two edges. In our system, all oscillators can be connected into one large atlas. Such connectedness of all oscillators is an important prerequisite for the evolvability of robustness, suggesting that a robust solution can be found by changing one regulatory interaction at a time without losing the ability to generate oscillations. These oscillators all contain at least one negative feedback loop, confirming that the negative feedback is a general requirement for generating oscillations (Novak and Tyson, 2008).

The atlas was laid out so that topological complexity (scaled with the number of edges) of the oscillators increased from bottom to top (Figure 3A). Oscillators of the same complexity were arranged within each row in decreasing order of Q values that spanned orders of magnitude, indicating a large variability of their ability to generate robust oscillations. The bottom-most eight topologies, which we define as 'oscillatory cores', serve as roots for all of the subsequent, more complicated, oscillators. They are minimized oscillatory networks that cannot be simplified further to another oscillatory network, and thus, the simplest topologies that sustain oscillation.

2.2.3. Oscillatory cores set the basic levels of robustness

These oscillatory cores exhibit a large variability of robustness among themselves, with the top three performing significantly better than the rest (Figure 3B). Affirming the validity of our methods, they match the three most well-known central structures of biological oscillators, namely the repressilator (core 1), activator-repressor (core 2), and delayed negative feedback (core 3).

To determine whether these oscillatory cores are responsible for the large range of robustness I observed among all networks, I clustered topologies based on oscillatory core composition. I first compared clusters of topologies that contained only one of the eight cores, and found that topologies containing core 1, 2, or 3 were on average significantly more robust than topologies containing any of the rest cores (Figure 4A). These results suggest that the core structures play an essential role in determining a network's robustness. These differences were compromised if we allowed topologies to contain more than one oscillatory core (Figure 4B). To quantify how combining cores can affect the network robustness, I clustered all topologies that contained any combinations of cores 1, 2, and 3 regardless of the presence or absence of all other less significant cores. I found that the average robustness of a cluster increases with the number

of the robust cores they contain, suggesting that multiple robust cores could combine to promote the robustness of the networks they are embedded in (Figure 4C).

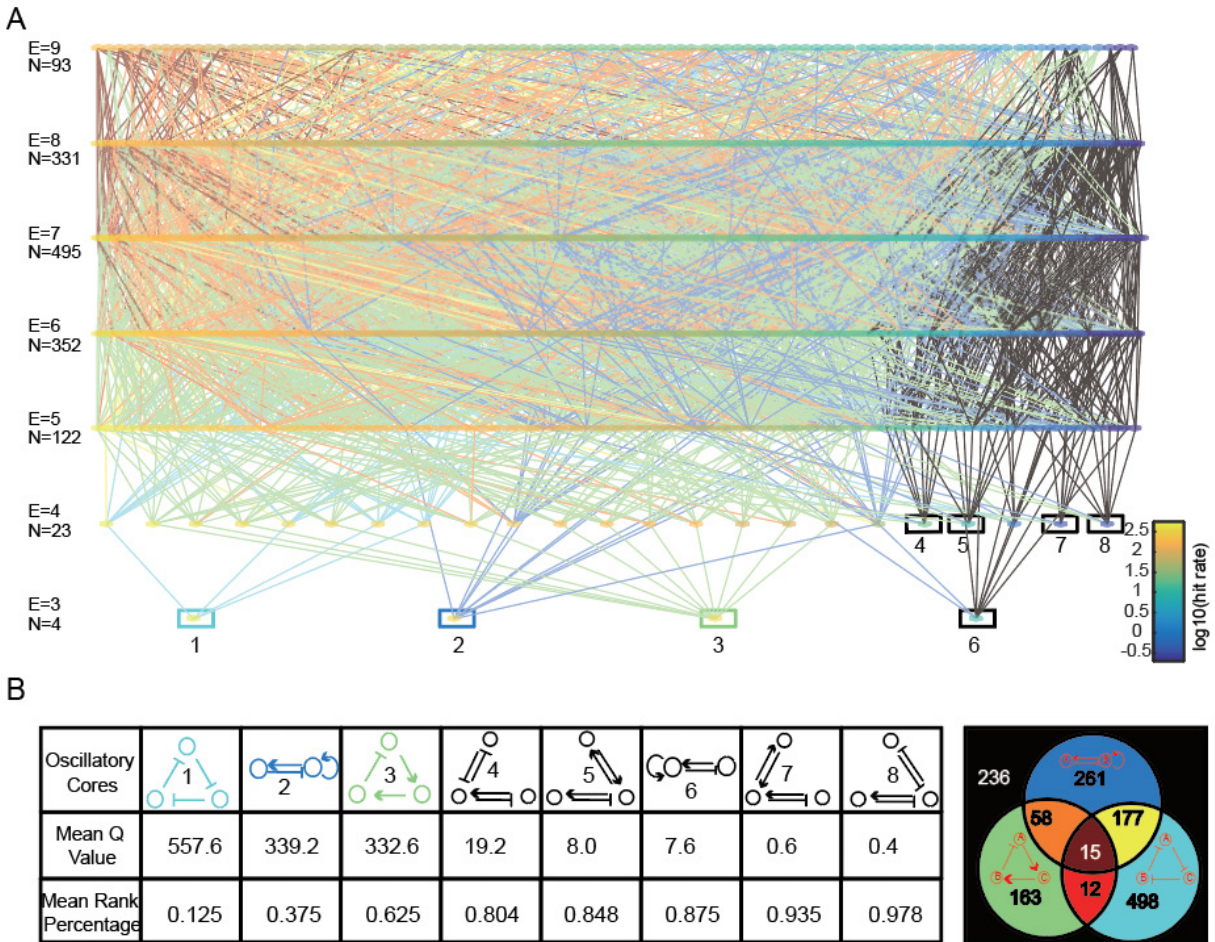


Figure 3 Building oscillator atlas of all 3-node network.

(A) A complete map of 1,420 oscillatory topologies, whose robustness values span orders of magnitude. Each node is one topology. All topologies are laid out such that the topological complexity, represented by the number of edges (E), increases from bottom to top. Topologies with the same complexity are color sorted within the same row, according to their Q values on a logarithmic scale. Each row contains a total number of N topologies. Eight “oscillatory cores” at the bottom of the atlas are highlighted by bordered boxes. Any two topologies with one edge difference are connected. The color of the connection between the two topologies of each pair matches the color for a certain combination of cores that the upper-layer topology contains. All possible combinations of cores with corresponding colors are shown in the Venn diagram in Figure 3B

(B) Eight oscillatory cores are listed in a table in decreasing (or increasing) order of mean Q value (or mean rank percentage of the Q value), each calculated from five replicates. The top three most robust cores are colored in cyan, blue, and green, and the rest cores are all colored in black. The Venn diagram on the right panel cluster all 1,420 topologies based on which combinations of the top three cores they consist of. The number on each region of the Venn diagram indicates the number of topologies in the set. The black region is for all topologies that contain none of the top three cores, i.e., topologies that contain only any one or more of the five non-robust cores.

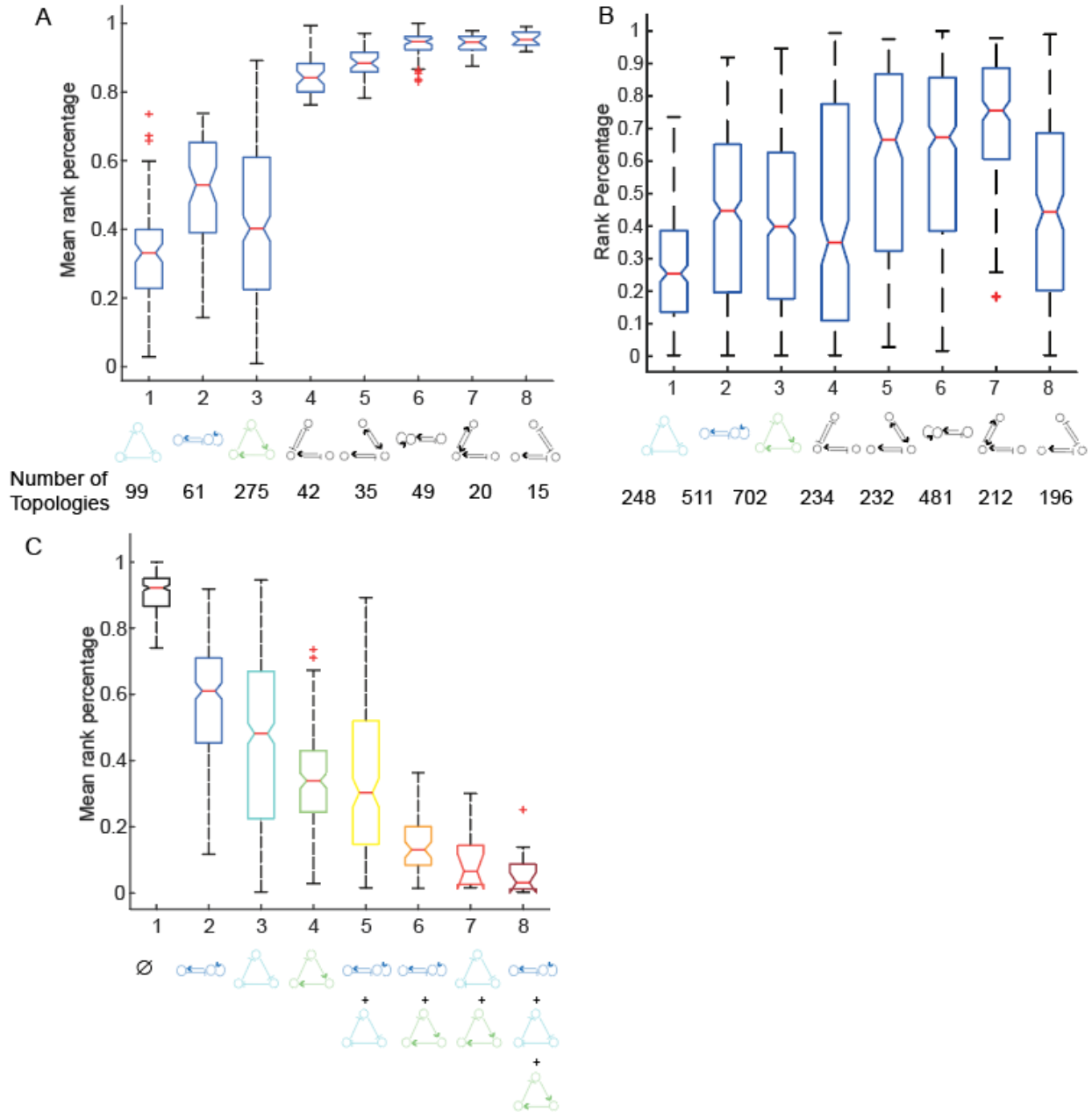


Figure 4 Effect of oscillatory cores on oscillator robustness.

(A) Boxplots of the mean rank percentage of topologies containing only one of each of the eight cores that are listed in the x-axis, showing that topologies with cores 1 to 3 are significantly more robust than those with all the other cores. The number of topologies within each cluster is also listed at the bottom.

(B) Boxplots of the mean rank percentage of topologies containing at least one of each of the eight cores that are listed in the x-axis,

(C) Boxplots of the mean rank percentage of topologies containing different combinations of robust cores (e.g. cores 1 to 3), regardless of the presence or absence of all other non-robust cores. The number of topologies within each cluster is listed in the Venn diagram in Figure 3B.

Despite the high dependence of the average robustness on oscillatory cores, I also observed a large variation of robustness within each of the clusters which cannot be explained by their cores alone (Figure 4C). In addition, it was unclear what mechanisms underlie the major differences in robustness among the cores themselves (Figure 3B). For example, cores 2 and 6 are both self-positive-plus-negative feedback loops except that core 2 has the self-positive feedback added onto the activator (node B), which in core 6 is to the repressor (node A). This seemingly subtle difference resulted in a 45-fold change in robustness. Notably, core 2 is well-conserved in natural and synthetic oscillators, while core 6 is rarely found in any biological oscillators. Together, these results suggest that, in addition to the core architecture, certain auxiliary local structures may play a significant role in robust network performance.

2.2.4. Incoherent inputs enhance the overall robustness of an oscillatory network

In addition to the oscillator core structures, I was also curious about how auxiliary structures affect oscillator robustness. I started by examining the influence of two auxiliary structures, namely positive feedback and negative feedback, both of which have been reported to improve the robustness of certain networks (Chen et al., 2015b; Tsai et al., 2008). The results, however, did not support a simple relationship between the addition of positive or negative feedback and robustness. Instead, the effect depends on the core structure and the node in the core onto which the feedback is added (Figure 5). I also analyzed the role of positive or negative interaction numbers, and neither has a simple relationship with the oscillator robustness (Figure 6 A and B). Therefore, I decided to systematically identify key structures that improve robustness independent of any specific oscillatory cores. To this end, I compared all neighboring topologies that differ by only one regulatory interaction but share the exact same oscillatory cores. Specifically, for each pair of these neighboring topologies, I decomposed them into smaller one-

edge (Figure 6) or two-edge (Figure 7) network. To identify which of the network structure components best predict the change in network robustness, I compared all eligible network pairs based on following two criteria: (1) their topologies only had one edge difference, and (2) they shared the exact same oscillatory cores. Thus, I obtained a list of $N = 1831$ entries of comparison, each of which was calculated from one pair of topologies and consisted of p covariates and a single outcome, y_i . Then, I performed LASSO on this dataset to select the most significant motifs that are responsible for the changes of robustness, by solving:

$$\min_{\beta_0, \beta} \left(\frac{1}{2N} \sum_{i=1}^N (y_i - \beta_0 - x_i^T \beta)^2 + \lambda \sum_{j=1}^N |\beta_j| \right)$$

Here, $x_i := (x_1, x_2, \dots, x_p)^T$ is the covariate vector for the i^{th} pair of oscillators, which contains p predictors, each as an integer. Each integer represents the difference between the pair with regards to their numbers of a certain motif (out of $p=4$ unique motifs for one-edge modifications and 21 for two-edge modifications). The outcome y_i is their robustness rank difference. λ is a nonnegative free parameter, to control for the amount of regularization of the fitting. The fitted coefficients β_0 and β are a scalar and p -vector respectively obtained at a certain λ value. I used ten-fold cross-validation and chose the largest λ such that generalization error (mean squared error) was within one standard error of its minimum value. The covariance test statistics was calculated, similar to a previous study (Lockhart et al., 2014), as a significant measurement for respective motifs.

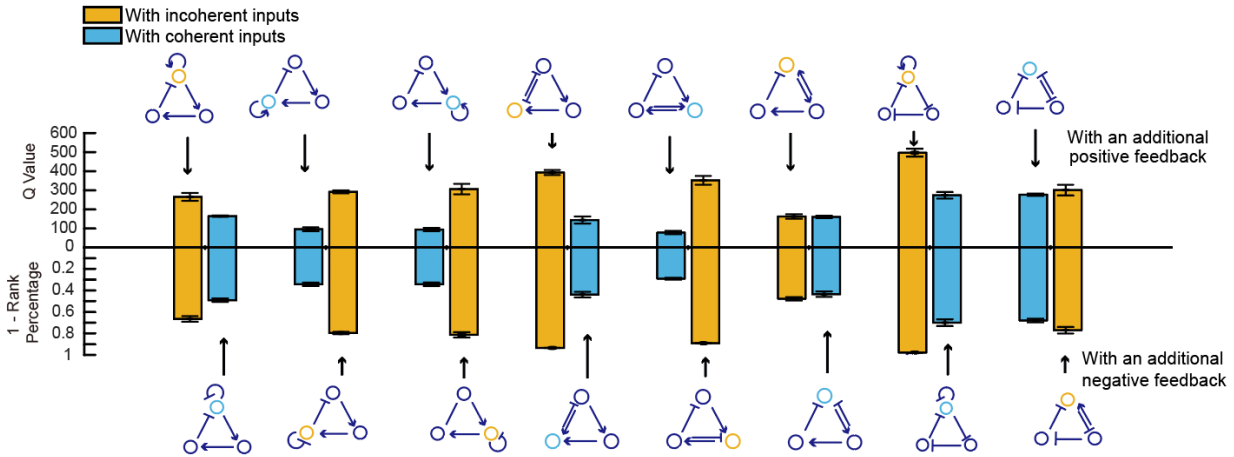


Figure 5 Comparison of the robustness of a few example topologies

To test whether adding a positive or negative feedback loop to an oscillator increases its robustness, topologies of each of the eight pairs are compared regarding their robustness levels, measured as Q value (bar plots on top) or Rank Percentage (bar plots on the bottom). The left bar plot of each pair corresponds to the topology with an additional positive feedback loop (top row), and the right bar plot of each pair corresponds to the topology with an additional negative feedback loop (bottom row). The color of each bar plot indicates whether the topology contains a node with incoherent inputs (orange) or a node with coherent inputs (cyan). It shows that adding a positive or negative feedback loop does not always result in a higher level of robustness. Instead, of each pair, the topology with incoherent inputs is unanimously more robust than the one with coherent inputs, regardless of whether positive or negative feedback is added, indicating that the ‘incoherent inputs’ principle can be a fundamental rule that unifies otherwise divergent results.

Results show that while some one-edge motifs seem to decrease robustness, none of the one-edge motifs significantly increased oscillator robustness (Figures 6C). But I discovered several two-edge motifs (Figure 7B) that had a major impact on robustness. Notably, all incoherent input structures (one node that receives both activation and inhibition) tend to increase the robustness, while the coherent inputs structures (one node that receives either two activations or two inhibitions) tend to decrease the robustness. To confirm these results, I also calculated Spearman’s rank correlation coefficients and partial rank correlation coefficients (PRCCs) (Appendix Figure A1), both of which resulted in the same conclusion. Remarkably, this simple “incoherent inputs rule” accurately predicted the differential influence of adding a positive or negative feedback loop to a core on its robustness (Figure 5), and therefore unified the apparently conflicting results in the literature where either positive feedback or negative feedback was reported to promote robustness in different contexts (Chen et al., 2015b; Gerard et

al., 2012; Tsai et al., 2008). The rule also explained the divergent robustness levels we observed for the pairs of cores with similar designs (e.g., cores 2 and 6, cores 4 and 8, cores 5 and 7) in Figure 3B.

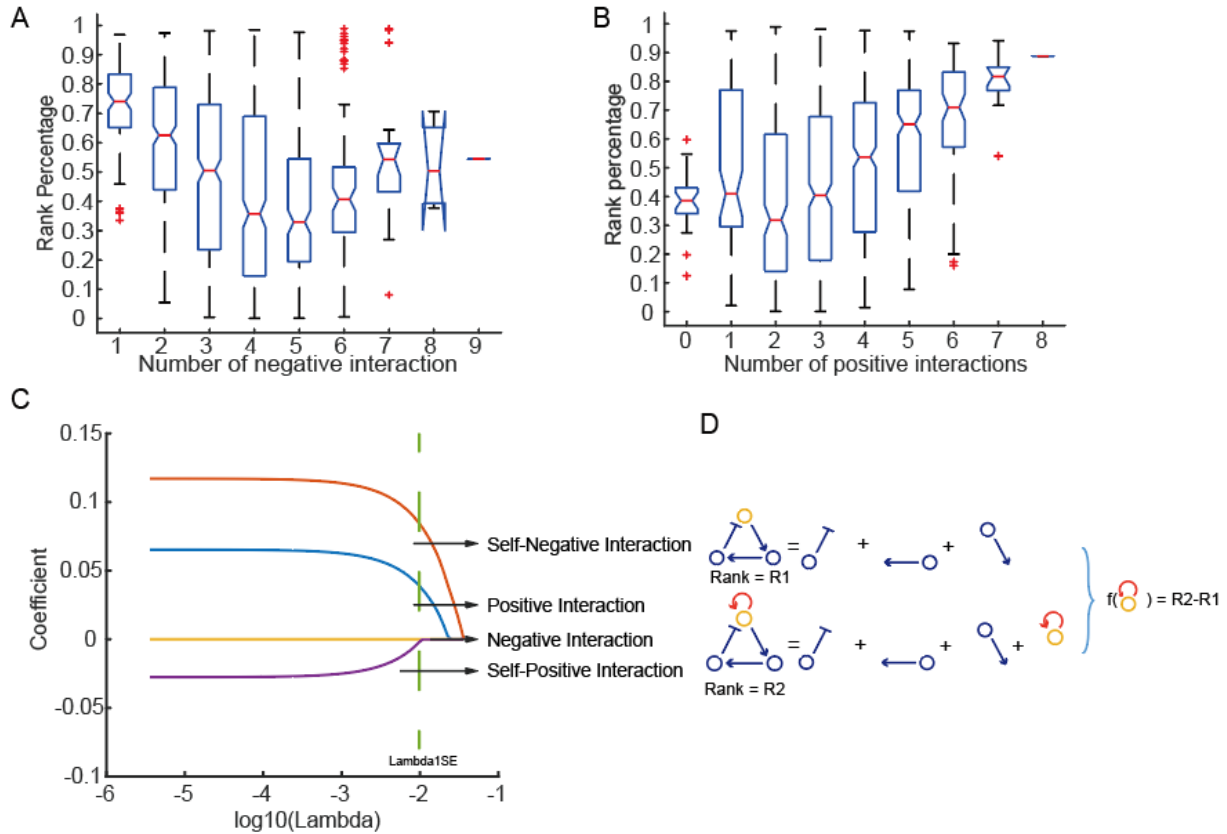


Figure 6 Analyzing the effect of one-edge motifs on network robustness (A, B) Distributions of the rank percentage of the Q value of topologies with various numbers of negative interactions (A) and positive interactions (B). (C) LASSO analysis on one edge modifications, showing that there are no significant one edge motifs that can increase the robustness without introducing new cores. (D) Schematic of comparing a pair of neighboring topologies by calculating the difference in their one-edge motif compositions and the resulting difference in their levels of robustness (measured as $R2 - R1$).

To examine whether these motifs contribute additively to the robustness of a network, I clustered all topologies based on the numbers of incoherent and coherent inputs embedded. The results show that the more incoherent inputs and the less coherent inputs a network has, the more robustly it behaves (Figure 7C). The same trends were also observed using different sampling

methods such as linear sampling (Figure 7H), or an alternative model function based on Michaelis-Menten kinetics (Figure 7I).

I also tested whether the effects of coherent and incoherent inputs on robustness scale in larger-size networks. To this end, I computationally simulated subsets of four or five-node networks using two complementary strategies. First, I enumerated all topologies that contained a core of a four- or five-node “delayed negative feedback” (Figures 7D and 7F). Second, I relaxed this constraint to randomly sample 50,000 topologies out of all configurations (Figures 7E and 7G). Both approaches led to the same conclusion: incoherent inputs and coherent inputs additively increased or decreased robustness in larger networks, respectively (Appendix figures S2A-D).

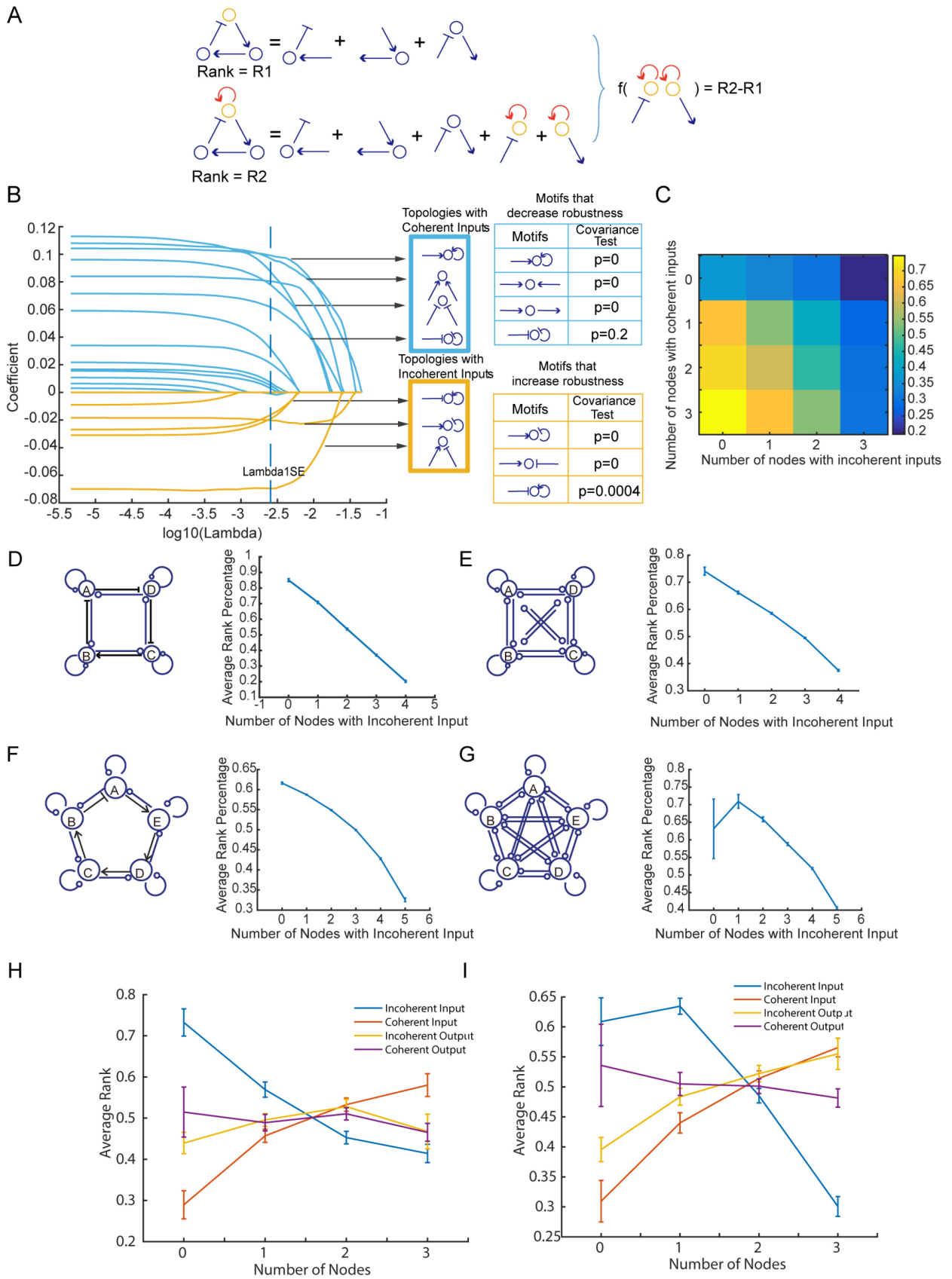


Figure 7 Analyzing the effect of two-edge motifs on network robustness

(A) Schematic of comparing a pair of neighboring topologies by calculating the difference in their two edge network structure compositions and the resulting difference in their levels of robustness (measured as $R_2 - R_1$).

(B) LASSO analysis on the dataset generated from (A) to estimate the coefficients (y-axis) for all two-edge motifs at a certain λ value (x-axis). Applying the one standard error rule, any curve with coefficients above zero at 1SE is for a motif that decreases the robustness, and below zero for a motif that increases the robustness. Interestingly, all motifs with incoherent inputs (highlighted in an orange bordered box) significantly increase the robustness, while all motifs with coherent inputs (highlighted in a cyan bordered box) significantly decrease the robustness. The p-values using covariance test statistics (Lockhart et al., 2014) are shown in tables on the right.

(C) Heatmap of the mean rank percentages of the Q value for all topologies that are clustered based on the number of nodes with incoherent inputs (x-axis) and the number of nodes with coherent inputs (y-axis) they contain.

(D-G) Incoherent inputs promote the robustness of larger-scale networks.

Left panels: (D) contains a total of 6,561 four-node topologies with a core four-node delayed negative feedback loop, and each topology is simulated with 10^6 parameter sets; (E) contains 50,000 topologies that are randomly selected from all four-node configurations, each of which is sampled with 100K parameter sets; (F) contains a total of 59,049 five-node topologies with a core five-node delayed negative feedback loop, each sampled with 100K parameter sets; (G) contains 50,000 topologies that are randomly selected from all five-node configurations, each sampled with 100K parameter sets.

Right panels: All topologies are clustered based on the number of nodes with incoherent inputs they contain, and the mean rank percentage of the Q value is calculated for each cluster. Error bars: the standard error of the mean (SEM) based on 5 replicates.

(H-I) The relationship between the mean rank percentage of the Q values and the number of nodes with different input logic. The calculation is done using linear sampling for parameter generation (H), or using Michaelis-Menten type interaction function (I)

To investigate which parameter is most strongly affected by adding incoherent inputs, I analyzed repressilator derived networks in a generalized enzymatic model. I projected the parameter volume of each topology that supports oscillations onto one of its parameter axes, and then compared the projected distributions along all parameter axes for each pair of topologies. The results (Figure 8A - C) show that the distributions of thresholds K and Hill coefficients n changed significantly in response to incoherent inputs versus coherent inputs, and the most sensitive parameter is the thresholds K from the nodes with incoherent inputs. This result is confirmed by bifurcation analysis from the centroid of the parameter volume that supports the oscillations of a repressilator. Namely, the incoherent input increases the oscillatory range of thresholds K of the node. In addition, the analysis of single parameter distributions also showed that the distribution that supports oscillation in networks with coherent inputs is included in the distribution that supports oscillations in incoherent inputs networks. This result shows that incoherent inputs could increase the robustness independent of the sampling methods.

To intuitively understand why incoherent inputs could improve robustness, I performed nullcline analysis on a node with a pair of incoherent or coherent inputs, or with a single input as a control. This analysis revealed that the range of steady-states of a node varied with its input logic (Figure 9). Specifically, the nullcline range of a node, comparing to the control (i.e. a node receiving only a single input), increased when it received incoherent inputs and decreased when receiving coherent inputs. The nullcline range seems to increase most dramatically from the control when the two input signals had opposite signs but a comparable strength. Since the oscillation trajectory needs to cross the nullcline, a larger nullcline range leads to larger freedom of oscillatory variables, which allows for more flexible parameter selections regarding those variables. Therefore, the wider the nullcline spans, the greater is the potential of a system to generate sustained oscillations. This explains why certain patterns of local interactions on a node impose a significant impact on the overall performance of a network.

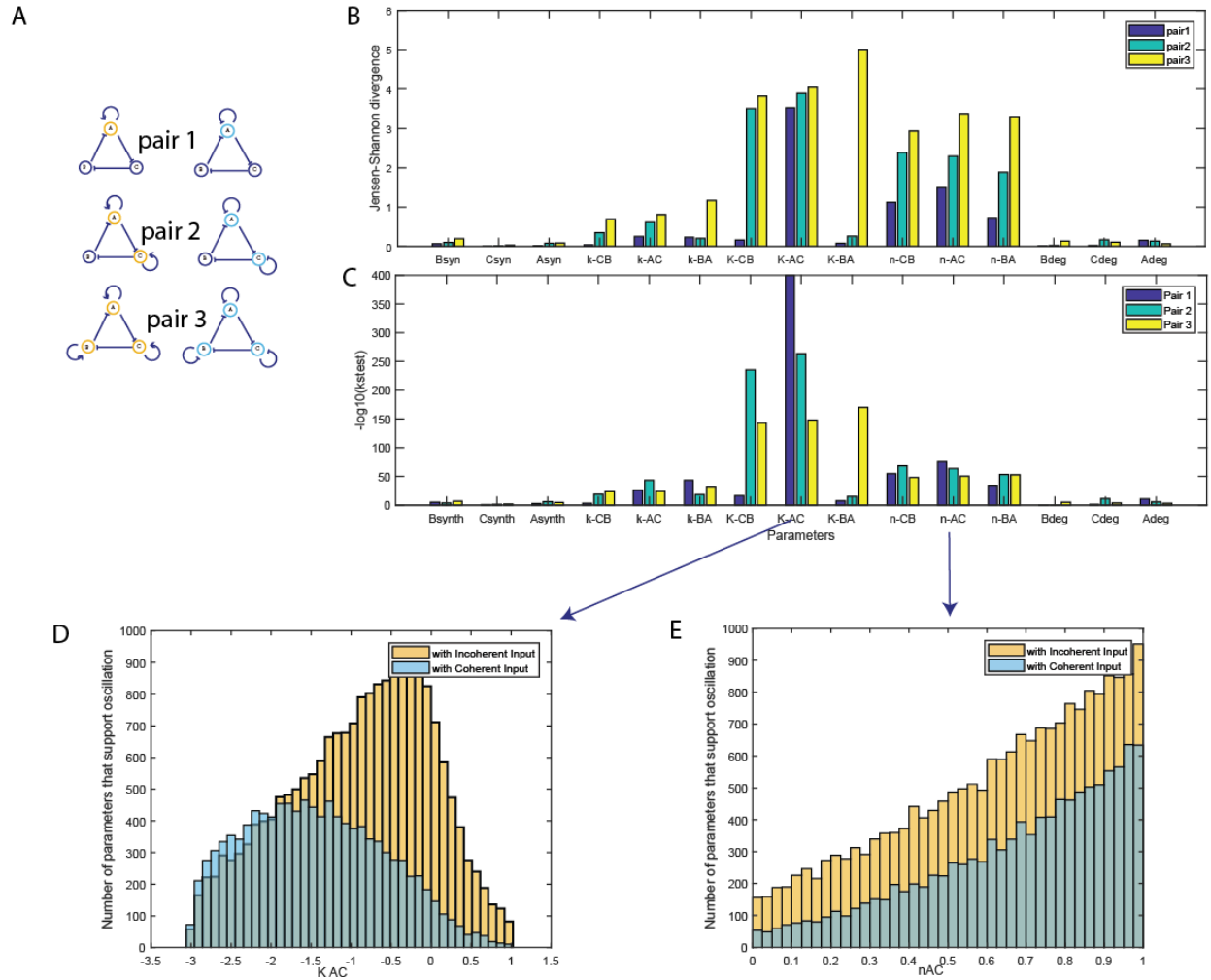


Figure 8 Effect of incoherent input is different on different parameters

A. Three topology pairs used for initial analysis. B. Jensen-Shannon divergence of single-parameter distributions between each pair of topology, showing that the distributions of K and Hill coefficient are changed the most. C. p-value of the two-sample Kolmogorov–Smirnov test, showing that the distribution of K is changed most significantly. D. Histograms of KAC, showing that the incoherent inputs result in more events favoring higher values of K. E. Histograms of nAC.

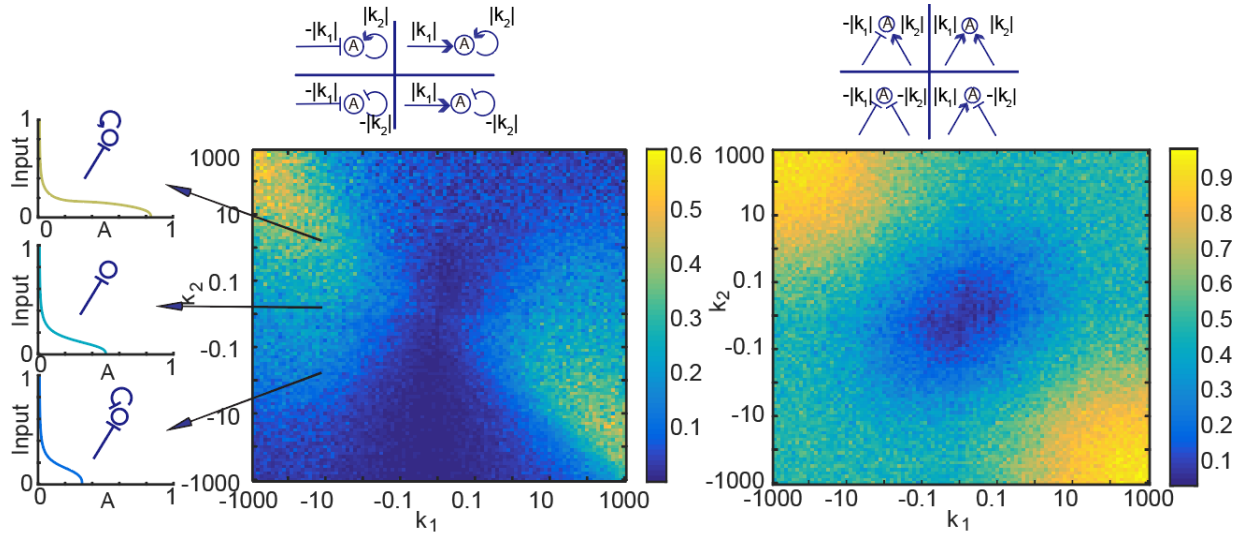


Figure 9 Comparing to a single input, incoherent (coherent) inputs increase (decrease) the nullcline range of a node. Left panel: Heatmap of the nullcline ranges of node A that receives both an input of strength k_1 and a self-feedback of strength k_2 . The value of k_1 (or k_2) can be positive or negative, representing activation or inhibition. The inset on the top shows the representative topologies for different combinations of k_1 and k_2 with positive or negative values. To eliminate any effect from parameters other than k_1 and k_2 , the mean nullcline range is calculated from 100 simulations, with all parameters except for k_1 and k_2 randomly sampled within the parameter ranges listed in Table 1. The inset on the left shows three examples of nullcline for a node with the same negative input on one leg but with an additional self-positive feedback, no additional input, or an additional self-negative feedback on the other leg (basal reaction rate = 0.1, self-regulation rate $|k_2| = 1$, input rate $|k_1| = 10$, $EC_{50} = 0.1$, $n = 2$). Each nullcline is colored according to its nullcline range. Right panel: Heatmap of the null-plane ranges of node A that receives both two inputs of strength $|k_1|$ and of strength $|k_2|$. All notations are the same as in Left panel.

2.2.5. Incoherent inputs increase robustness in real biological networks

To better understand the importance of incoherent inputs in “real-world” biological systems, I analyzed two well-known biological oscillators: embryonic cell cycles and the p53 signaling system, both of which are highly conserved among organisms and have been extensively studied with well-established mathematical models and have been measured parameters (Batchelor et al., 2011; Tsai et al., 2014a). The embryonic cell cycle (Figure 10A) centers on a core of delayed negative feedback that is modified by a double positive feedback loop through phosphatase Cdc25 and a double negative feedback loop through kinase Wee1. Although both are self-reinforcing loops, Cdc25 forms an incoherent input to

Cdk1-cyclin B1, while Wee1 forms a coherent input. Therefore, this system provides an ideal platform to test my prediction. By adopting a published model with experimentally estimated parameters (Tsai et al., 2014a), I found that removal of the incoherent inputs (set *cdc25-cdk1* interaction strength to 0) disrupted the ability of the system to oscillate, while removal of the coherent inputs (set *wee1-cdk1* interaction strength to 0) did not (Figure 10C, Appendix figureA 3A). By random parameter sampling centered on the experimentally measured parameter values (see parameter ranges in Appendix 2), I found that the robustness of the oscillator, measured as the percentage of parameters that yielded sustained oscillations, increased with the strength of the Cdc25 loop until it reached a plateau (Appendix figureA 3A). An opposite trend was observed for the Wee1 loop (Appendix figureA 3A). These results suggested that Cdc25, as an incoherent input modification, is essential to maintain a robust cell cycle. The impact of Cdc25 on the cell cycle robustness was further confirmed in both nullcline analysis and bifurcation analysis—as the strength of Cdc25 increased, so did the range of steady-state Cdk1-cyclin B1 activities (Figure 10E), and the ranges of several key bifurcation parameters (e.g., cyclin B1 synthesis rate in Figure 10G; Hill coefficients in Appendix figuresA3B, C), within which sustained oscillations occurred. In contrast, the strength of Wee1, as part of the coherent inputs' modification to the core negative feedback architecture, played an opposite role.

In the second example, I studied the signaling network of the tumor suppressor p53, which cells utilize to respond to stresses such as DNA damage. Interestingly, the p53 network wires differently under different stimulations, leading to distinct dynamics and cell fates (Purvis et al., 2012). Explicitly, the p53 network oscillates in response to double-strand break (DSB), while exhibits a single pulse under ultraviolet radiation. The key structure to sustain the oscillations is a negative interaction from Wip1 to ATM (Batchelor et al., 2011) (Figure 10B).

This negative regulation from Wip1 (Shreeram et al., 2006), together with the positive regulation from the DSB-sensing complex (Mre11-Rad50-Nbs1) (Lee and Paull, 2005), form incoherent inputs to ATM. Removing either of the inputs terminated the oscillations (Figure 10D), and increasing the reaction rate constant of either input resulted in an extended nullcline range of ATM (Figure 3F). Similarly, through bifurcation analysis, the range of the DSB signaling input level that supports oscillations also widened with increasing rate constant of Wip1 -| ATM (Figure 3H). Together, these results strongly demonstrated the significance of incoherent inputs in promoting robust biological oscillations

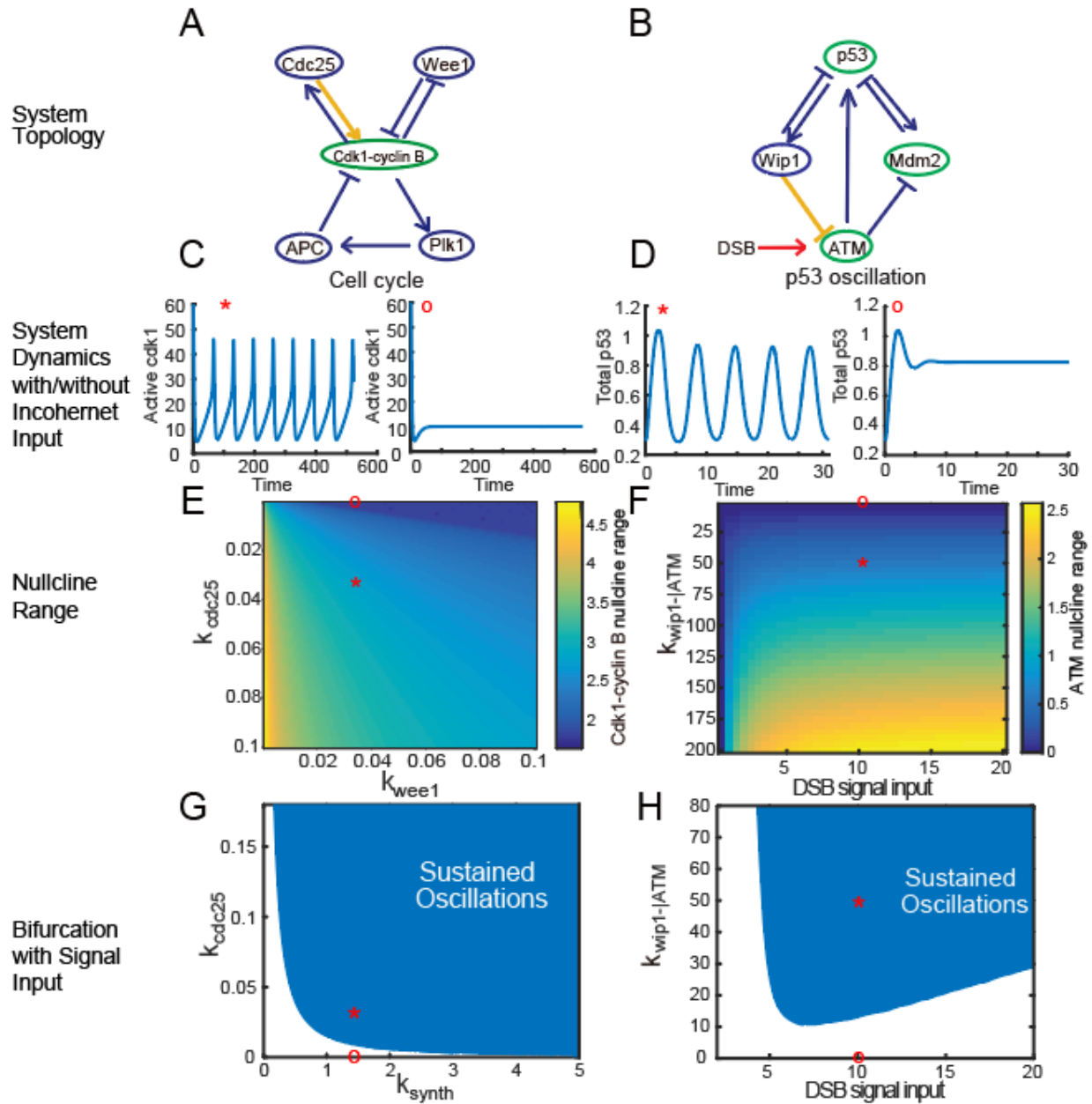


Figure 10 Two examples of the real biological oscillator

(A, B) Topologies of the cell cycle (A) and p53 oscillator (B), where the nodes that receive incoherent inputs are labeled in green and the interactions of interest in yellow.

(C, D) Time courses of active Cdk1 levels (C) and total p53 levels (D), either with (labeled with *) or without (labeled with o) the interactions labeled in yellow in (A, B). The results show that incoherent input is necessary for oscillation. The rest of the parameter values are unchanged from the literature values (Batchelor et al., 2011; Tsai et al., 2014a).

(E, F) Heatmaps of the nullcline ranges of Cdk1-Cyclin B (E) and ATM (F), indicating that the strength of any of the incoherent inputs such as Cdc25, Wip1-|ATM, and DSB signal input is positively correlated with the nullcline range, while the coherent input strength of Wee1 is negatively correlated with the nullcline range. The points labeled with * and o correspond to the same systems as in (C, D).

(G, H) Bifurcation analysis. The shaded regions denote the parameters compatible with sustained oscillations. The parameter ranges of the cyclin B synthesis rate constant k_{synth} (G) and DSB signal input strength (H), both as the

essential clock inputs, become wider as the incoherent input strength k_{Cdc25} (G) and $k_{Wip1-|ATM}$ (H) increase. These results indicate that incoherent inputs increase the parameter choice for oscillation, and thus increase the robustness of the system. The points labeled with * and o correspond to the same systems as in (C, D).

2.3. Positive feedback increases the tunability of biological oscillators

Tunability (specifically frequency tuning) is the ability of oscillators to change their cycle frequency, another critical feature of many biological oscillators. Oscillators like heartbeat or breathing regulate biological processes that require adaption to the changing environment and physiological conditions. Frequency tuning is also a property for many cellular oscillators. For example, the period of the cell cycle can range from half an hour in early embryos to days in adult cells. In addition, certain neural spikes range a wide range of oscillation frequency to encode information. The recent work also showed benefits of frequency tuning in transcription regulation. It is suggested that transient pulse of transcriptional factors ensures high concentration inside the nucleus so that they can coordinately activate genes even if these transcriptional factors have different binding coefficient with DNA (Levine et al., 2013). For example, Cai L. et al showed that the calcium-sensing yeast transcriptional factor Crz1 oscillates during activation, with similar spike width but different frequency (Cai et al., 2008). However, tunability is not a required feature for all biological oscillator. For example, oscillators like circadian clocks are not easily tunable in their periods, which is a critical feature for their role of timekeeping.

As described in Section 2.2, I have built a network atlas to investigate the role of topologies on oscillator robustness, which also provides an ideal platform to systematically analyze the relation between network structure and other oscillator properties such as tunability. Previously, there have been several theoretical studies that examined the regulation of oscillator tunability, which showed that positive feedback could enhance the oscillator tunability (Tsai et

al., 2008), a currently widely accepted conclusion. Recent advances in synthetic biology have further promoted the study of oscillator tunability by developing real-world synthetic oscillators to test the theoretical predictions (Tomazou et al., 2018). On the other hand, computational studies have simulated specific biological oscillators to test parameters that affect their tunability. One recent work examined repressilator centered models and suggested that longer negative feedback also increase the tunability (Maeda and Kurata, 2018). Another computational study using models from synthetic biology also showed that amplitude tuning and frequency tuning can be independently achieved when tuning different parameters (Tomazou et al., 2018). However, all previous studies only focused on a few specific topologies or topologies derived from the same oscillatory core, therefore it is unknown whether the conclusions can be applied to other oscillators or network topologies. To facilitate systematic understanding of frequency control among biological oscillators, I applied the network enumeration pipeline described in Section 2.1 to systematically permuted model parameters and measure the effects on the oscillator frequency. This work provided a rich dataset to systematically examine the relationship between oscillator tunability and network structures.

2.3.1. Method to calculate oscillator tunability

Oscillator tunability in my study refers specifically to frequency tunability. It is defined as the frequency range of an oscillator when a given tuning parameter is changed. Obviously, according to the definition, oscillator tunability depends on the choice of the tuning parameters. In reality, tuning different parameters will lead to different frequency changes. Since our goal is to find the role of network topology, we introduced two measurements to summarize frequency tunability of oscillatory network topology. 1). In section 2.3.2, I used average frequency tuning range of all parameters as a measurement for topology tunability, which is straightforward to

calculate and amenable for statistical analysis. 2). In section 2.3.3. by analyzing the relationship between frequency tuning and amplitude tuning, I identified two prominent types of tunings. For each topology, I used the percentage of frequency tuning type among all random parameter set and tuning parameters as a measurement of oscillator tunability. Note that in my analysis, since the number of parameters is large, not all of them are systematically tuned. Specifically, EC50, which represents the binding coefficient between two proteins, and Hill coefficient, which represents the cooperativity of a reaction, are not tuned in my analysis since they are unlikely to change without structural changes of the proteins.

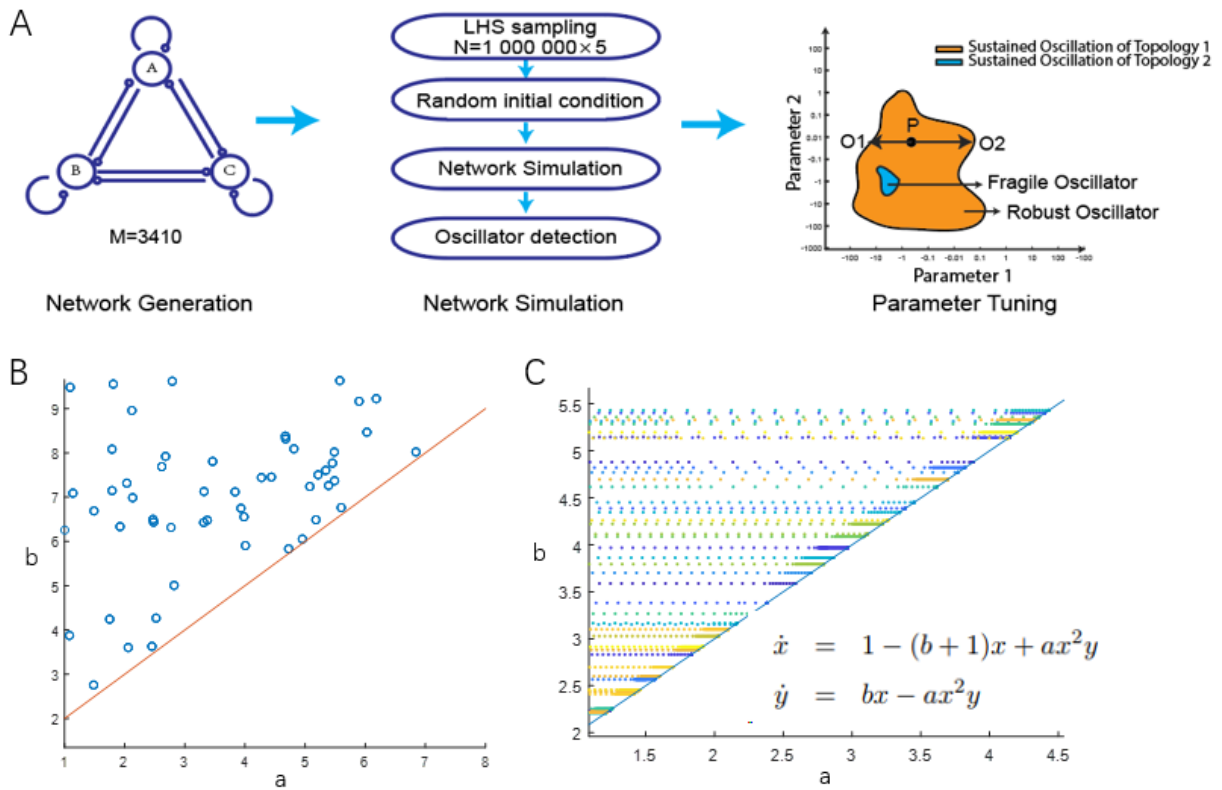


Figure 11 Pipeline to investigate oscillator tunability

(A) Schematic of a computational workflow for topology-to-function mapping of biological oscillators. Left panel: A complete enumeration of topologies with three nodes or fewer. Each node can generate outputs to (analogous to enzymes) or receive inputs from (analogous to substrates) other nodes, leading to 3,325 unique topologies. Middle panel: Each topology is simulated (using the Runge-Kutta Dormand-Prince, or RKDP method) with 10^6 parameter sets (and 5 replicates) using LHS sampling in Log-space. Right panel: Robustness of each topology is calculated as the number of parameters that support oscillations (Q value) or as the rank percentage of the Q value, then the parameter is systematically tuned once at a time until reaching the parameter range boundary or reach the bifurcation when the system stops oscillating. (B) Example of Brusselator, each dot represents an oscillator detected in the

previous pipeline for robustness estimation. (C) The same example as in (B), but each dot is permuted on the parameter a , until it reaches parameter boundary (here $a=1$) or meets bifurcation, and the trace of tuning is shown.

To calculate tunability levels for different networks, I followed a similar procedure of the oscillator robustness analysis (Section 2.1). First, I generated the whole list of network topologies with three nodes. Then, I simulated the networks with random parameters and initial conditions to detect oscillations as described in Section 2.1. Lastly, for each oscillator, I tuned one parameter at a time until the system stops oscillating or reaches the boundary of pre-defined parameter ranges (Figure 11A), then repeat for parameters. Figure 11 B and C show an example of parameter tuning in the Brusselator, a well-established chemical oscillator. Each point in panel B represents a network with a unique parameter set, then for each of this system, parameter a is tuned adaptively until it reaches the Hopf bifurcation or parameter boundary. Specifically, when tuning the parameter, I started by adding/deleting a small value, and increase this step size exponentially until it passes the boundary or bifurcation point, then we use bisection method to find the specific critical point.

2.3.2. Positive feedback increases the average frequency range of oscillators

After screening the tunability of all topologies, I found that these topologies can be divided into two categories according to their parameter sensitivity of period/frequency and amplitude (Figure 12). In one group, period and amplitude of topologies change proportionally with the parameter, and in the other groups, period and amplitude of topologies maintain relatively constant across the tested range of the parameters. This has led to the questions of whether the observed bimodal distribution is determined by network topologies, and what particular network structures contribute to the difference in tunability.

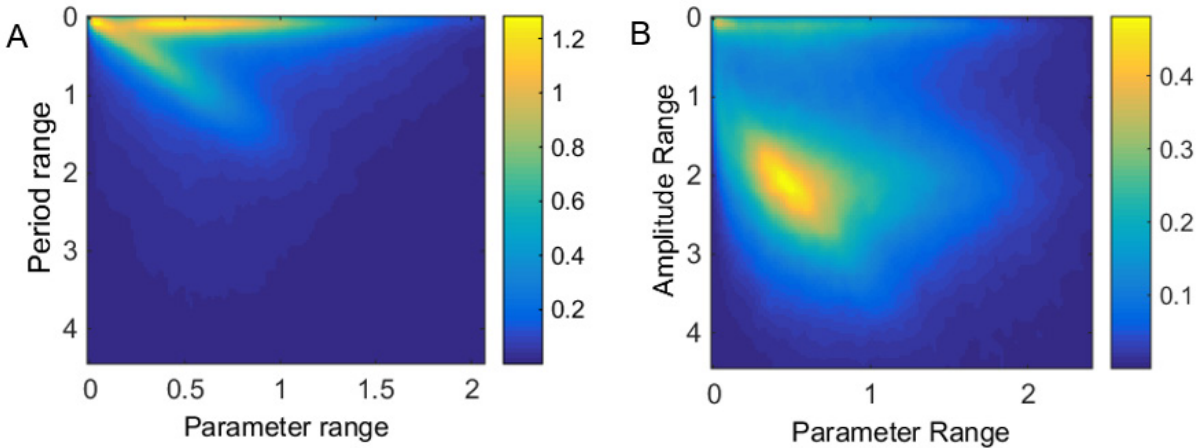


Figure 12 Relationship between parameter tuning range and oscillator property tuning range. Kernel density estimation for the joint distribution between parameter range and period range (A) or amplitude range (B). All ranges are in the logarithm scale. Gaussian kernel with standard deviation 0.05 is chosen. Results show the bimodal distribution in both cases.

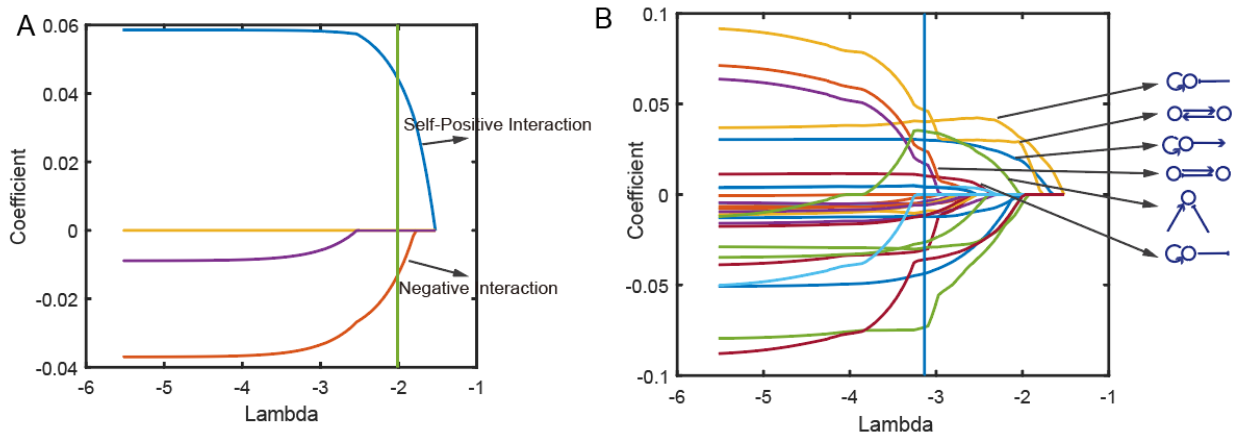


Figure 13 Statistical analysis to find the motif that is responsible for high oscillator tunability. LASSO analysis of the frequency range difference to estimate the coefficients (y-axis) for all one-edge (A) or two-edge (B) motifs at a certain λ value (x-axis). Applying the one standard error rule, any curve with coefficients above zero at 1SE is for a motif that increases the tunability, and below zero for a motif that decreases the tunability. In general, positive feedbacks increases the tunability of oscillators.

I again used LASSO to find the responsible network motif(s) for average period tuning range. For one edge motifs, I found that self-positive interaction significantly increases the network tunability (Figure 13A), in accordance with conclusions in previous research (Novak and Tyson, 2008; Tsai et al., 2008). In contrast, self-negative interactions tend to decrease parameter tunability. It should be noted, however, that the number of self-negative feedback

loops and self-positive feedback loops of a topology always adds up to no more three in a 3-node network, meaning that the two quantities are artificially correlated in my analysis. Therefore, the role of self-negative feedback, which is less significant than self-positive feedback, may come from its artificial correlation with self-positive feedback. For two edge motifs, I similarly found that the positive feedback loops, including topologies with self-positive feedback and positive feedbacks with two nodes, are the top-ranked topologies associated with high tunability (Figure 13B). Interestingly, incoherent inputs, which has been shown to affect oscillator robustness (Section 2.1) seem to also promote oscillator tunability. As shown in Figure 12, the topologies are less likely to have a high tunability when they have a small parameter range (i.e., low robustness). This makes intuitive sense that a non-robust oscillator is less likely to be tunable with a narrower range of parameters that support oscillation. In this study, I showed that the motif of positive feedback will increase the average frequency tuning range of biology oscillators.

2.3.3. Analysis on the waveform of biology oscillators

While average frequency tunability is straightforward to calculate, it does not capture the details of the frequency tuning with different parameters. In addition, even for the same tuning parameters, the frequency tuning range may have large variation within different random parameter set and initial conditions.

After identifying positive feedback as a major responsible motif for increasing network tunability, I examined the frequency and amplitude tunability distribution of individual topologies with all tuning parameters and random parameter set (Figure 14). This result interestingly shows that frequency tuning and amplitude tuning are almost mutually exclusive. Accordingly, taking advantage of previous research on oscillator theory (Forger, 2017), I have

classified these oscillators into the two types depending on their bifurcation types: 1) a type 1 oscillator, which is capable of frequency tuning, has saddle-node on invariant cycle bifurcation, and 2) a type 2 oscillator, which is capable of amplitude tuning, has Hopf bifurcation. To discriminate these two types of oscillators, I introduced the measurement ϕ which equals $\arctan(\text{Amplitude range} / \text{Period range})$. While a ϕ value close to 0 means frequency tuning, a value close to $\pi/2$ indicates amplitude tuning. Statistical analysis on all networks shows that the distribution of angle ϕ is bimodal (Figure 14B), suggesting that most of the parameter tunings are either amplitude tuning or frequency tuning. In the following analysis, I used ϕ as the indicator of frequency tunability level and calculated the percentage of frequency tunings and amplitude tunings. Specifically, two arbitrary thresholds are chosen, and ϕ smaller than $\pi/8$ is considered frequency tuning, and ϕ larger than $3\pi/8$ is considered amplitude tuning. I measured the percentage of frequency tuning and amplitude tuning types of all topologies, and the results showed that the increased number of positive feedback loops increased the percentage of frequency tuning parameters and decreased the number of amplitude tuning parameters. This result suggests that the effect of positive feedback on this percentage seems to be additive.

It is well-known that the positive feedbacks may lead to relaxation oscillation and increase of tunability (Tsai et al., 2008). Most of the biological oscillators responsible for information transfer are among this type. From traditional neural spike to transcriptional oscillation (Cai et al., 2008; Hodgkin and Huxley, 1952d), experimental results showed the pulsatile relaxation oscillation, with constant pulse width. On the other hand, there are also biological oscillators like circadian rhythm that generally show sinusoid shapes (Bell-Pedersen et al., 2005). To verify whether relaxation oscillation can explain the frequency tuning, and to explore how waveform of oscillation is correlated with its tunability, I took a closer look into

oscillation time series. To discriminate the sinusoidal and pulsatile oscillations, I defined the oscillation peak time, which is the duration of the period when a variable is more than half maximum of its amplitude (note: if this time is larger than half period, flip the signal along the x-axis).

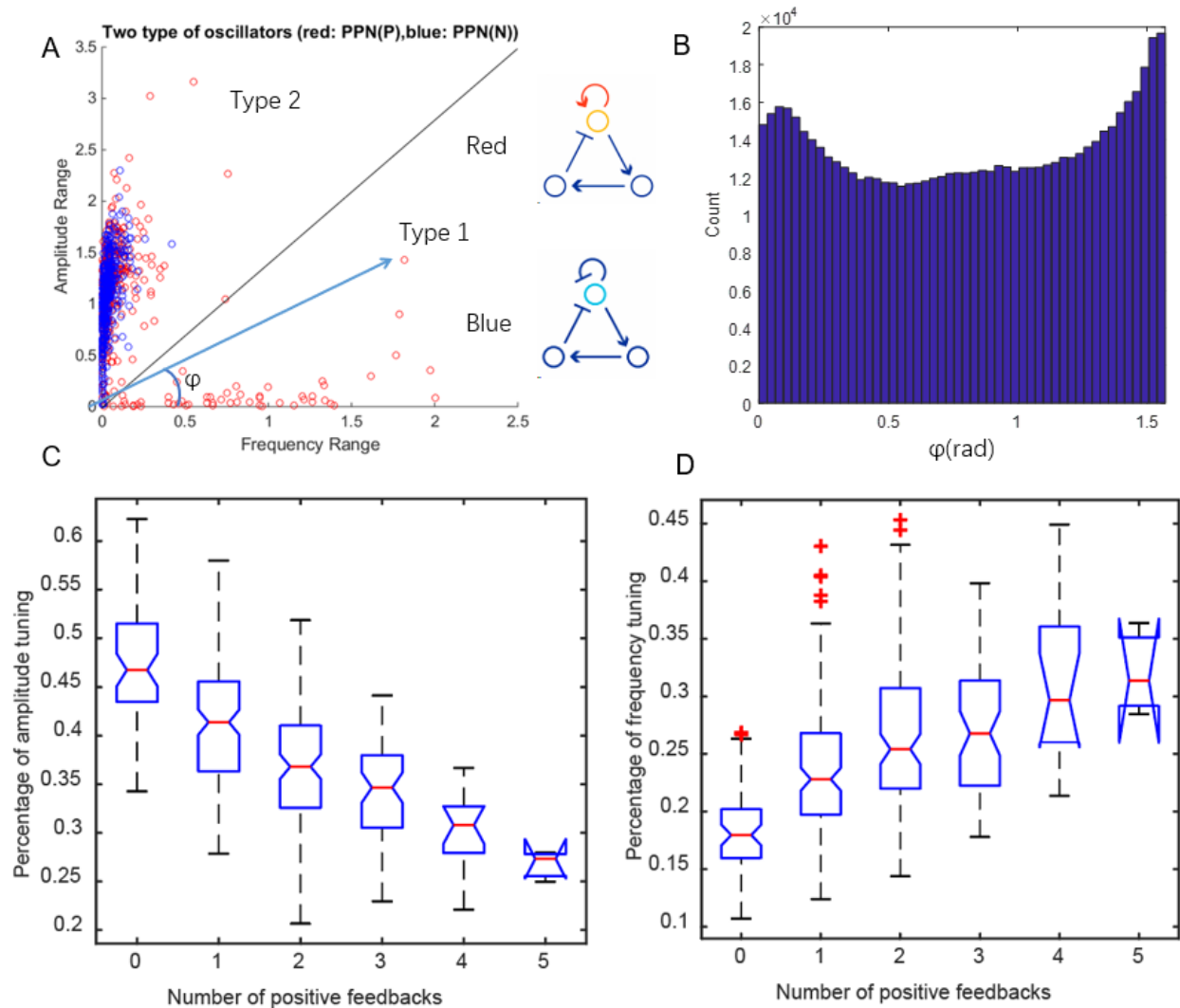


Figure 14 Analysis of tunability distribution of single oscillators

(A) Example of tunability of two topologies. Each sample of interlinked positive and negative feedback (upper) is colored red and the sample of interlinked negative feedback (lower) is colored blue. Angle ϕ is defined as a measurement of tunability. Basal inactivation parameters of the colored nodes are used as tuning parameter. Each node represents a tuning on a randomly selected parameter set. The distribution of dots shows two different tuning patterns: amplitude tuning and frequency tuning. (B) Distribution of ϕ for all system parameters, tuning parameter, and all topologies, showing two modal distribution and the peaks are at around 0 and $\pi/2$. (C) Relationship of the number of positive feedbacks on amplitude tuning percentage for all topologies. (D) Effect of positive feedback number on frequency tuning percentage for all topologies.

The analysis of the relationship between period and peak time showed clear differences between amplitude tuning and period tuning oscillators (Figure 15). In topologies with only amplitude tuning, the peak time is linearly correlated with the oscillator period, indicating sinusoidal-like oscillations. On the contrary, in topologies with frequency tuning, tuning of certain model parameters results in pulsatile behavior with constant peak time across a range of period. Systematic analysis with all topologies also shows that the positive feedbacks are needed for peak time and period to deviate from a linear relationship (Figure 15C). Interestingly, in addition to the sinusoidal and pulsatile waveform, the analysis also identified other types of waveforms. As shown in Figure 15D, the exemplified topology allows tuning of both peak time and period independently. Preliminary analysis showed that this kind of rich behavior on waveform type could only occur in topologies with more than one oscillatory core (coupled oscillators), and the detailed mechanism still needs further investigations.

2.4. Conclusion

Previous work using computational search for functional network motifs of biological oscillators has mainly focused on the core topologies. Much fewer studies have investigated the functional role of auxiliary structures. These studies have selectively examined the influence of one-edge structures on a few predefined oscillatory cores, resulting in a lack of generality. Different from the previous studies, I found the most significant local motifs for oscillator robustness are two-edge structures, namely the incoherent or coherent inputs. This finding has implied the importance of interactions between signals and helps elucidate how biological oscillators can improve robustness through gradual evolution. In addition, identification of

incoherent inputs provides useful guidance for designing robust synthetic oscillators and present a convenient way to modify known biological oscillators, of which the core structures are difficult to manipulate.

In the analysis, we have generated a complete map of three-node oscillators where any pair of topologies that differ by only one regulatory interaction are connected. A similar connection map has been reported in a study on the evolution of robustness in circadian clocks by evolutionary search (Wagner, 2005). The high connectivity we observed in the oscillator design space suggests that an oscillator can be evolved by adding or deleting one regulatory interaction at each step without stopping oscillations. Interestingly, I found the effects of multiple local motifs are additive for both robustness and tunability. That is, the robustness or tunability of an oscillator can increase or decrease with the numbers of respective motifs. This implies that natural evolution could repeatedly use the same strategy to achieve robust or tunable oscillators.

Indeed, both incoherent inputs and positive feedbacks are highly enriched in well-known biological oscillators. Incoherent inputs are observed in nearly all oscillators, ranging from circadian clocks to signaling networks (Figure 1), as well as many robust synthetic biological oscillators (Figure 2). The only exception is the repressilator (Elowitz and Leibler, 2000), the first synthetic gene oscillator, which did not show great robustness until recent modifications (Potvin-Trottier et al., 2016). Positive feedbacks, which were shown to increase oscillator tunability, are also highly enriched in oscillators that requires frequency tunability, from the neural spike, cardiac oscillation to cell cycles (Figure 1). A recent study on frequency tuning and amplitude tuning suggests that the tunability is a critical feature of biological oscillator and plays an important role in transcription regulation (Levine et al., 2013). Detailed analysis on parameter

response in our study provides valuable guidance for designing robust and tunable synthetic oscillators as well as understanding evolutionary strategy to improve the robustness and tunability of an oscillator.

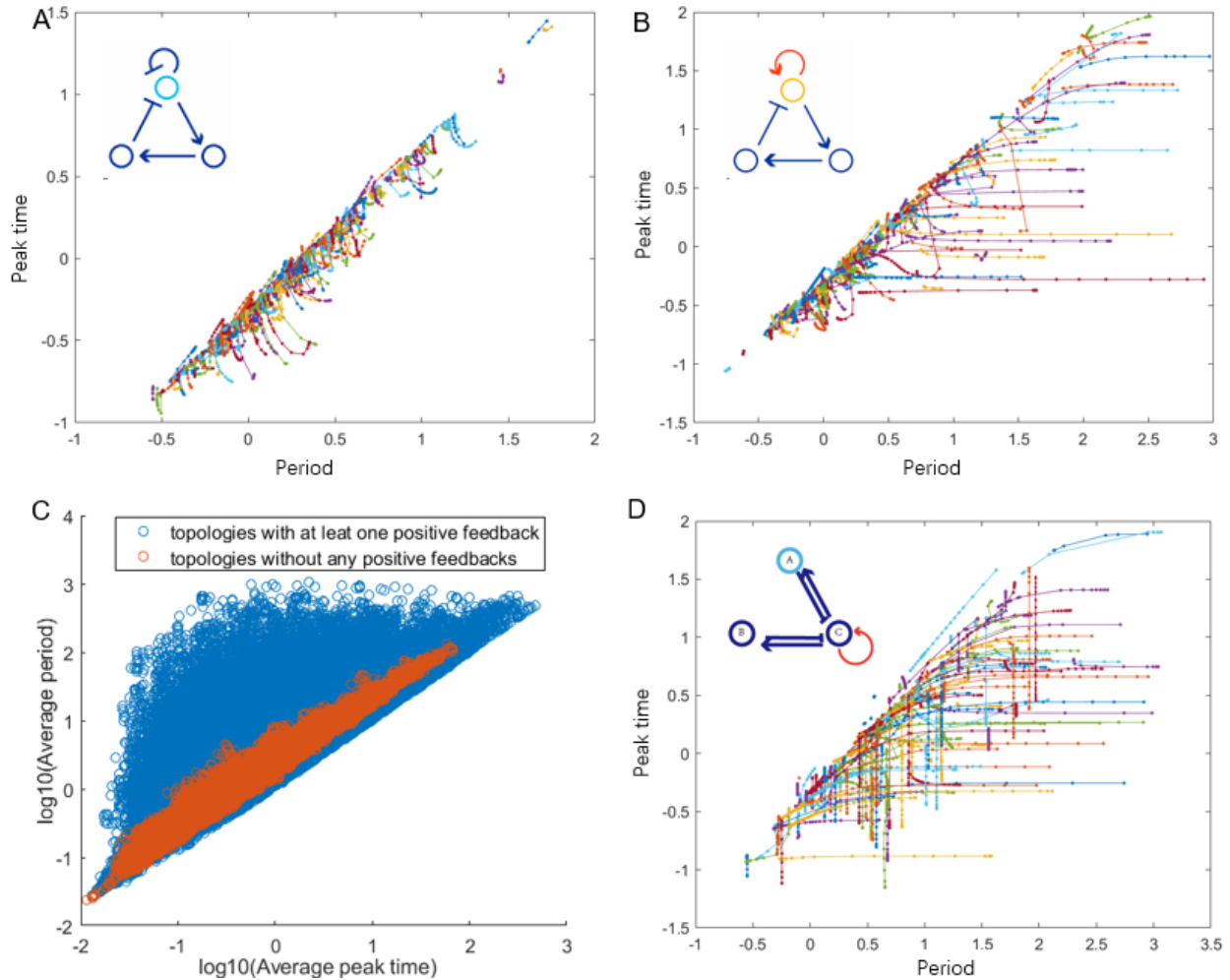


Figure 15 Relationship between peak time and oscillation period (A-B) Relationship between period and peak time of interlinked negative feedback (A) and interlinked positive feedback and negative feedback (B). (C) Joint distribution of average peak time and average period for all samples. Samples of topologies without positive feedback are labeled red, and the samples with positive feedback are labeled blue. (D) Relationship between period and peak time of a coupled oscillator, showing multiple forms of waveform tuning pattern.

Chapter 3 Investigating network circuits of cell cycle oscillator using cell-free *Xenopus* extract droplets

The computational and theoretical study described in Chapter 2 has produced various interesting predictions for how network circuits affect the dynamics properties of biological oscillations. However, given the level of abstraction in the computational models, it is critical to experiment with real-world oscillatory systems to test the predictions derived from mathematical modeling. In this Chapter, I describe my efforts on first building an artificial cell system that reconstitutes cell cycle with cell-free extracts from *Xenopus* eggs, and then using this system to perform various experiments to test the predictions from my theoretical study.

Extracts of *Xenopus* eggs were one of the few early classical models used to study cell cycle regulation (Lohka et al., 1988). Detailed dissections of the cell cycle circuits using these extracts have revealed an architecture of interlinked positive and negative feedbacks (Pomerening et al., 2005). Compared to cellular systems such as cultured cells or developing embryos, it is more convenient to reconstitute molecular circuits in cell-free extracts by adding well-defined recombinant molecules. Cell-free extracts are more amenable to the systematic design, manipulation, and quantitative biochemical measurements, bringing a unique advantage to test model predictions. However, most *in vitro* reconstitutions of biological oscillators up to date can only sustain short lifetimes of oscillations. This is because the previous methods usually constructed oscillations in well-mixed bulk solutions which tend to produce quickly damped oscillations. Additionally, these bulk reactions lack the similarity to the actual cell dimensions and the ability to generate oscillations with different frequencies in a high-throughput manner.

These limitations make it difficult to systematically study oscillator properties, especially period tunability.

In this chapter, I will introduce our approaches to tackle these challenges. In part 3.1, 3.3 and 3.4, I will discuss our efforts to develop an artificial mitotic cycle system by encapsulating reaction mixtures containing cycling *Xenopus* egg cytoplasm in cell-scale micro-emulsions. This is a published work in collaboration with Ye Guan (Guan et al., 2018), a previous graduate student in the lab, who did most of the experiments, and some of the paragraphs and figures are adapted from previous publications (Guan et al., 2018). We showed that energy level may play an important role in cell cycle progression. In part 3.2, I'm going to present the experimental evidence I collected supporting that incoherent input increases the oscillator robustness. Part 3.5-3.7 is ongoing projects in collaboration with Meng Sun, a postdoctoral researcher in the lab with expertise in nanofabrication and droplet microfluidics, and we further developed artificial mitotic cycle system using microfluidic devices to allow for reliable high-throughput analysis. Using this system, we collected experimental evidence supporting positive feedbacks increasing the oscillator tunability. In the meantime, and we also verified that the cell cycle is a pulsatile oscillator with consistent mitotic phase and variable interphase.

3.1. Droplets of *Xenopus* egg extracts reliably drive the periodic progression of multiple mitotic events

To generate the extracts droplets, we have developed and optimized a protocol to encapsulate cell-free cycling extracts into microfluidic droplets and have used fluorescent imaging to examine their cell cycle activities. Cell-free cycling extract was made from *Xenopus* eggs (Figure 16) using a published protocol (Murray, 1991) with a small modification and tested for biological activities. The modification we made was in the cell cycle activation method in

which we replaced the electrical shock activation by adding calcium ionophore A23187 (200 ng/ μ L). The extract was then mixed with surfactant oil 2% PFPE-PEG, and vortexed to generate droplets (Ho et al., 2017). This method could compartmentalize cycling *Xenopus* egg extracts into microemulsion droplets, with radii ranging from 10 μ m to 300 μ m (Figure 16A). After vortexing, the droplets were loaded into a Teflon-coated chamber with a height of 100 μ m and recorded using long-term time-lapse fluorescence microscopy.

To enable measurement of cell cycle activities, we added cell cycle reporters in the extract which allowed high-resolution measurements of the cell cycle dynamics. The fluorescence time courses of each droplet were then analyzed to obtain information of its cell cycles including period, reporter amplitude, number of sustained cycles, and droplet size. Specifically, we added securin-mCherry mRNA, de-membranated sperm chromatin, purified green fluorescent protein-nuclear localization signal (GFP-NLS), and Hoechst 33342 dye to the cytoplasmic extracts, which together visualize cell cycle dynamics of individual droplets (Figure 17A). Securin is an anaphase substrate of APC/C. Therefore, the securin-mCherry reporter is periodically degraded and indicates the oscillation of cell cycle. The sperm chromatin, GFP-NLS and Hoechst dye in combination visualize the breakdown and reconstruction of the nucleus as well as the condensation and relaxation of chromatin that oscillates between interphase and mitosis. In interphase, the presence of sperm chromosomal DNA, labeled by Hoechst, initiated the self-assembly of a nucleus, upon which GFP-NLS protein was imported through the nuclear pores. The spatial distributions of Hoechst and GFP-NLS thus coincided in an interphase nucleus (Figure 17A columns 1, 3, and 5). As the artificial cell entered mitosis, the chromosome condensed resulting in a tighter distribution of Hoechst, while the nuclear envelope broke down and GFP-NLS quickly dispersed into a uniform distribution in the whole droplet (Figure

17A columns 2 and 4). In another set of experiments, we also supplied the system with purified mRNAs of full-length cyclin B1 fused to YFP (cyclin B1-YFP), which function both as a reporter of APC/C activity and as an activator of Cdk1. A droplet supplied with both cyclin B1-YFP and securin-mCherry mRNAs exhibited oscillations with highly correlated signals, suggesting that both are reliable reporters for the cell cycle activity. Altogether, these experiments showed that the droplet system successfully reconstituted a cell-free mitotic oscillator centered on Cdk1 and APC/C that can reliably drive the periodic progression of downstream events including chromosome morphology change and nuclear envelope breakdown and re-assembly, like what occurs *in vivo*.

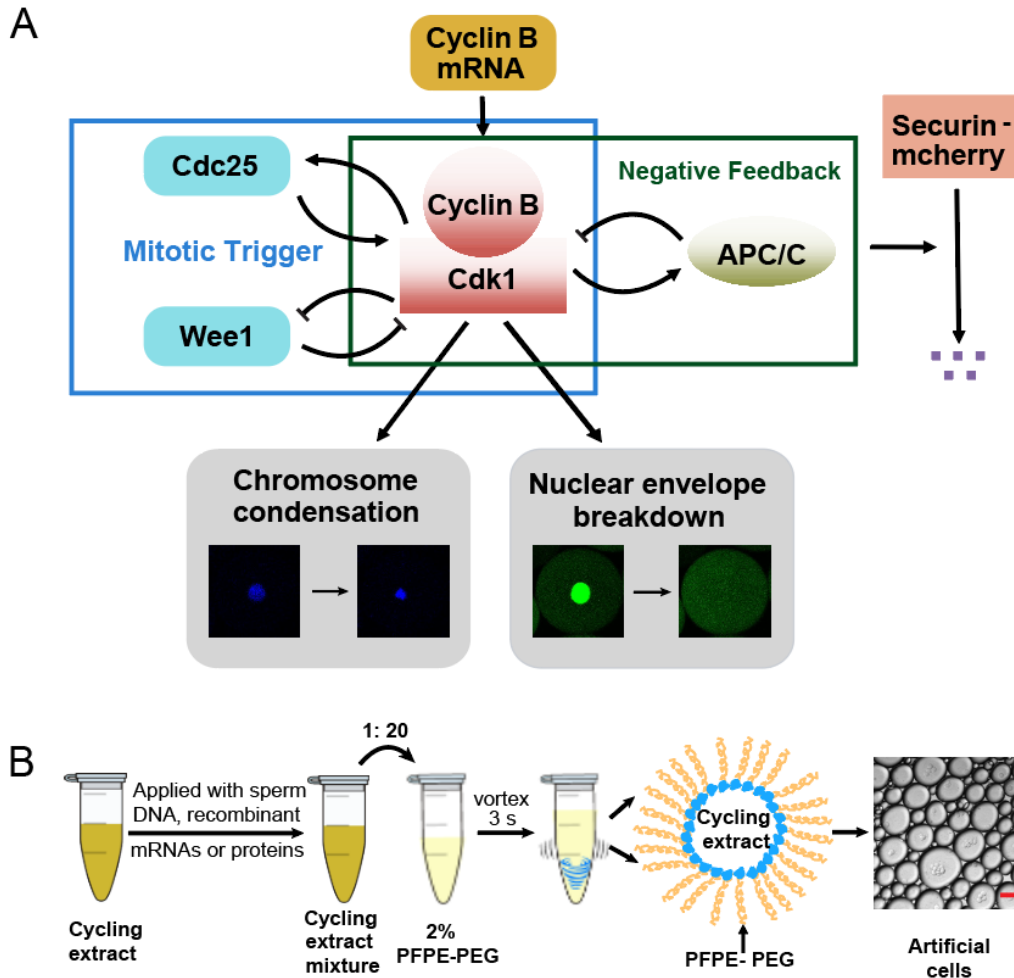


Figure 16 Making cell-free cell cycle extract from *Xenopus* eggs

(A) Schematic view of a cell cycle oscillator that consists of coupled positive and negative feedback loops. The central regulator, cyclin B-Cdk1 complex activates its own activator, phosphatase Cdc25, forming a positive feedback loop, and inhibits its own inhibitor, kinase Wee1, forming a double negative feedback loop. Additionally, cyclin B-Cdk1 activates the E3 ubiquitin ligase APC/C, which targets cyclin B for degradation and completes a core negative feedback loop. Active APC/C also promotes the degradation of another substrate securin. Once the cyclin B1-Cdk1 complex is activated, the circuit drives a set of mitotic events including chromosome condensation and nuclear envelope breakdown (NEB). (B) Experimental procedures. Cycling *Xenopus* extracts are supplemented with various combinations of recombinant proteins, mRNAs, and de-membrated sperm DNAs, which are encapsulated in 2% Perfluoropolyether-poly (ethylene glycol) (PFPE-PEG) oil microemulsions. Scale bar is 100 μm .

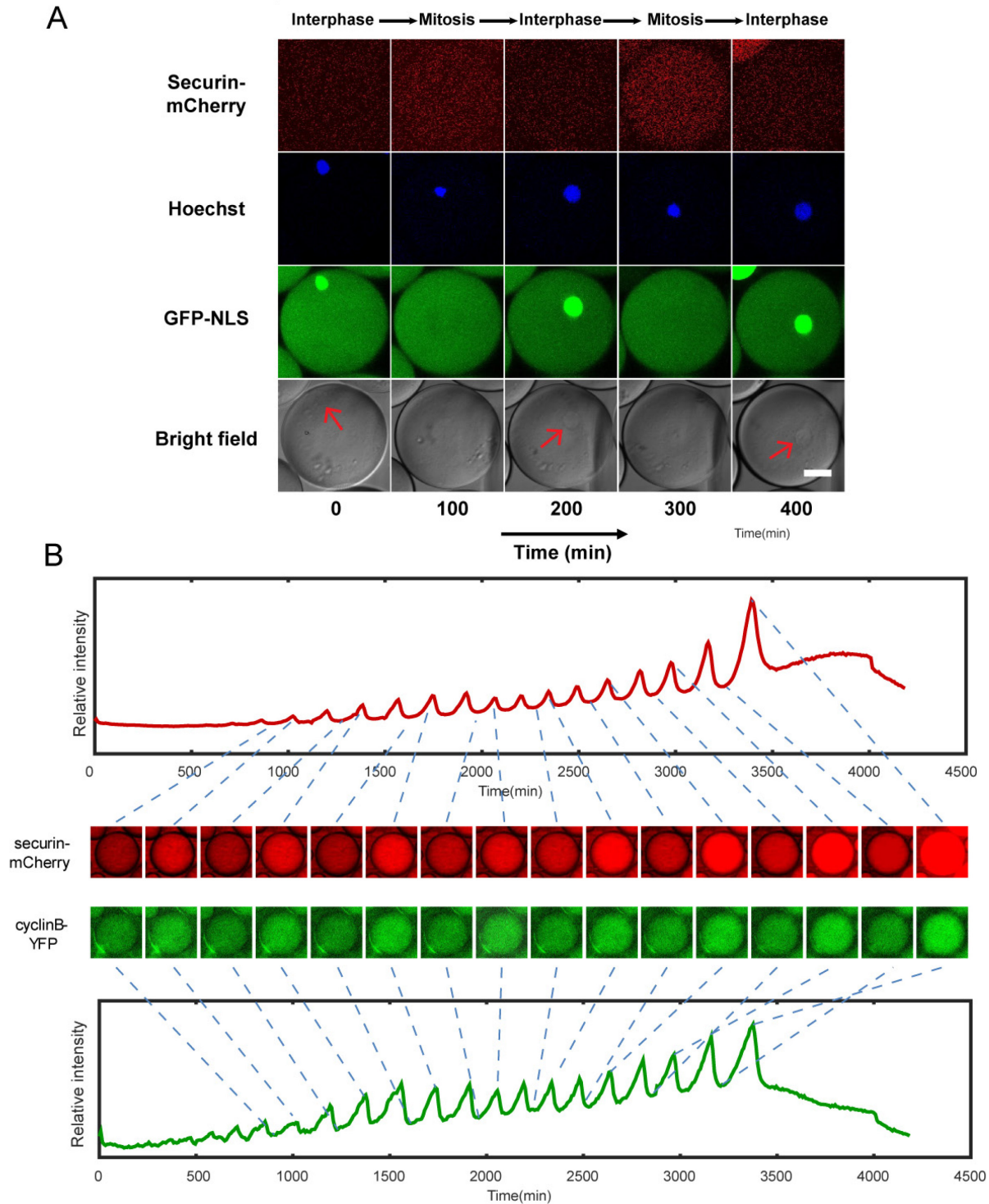


Figure 17 *Xenopus* extract cell cycle oscillator reliably drives the periodic progression of multiple mitotic events (A) Snapshots of a droplet were taken periodically both in fluorescence channels (top three rows) and bright-field (the last row). The cyclic progression of the cell cycle clock and its downstream mitotic processes are simultaneously tracked by multiple fluorescence reporters. The clock regulator APC/C activity is reported by its substrate securin-mCherry, chromosomal morphology changes by the Hoechst stains, and NEB by GFP-NLS. Nuclear envelopes (red arrows) are also detectable on bright field images, matching the localization of GFP-NLS indicated nuclei. Scale bar is 30 μ m. (B) Simultaneous measurements of fluorescence intensities of securin-mCherry

(upper panel) and cyclin B-YFP (lower panel), showing sustained oscillations for about 58 hr. The mRNA concentrations of securin-mCherry and cyclin B-YFP are 10 ng/ μ L and 1 ng/ μ L. The series of mCherry and YFP images correspond to selected peaks and troughs in the time courses of fluorescence intensities. The two channels have coincident peaks and troughs for all cycles, suggesting that they both are reliable reporters for the cell cycle oscillator.

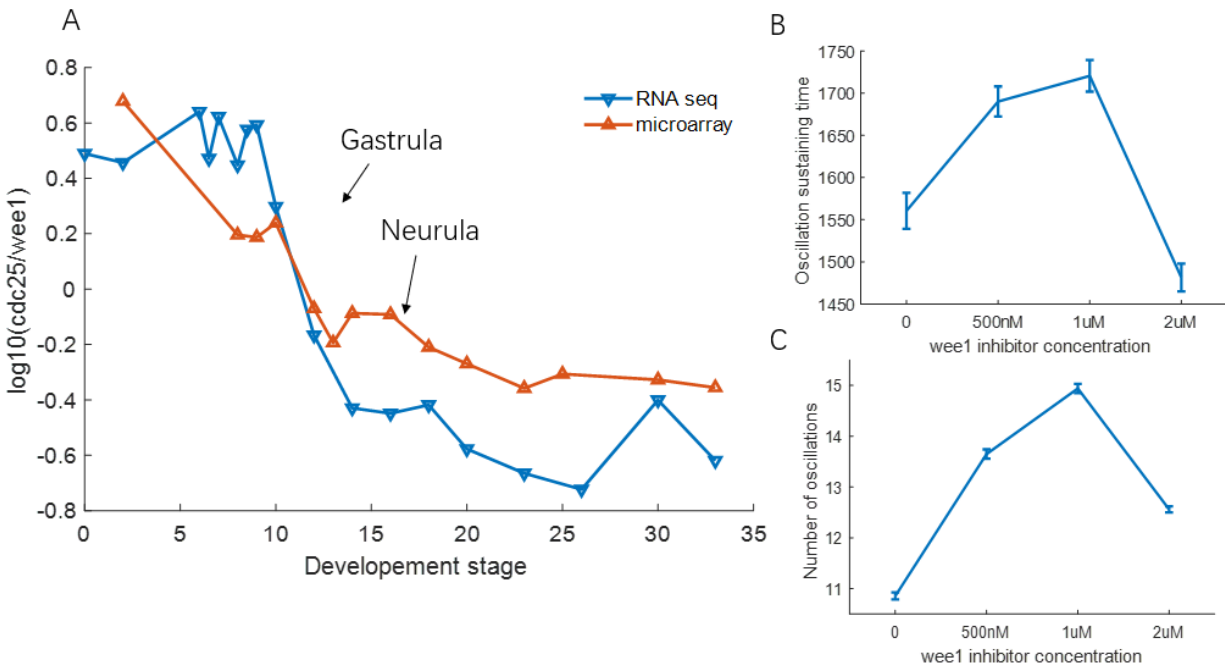


Figure 18 *wee1* inhibitor could increase the cell cycle oscillation number and sustaining time. (A) The expression level of *cdc25* divided by the expression level of *wee1* during the development of *Xenopus* embryos. Calculated from the database of a previous study (Peshkin et al., 2015). (B) Relationship between *wee1* inhibitor concentration and cell cycle oscillator sustaining time. (C) Relationship between *wee1* inhibitor concentration and cell cycle oscillation number

3.2. Oscillation duration of *Xenopus* extract is effectively tuned by *wee1* inhibitors.

Cell cycle oscillations in *Xenopus* egg extract mainly consist of two phases, mitotic phase and interphase, and its transition (also called G2/M transition) is mainly driven by the Cdk1-cyclinB complex. The molecular mechanisms underlying G2/M transition has been reviewed in detail in (Kastan and Bartek, 2004). In brief, kinase *wee1* phosphorylate Cdk1 and inhibits its activity; conversely, *cdc25*, a phosphatase can dephosphorylate and activates Cdk1. Cdk1, in return, phosphorylates both *cdc25* and *wee1*, which activates *cdc25* but inhibits *wee1* (Figure

16A). As a result, *cdc25* and *wee1* each forms a positive feedback loop on Cdk1-cyclinB complex respectively. After activation, Cdk1 can drive a series of downstream events including the phosphorylation of the APC/C complex, an E3 ligase. The APC/C complex is activated by a series of phosphorylation events and could mediate ubiquitin-mediated degradation of cyclin B with the help of *cdc20*, which forms a negative feedback to the Cdk1-cyclinB complex. As a result, APC/C and *wee1* form a pair of coherent inputs to regulate Cdk1 activity while APC/C and *cdc25* form a pair of incoherent inputs to regulate Cdk1. According to the predictions from my computational work (Chapter 2), the robustness of the cell cycle oscillator should be enhanced by *cdc25* activity and inhibited by *wee1* activity.

To test this prediction, I first examined published data on cell cycle during development (Peshkin et al., 2015) and calculated the ratio between *cdc25* and *wee1* during different developmental stages (Figure 18A). I found that the ratio of *cdc25* to *wee1* activity remains relatively high and decreases rapidly during gastrulation, and remained low at later developmental stages, which supports my prediction as cell cycle is more likely to sustain oscillation during early developmental stages. Then I experimented with the *Xenopus* cyclin B extract droplets and performed perturbations to the cell cycle circuits. While a specific inhibitor of *cdc25* is difficult to find, several specific *wee1* inhibitors have been developed. Specifically, I have used PD0166285, a previously tested *wee1* inhibitor (Tsai et al., 2014a), to inhibit *wee1* activity. Since it is difficult to measure parameter volume that supports oscillations experimentally, we proposed several measurements to indicate oscillator robustness, including 1) The percentage of droplets that shows oscillations. 2) The sustaining time of oscillation droplets. 3) The number of cycles the system could perform. From our results, I observed that adding *wee1* inhibitor has little effect on the percentage of droplets that show oscillations at time zero

(data not shown). However, treatment of wee1 inhibitor had a significant effect on the number of oscillations and total oscillation duration a droplet sustains. Specifically, wee1 inhibitor PD0166285 below 1 μ M increase both the oscillation sustaining time (Figure 18B) and the number of oscillations in the extract system (Figure 18C). This result suggests that inhibit wee1 activity may increase the robustness of cell cycle oscillations. Somewhat surprisingly, wee1 inhibitor treated at concentrations above 1 μ M reverses this increase. This is probably a result of substrate depletion of cdc25 when wee1 activity is vastly reduced.

3.3. Cell cycle frequency can be effectively tuned with cyclin B1 mRNAs and is sensitive to droplet size

Frequency tunability, the ability to adjust oscillation frequency is an important feature shared by many oscillators (Tsai et al., 2008) (also in Chapter 2.3). The *Xenopus* egg extract droplets which support multiple oscillations of cell cycles provide an effective experimental solution to study tunability of the biological oscillators. To avoid interference from the complicated nuclear dynamics, I used a minimal mitotic oscillatory system with no addition of sperm chromatin, therefore forms no nuclei. This simple, cytoplasmic-only oscillator produced highly robust, undamped, self-sustained cell cycle oscillations up to 32 cycles over a lifetime of 4 days, significantly better than many existing synthetic oscillators (Guan et al., 2018) (Figure 17).

Cyclin B1-YFP is used in the experiment to both visualize the cell cycle dynamics and manipulate cyclin B1 expression. With increasing concentrations of cyclin B1-YFP mRNAs added to the system, I observed a decrease in the average period (Figure 19B), meaning that higher cyclin B1 concentrations tend to speed up the cell cycle. However, the average number of cycles (Figure 19A) reduces with increased cyclin B1 concentrations, resulting in a negative

correlation between the lifetime of oscillations and the amount of cyclin B1 mRNAs, and the extracts will eventually arrest at a mitotic phase in the presence of high concentrations of cyclin B1. We have proposed an energy-related model to explain this phenomenon which is detailed in the next section.

In the experiments, we have generated droplets with radii ranging from a few μm to 300 μm . This enabled the characterization of size-dependent behaviors of cell cycles. At the scale of a cell, the dynamics of biochemical reactions may become stochastic. Although stochastic phenomena have been studied extensively in the context of steady-state gene expressions, studying a stochastic system that is out of steady-states can be challenging in living organisms due to low throughput and complications from cell growth and division. These limitations can be overcome by reconstitution of *in vitro* oscillators inside cell-scale droplets, which omit cell growth and divisions. Parallel tracking of droplets also enables high-throughput data generation for statistical analysis. *In vitro* compartmentalization of molecules, especially rate-limiting molecules such as cyclin B1 mRNAs, into cell-sized droplets may have a major effect on the reaction kinetics of cell cycles. The smaller the size of a droplet, the smaller the copy number of molecules encapsulated inside the droplet and the larger the inherent stochasticity of biochemical reactions. Additionally, the partition errors of these molecules resulting from compartmentalization may further contribute to the variation of droplet behaviors in a size-dependent manner. Figure 19C shows that smaller droplets have slower oscillations with a larger variation in the periods. This is similar with the size effect reported on an *in vitro* transcriptional oscillator (Weitz et al., 2014), further suggesting that the size effect on oscillation period is likely a result of stochasticity in the system independent of specific oscillating molecules. We also observed a reduced number of oscillations in smaller droplets (Figure 19B). Interestingly, these

size effects become less dramatic for droplets with larger sizes or with higher concentrations of cyclin B1 mRNAs, suggesting that stochasticity effects diminish as the molecule number increases.

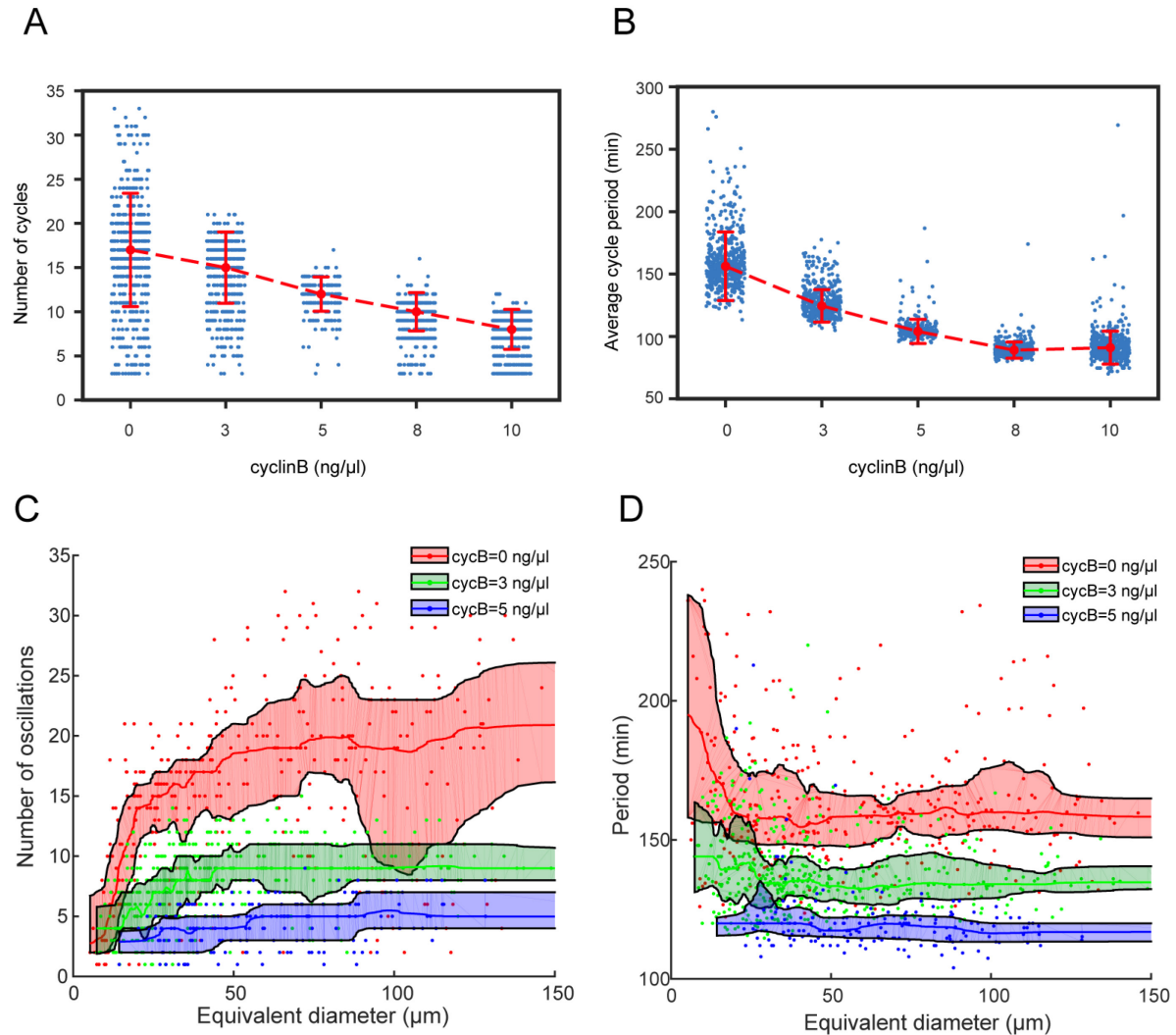


Figure 19 Effect of external cyclinB concentration and droplet size on cell cycle number and period. (A, B) The oscillator is tunable in frequency (A) and the number of cycles (B) as a function of the concentration of cyclin B mRNAs. Cyclin B not only functions as a substrate of APC/C but also binds to Cdk1 for its activation, functioning as an ‘input’ of the clock. Each data point represents a single droplet that was collected from one of the loading replicates. Red dashed line connects medians at different conditions. Error bar indicates median absolute deviation (MAD). (C, D) Droplets with smaller diameters have larger periods on average and a wider distribution of periods (C) and exhibit a smaller number of oscillations on average (D). Colored areas represent moving 25 percentiles to 75 percentiles and are smoothed using the LOWESS smoothing method. The equivalent diameter is defined as the diameter of a sphere that has an equal volume to that of a droplet, estimated by a volume formula in literature (Good et al., 2013). Note that these size effects are smaller for droplets with higher cyclin B mRNA concentrations.

3.4. Energy depletion model recapitulates dynamics of the oscillator

As discussed in the previous section, the period of the *Xenopus* cycling extract can be tuned by cyclin B1 mRNA concentration and droplet size. Interestingly, the period and number of cycles are affected by droplet sizes in opposite directions, but changes in the same direction when affected by the level of cyclin B1 mRNAs (Figure 19). This means that the lifespan of the oscillatory system is sensitive to cyclin B1 mRNA concentration but not droplet size (Figure 19). Moreover, I have observed that both securin-mCherry and cyclin B1-YFP levels exhibited increased amplitude, baseline, and period over time. These trends cannot be explained by any existing cell cycle models (Tsai et al., 2014a; Yang and Ferrell, 2013b).

To explain these phenomena, we explored factors of cell-free extracts that differ from existing cell cycle models. Unlike intact embryos, cell-free extracts lack yolk which is an energy source for embryo development and exclude some of the mitochondria which are responsible for energy regeneration. We postulated that energy is an important regulator for the droplet system with a limited amount of energy sources to consume over time.

To gain insights into our experimental observations and to better understand the in vitro oscillator system, we built a computational model to examine how energy consumption affects the cell cycle oscillation behaviors. This energy depletion model is modified based on a well-established cell-cycle model (Tsai et al., 2014b; Yang and Ferrell, 2013a) by introducing ATP into all phosphorylation reactions (Appendix Tables A2, A3). In the cell cycle network, the activation of Cdk1 is co-regulated by a double positive feedback through a phosphatase Cdc25 and a double negative feedback through a kinase Wee1. The balance between Wee1 and Cdc25 activity was suggested to be crucial for the transition of cell cycle status during early embryo

development (Tsai et al., 2014a). In light of this, we defined the balance between Wee1 and Cdc25 by the ratio $R = \frac{k_{Wee1}[Wee1]}{k_{Cdc25}[Cdc25]}$. We noted that ATP-dependent phosphorylation of Cdc25 and Wee1 can decrease R by activating Cdc25 and inhibiting Wee1 simultaneously, resulting in a high dependence of R on the ATP concentration (Figure 20B).

Using this model, we further investigated the relationship between ATP and oscillation behaviors. We introduced a parameter r into our system to systematically change the ratio R . In Figure 20C, the phase plot of the two-ODE model shows that at a low r (e.g. 0.5), the system will stay in a stable steady-state with low cyclin B concentration. Conversely, at a high r (e.g. 2.5), the oscillation will be arrested in a stable steady-state with high cyclin B concentration. At an intermediate value, increasing r produced oscillations of increased amplitude, baseline and period (Figure 20C, D). We assume that the available ATP concentration decreases over time which makes sense in the case of our droplets with no energy reserve. This model therefore successfully recapitulates the experimentally observed increment of amplitude, baseline, and period of the cyclin B time course (Figure 20E).

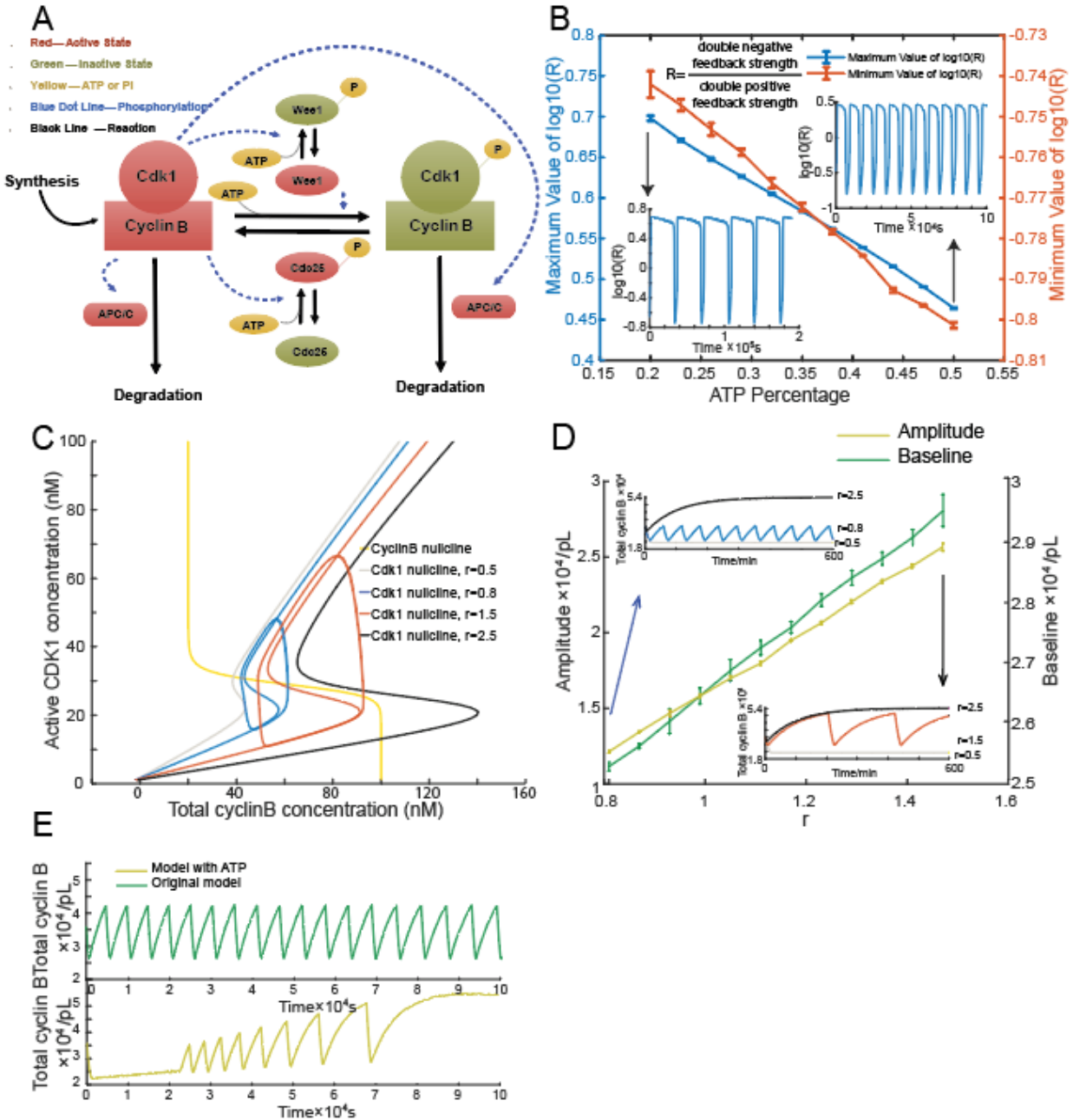


Figure 20 Energy depletion model of cell cycle

(A) Schematic view of the cyclin B-Cdk1 oscillation system. Note that ATP is taken into consideration. Activated molecules are marked in red, inactivated molecules in green and ATP or Pi in yellow. Black line indicates a reaction and blue dotted line phosphorylation. (B) Relationship between ATP percentage and R value, showing that decreasing the ATP concentration leads to a higher R value. Error bars represent ranges from three simulations. Two inserts represent the dynamics of R value over time when the ATP percentage $[ATP]/([ATP]+[ADP])$ is set as 0.2 (left) and 0.5 (right). The model is simulated using the Gillespie algorithm. (C) Phase plots of the two-ODE model. Parameters for the cyclin B nullcline (Ncyc) (Yang and Ferrell, 2013) and the Cdk1 nullclines with a variety of values of r were chosen based on previous experimental work (Pomeroy et al., 2003). Note that the r here is a parameter and is different from R in Figure 20B. Two sample traces of limit cycle oscillations are plotted for $r = 0.8$ and $r = 1.5$, showing that a larger r value leads to a higher amplitude and baseline. In addition, $r = 0.5$ generates a low stable steady-state of cyclin B, while $r = 2.5$ a high stable steady-state of cyclin B. (D) Relationship between the oscillation baseline and amplitude values and ATP concentration (positively correlated with r). Error bars indicate

the ranges of 3 replicates. Inserts show two example time courses of total cyclin B with different r values (upper: $r = 0.8$, lower: $r = 1.5$), colors of which match the ones in Figure 20C. Simulation is done using the Gillespie algorithm. (E) Time series of total cyclin B molecules from the model without ATP (top panel, green line) and with ATP (bottom panel, yellow line).

3.5. Building artificial cells with a uniform size

Given the sensitivity of the oscillator period on droplet size, when tuning frequency with mRNA concentrations, the system shows high variation among droplets with the same mRNA concentrations. To systematically investigate the oscillator tunability without this additional variable, I worked with Meng Sun to use the microfluidic system to produce droplets with uniform sizes and shape. Droplet microfluidic technology is a state-of-art technology (Damiati et al., 2018) that is capable of producing cell-like compartments and sub-compartments of controlled size at a high level of precision. Recent studies have used microfluidic systems to generate nucleus (Guan et al., 2018), microtubules (Sanchez et al., 2012), and spindle (Good et al., 2013) in uniform-sized droplets. Microfluidic systems can generate large quantities of monodispersed droplets of controlled sized and content from small sample volumes at high speed. It allows expeditious processing of raw samples prepared from live embryos or cells that oftentimes have unpredictable and limited quantities and thus can help maximally preserve the biological activities of the samples *in vitro*. However, to obtain accurate and high-resolution measurements for a large number of droplets, it also requires compatible droplet detection techniques, analytical throughput, and spatiotemporal resolution. In addition, for those artificial droplet cells that mimic dynamic cellular behaviors and biological processes, it becomes difficult computationally to extract the sophisticated dynamics and morphological details in the droplets with long-term live monitoring. These challenges have limited the technology to be generalized for biological applications.

To tackle the challenges, we have developed a droplet microfluidic toolbox (Figure 21A) and an image-based droplet analysis framework (Figure 21B) that address the aforementioned challenges to create and analyze artificial droplet cells. As shown in Figure 21B, droplets are generated in a flow-focusing device and loaded from an on-chip reservoir into rectangular shaped thin glass tubes. Compared to traditional methods which use micro-wells or -traps fabricated on a chip, our method largely reduces the complexity of manipulating fluid dynamics in the microchannel network (Du et al., 2009). A key challenge is to trace the origin and constitution of individual droplets which we addressed by using automated droplet tracking. After loading the droplets to the tubes, they are then immersed and arrayed in an oil dish for long-term droplet incubation and imaging. Unlike previously reported tracking methods using fluorescence markers (Genot et al., 2016), which may be subject to cross-talk, photobleaching, fluctuations, and photo-toxicity to biological samples, we developed an automatic image analysis method using bright-field images to segment and track every single droplet over the entire acquisition time.

The detailed image analysis pipeline is shown in Figure 22. Images are preprocessed with background subtraction to compensate illumination difference. An LoG (Laplacian of Gaussian) filter is then applied to the image to increase the contrast of edge and suppress noise. Hough circle transform is used to detect circular objects (droplets), and the detected circles are trimmed to avoid overlapping. Automated lineage tracking is performed on features calculated during segmentation. Segments are organized in K-D trees for faster searching. Droplets from each time point T were compared with the ones from $T+1$ to search for the globally optimal matches between neighboring time points (Huh et al., 2011). Parameters used for tracking were automatically calculated based on the distribution of droplets features and confirmed in

subsamples by eye. As an output from tracking, each track starts at the first time point, or when the droplet moves into the image field and ends at the last time point, or when the droplet moves out of the image field. After tracking, individual droplet tracks are further filtered based on tracking length, droplet shape/size, and the fluorescent intensity of cell cycle reporters are measured and recorded frame by frame over all the captured time-lapse images.

Having the combined advantages of high-throughput droplet generation, long-term incubation, as well as accurate tracking and detection, our droplet microfluidic framework can be flexibly adapted for a wide variety of chemical and biological applications.

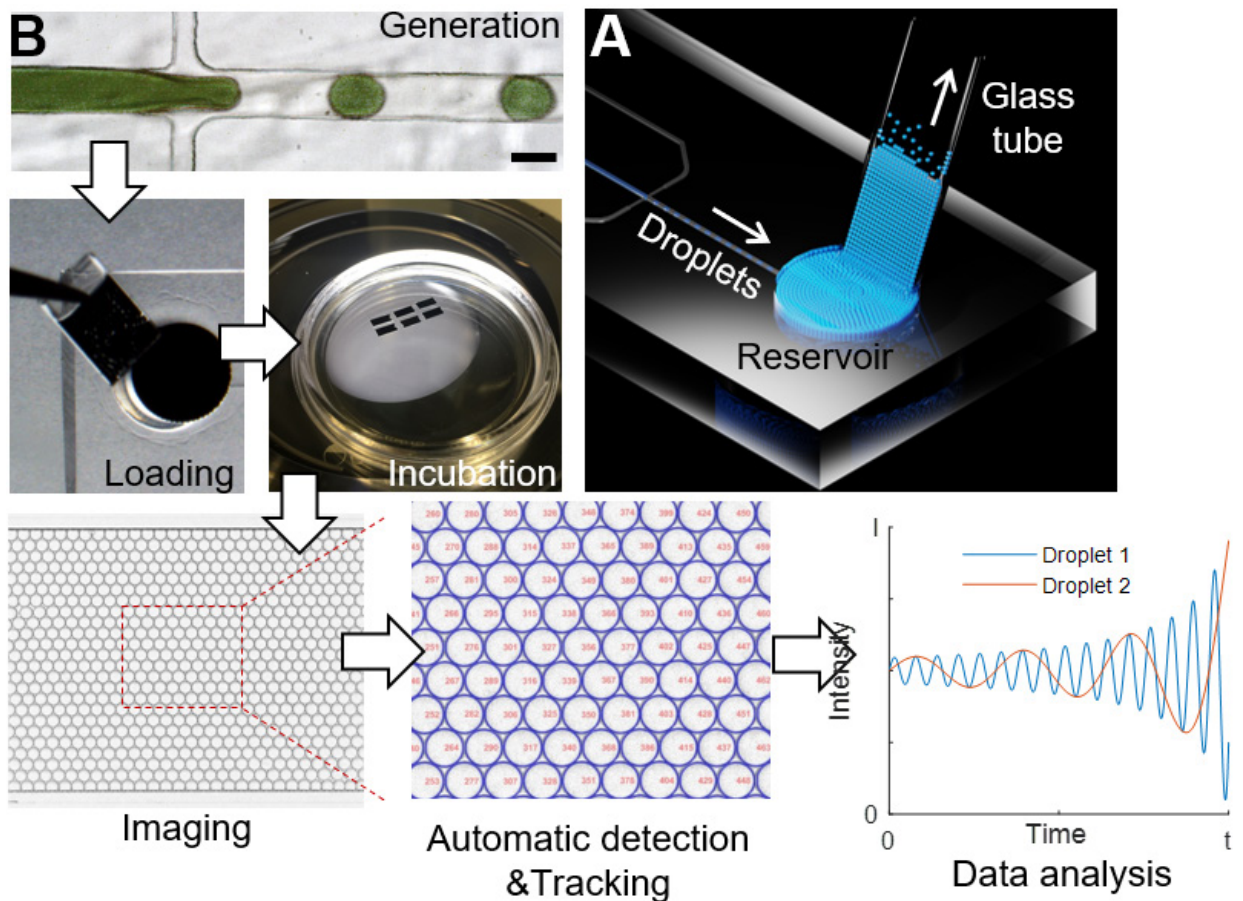


Figure 21 Droplet microfluidic platform.

(A) Schematic diagram showing droplet generation and loading into a glass tube: a reservoir opened at the end of a flow-focusing device with a diameter of 3 mm; the tube width is 2.1 mm. The arrows indicate the flow direction of droplets. (B) Droplet microfluidic workflow.

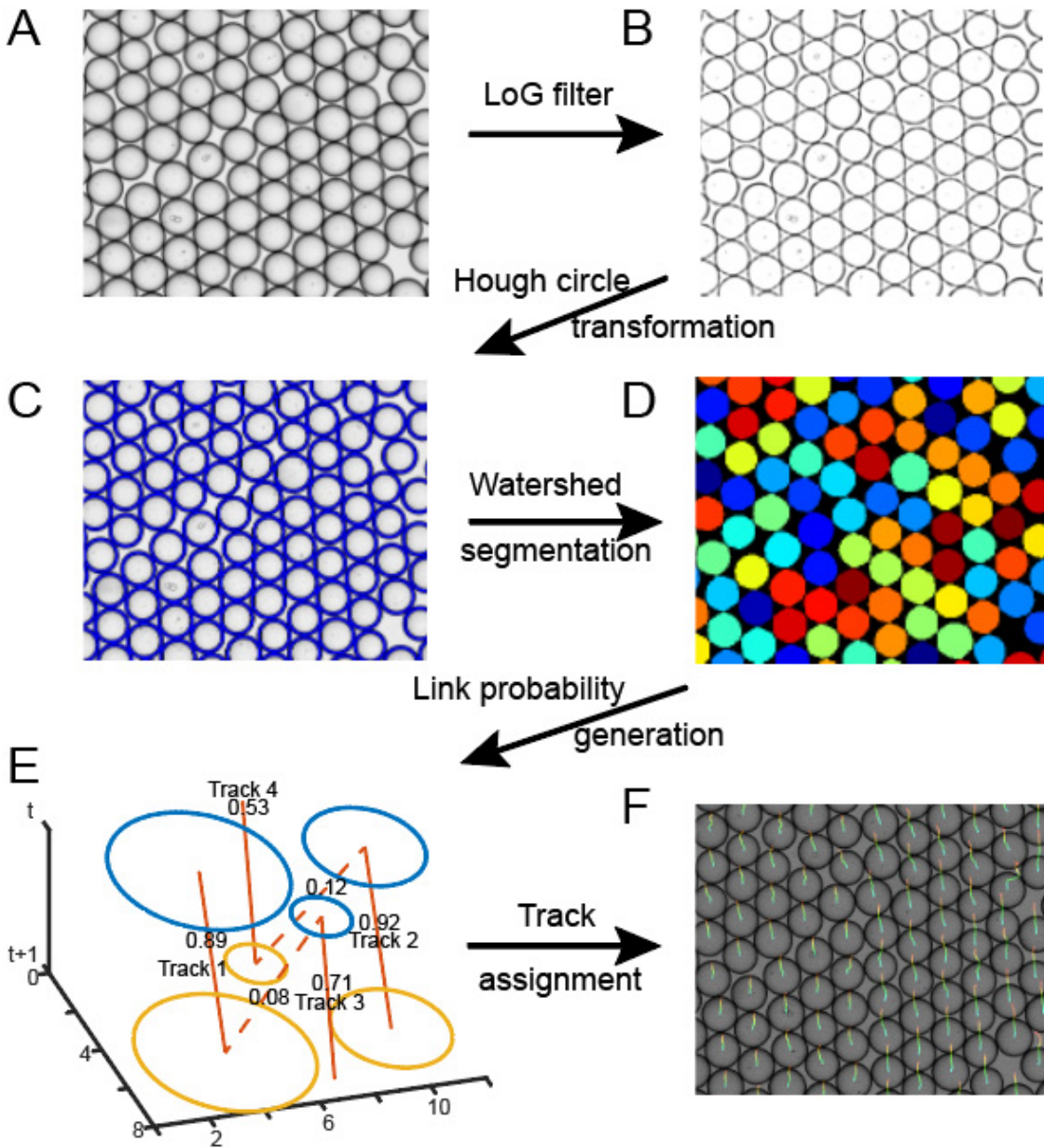


Figure 22 Image processing pipeline for automatic droplet analysis. (A) A section of an original Image. (B) Image after LoG filter ($r_1=6$ pixel, $r_2=2$ pixel). (C) Hough circle transformation followed by thresholding and overlap detection. (D) Watershed segmentation with seeds generated from circle detection. (E) Illustration of the linking process. 6 possible links found between two frames with 3 segments. The number next to tracks represent linking probability. After optimizing maximum probability, 4 of the links (solid line) are adopted and added to tracks, while the rest (dashed line) are discarded. Note that track 4 represents the droplet moving in from outside while track 3 represents the droplet moving out of the view (F) Example of tracking results

3.6. Disruption of positive feedback reduces the tunability of cell cycle oscillators.

Using the microfluidic system, we generated droplets of controlled size and content to study the control of frequency tunability of the cell cycle. In Chapter 3.3, it has been showed that external human cyclinB1-mRNA can reliably tune the cell cycle oscillator frequency, suggesting that cyclin B1 level is an ideal candidate tuning parameter. However, adding external cyclin B mRNA can only increase, but not decrease the oscillator period, which restricts the dynamical range of the cell cycle period. To solve the problem, we used morpholino, a polymer that binds to specific mRNA to block translation. We applied cyclin B morpholinos to the droplets to inhibit internal cyclin B mRNAs which effectively tuned the cell cycle oscillator to a longer period. As shown in Figure 23, we added a mixture of 4 morpholinos to the extracts droplets, targeting *Xenopus* cyclinB1a (ACATTTTCCCAAACCGACAACCTGG), *Xenopus* cyclinB1b (ACATTTTCTCAAGCGCAAACCTGCA), *Xenopus* cyclinB2l (AATTGCAGCCCGACGAGTAGCCAT), *Xenopus* cyclinB2s (CGACGAGTAGCCATCTCCGGTAAAA) respectively, and the average period of the cell cycle significantly increases. In comparison, the droplets treated with control morpholinos (a mixture of random 25mers) shows no significant change. This indicates that the morpholino mixture can reliably block the translation of internal cyclin B mRNAs. As an additional control, the effect of morpholino on cell cycle period is compensated when we added 10ng/ul external human cyclinB1 mRNA to the extract. This confirms that the effect of morpholino is specific and we can use a combination of morpholino mixture and cyclin B mRNA to increase the dynamical range of frequency tuning.

We developed microfluidic platforms to identify the operating concentration range of morpholino and mRNAs (Figure 23B, C). We added fluorescent dyes to both the morpholino

mixture and external cyclin B mRNA to facilitate measurements of their concentrations in individual droplets. We use microfluidic devices to fine tune the volume of morpholino mixture or external cyclin B mRNA added to the droplets. As the molecule numbers of both the dye and morpholino/mRNA are large enough, we assume that the intensity of the fluorescence dye linearly correlates with the concentration of morpholino/mRNAs in the droplets. By changing the pressure of two microfluidic inlets, we can continuously change the value of the tuning parameter. After imaging and data analysis, we binned the data based on the morpholino or mRNA concentrations. The result shows that by increasing morpholino or mRNA concentration, the percentage of oscillators that support oscillation decreases and reached 0, which means that we have identified the bifurcation point of this oscillatory system. The critical condition for morpholino is around $2.5\mu\text{M}$. As a result, we can add mRNAs in extract supplemented with $3\mu\text{M}$ morpholino to achieve full range parameter scan. Under this condition, the bifurcation point for mRNA is around $10\text{ng}/\text{ul}$ (Figure 23C).

We then used the microfluidic design with three inlets channels. This design allows for systematically tuned both mRNA concentration and wee1 inhibitor concentration with the droplet system as guided by previous research (Genot et al., 2016). The result shows that when wee1 inhibitor concentration increases, the range of cell cycle oscillation period decreases (Figure 23), supporting the computation prediction in Chapter 2. To fully address the role of positive feedback on tunability, it helps to have further experiments with more tuning parameters and different circuit perturbations.

Investigation of tunability in real biological oscillator will provide valuable data to understand the control mechanisms of the biological oscillator. In addition, by dissecting cell cycle circuits *in vivo*, this work represents the first reported experimental effort to systematically

analyze the mechanism of changing tunability in the cell cycle. This study also provides an optimized scheme for cell cycle period control, which may help inspire the development of novel target for diseases caused by cell cycle malfunctions. Furthermore, as the frequency range in the cell cycle is changing drastically from embryo to adult, a study on frequency range may provide useful information on organism development and cell differentiation.

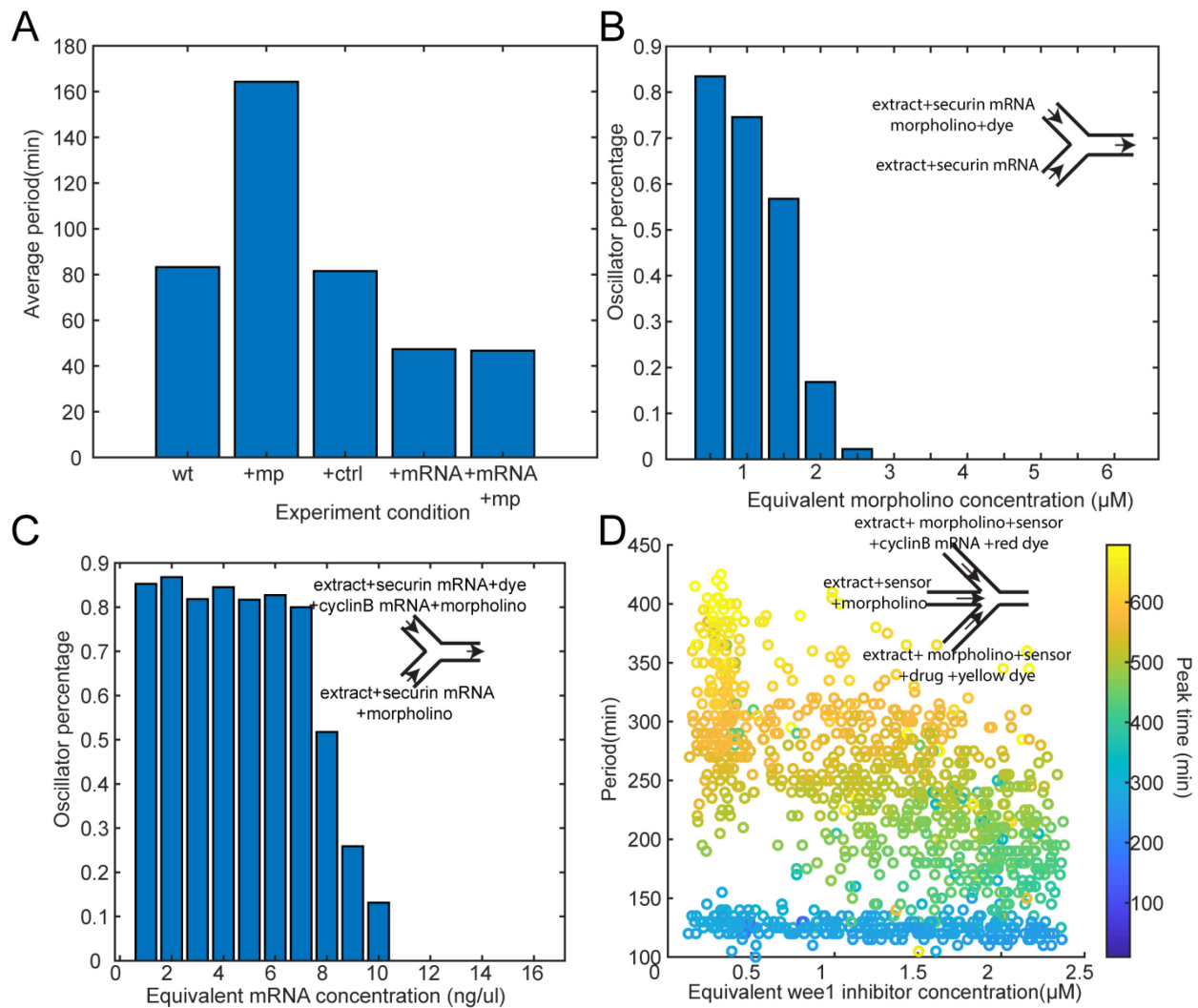


Figure 23. Investigation of the effect of the wee1 inhibitor on cell cycle tunability in response to cyclin B mRNAs. (A) Effect of different experimental conditions on average cell cycle oscillator period (min). wt, pure *Xenopus* extract; mp, add anti-*Xenopus* cyclinB morpholino mix; ctrl, add control morpholino (targeting random sequence); mRNA, add human cyclinB1 mRNA. (B) Tune cell cycle oscillator using morpholinos. The microfluidic setup scheme is shown on the upper right corner. By changing the relative pressure of two channels, the morpholino concentration is changed continuously. The x-axis shows the equivalent morpholino concentration measured by

fluorescent dye. Y-axis shows the percentage of all droplets tracked that oscillate for least two cycles. (C) Tune cell cycle oscillator using mRNAs. The microfluidic setup scheme is shown on the upper right corner. The x-axis shows the equivalent mRNA concentration measured by fluorescent dye. Y-axis shows the percentage of all droplets tracked that oscillate for least two cycles. (D) Role of wee1 inhibitor on the period range. Showing all cycles within 700 min. The microfluidic setup scheme is shown on the upper right corner, both cyclin B mRNA and wee1 inhibitor concentration is tuned continuously. The result shows a reduced cell cycle period range under high wee1 inhibitor concentrations.

3.7. Cell cycle oscillation shows a pulsatile waveform

Another advantage of having uniform droplet size is the ease of image analysis, in particular, identification of nuclei in the droplets. Accurate identification of nuclear breakdown and reconstruction allows us to precisely capture the initiation and termination of the mitotic phase. Therefore, we used the microfluidics generated droplets to analyze the relative timing of the interphase vs mitotic phase in the mitotic cycle.

To generate nucleus-containing droplets, we used similar protocols as described in Chapter 3.1. In brief, we supplemented the droplets with demembrated sperm chromatin to trigger self-assembly of nuclei surrounding the sperm DNA. We used a GFP-tagged nuclear localization signal (GFP-NLS) to report nuclear formation, and additionally added an ATP energy regeneration system (creatine - creatine phosphate system). These enable the creation of an artificial cell with a nucleus that exhibits periodic morphological changes across cell cycle oscillations. Figure 24 demonstrates an example droplet from the experiment showing that a nucleus forms during interphase when GFP-NLS translocates to the nucleus forming a bright dot in the droplet (Figure 24A, upper-row images), while nuclear envelope breaks down during mitotic phase, with NLS-GFP evenly distributed throughout the droplet (Figure 24A, bottom-row images). To accurately discriminate the droplets with nucleus (at mitotic phase) vs the ones without a nucleus (at interphase), I calculated the standard deviation of GFP-NLS fluorescence within each droplet and applied supervised learning based on support vector machine to classify interphase and mitotic phase droplets.

Similar to the droplets containing no nuclei, we found that the period of oscillations increased over time (Figure 24A). Interestingly, the impact seems to be predominantly on the interphase which gets longer at each cell cycle (Figure 24B), while the length of the mitotic phase maintains almost constant (Figure 24C). Using a cell cycle model discussed in Chapter 3.4, we further recapitulated such differential behaviors of interphase and mitotic phase in response to energy reduction (Figure 24D). Together, it confirms that cell cycle behaves as a relaxation oscillator, as suggested by previous studies in bulk solutions (Yang and Ferrell, 2013b) and in mammalian cell lines (Araujo et al., 2016). Building on a hysteretic switch by the Cdk1-Cdc25-Wee1 interlinked positive feedback loops, cell cycle (Araujo et al., 2016; Yang and Ferrell, 2013b) alternates between a long relaxation interphase period that is subject to environmental perturbations and a short impulsive mitotic period that is temporally insulated from variability.

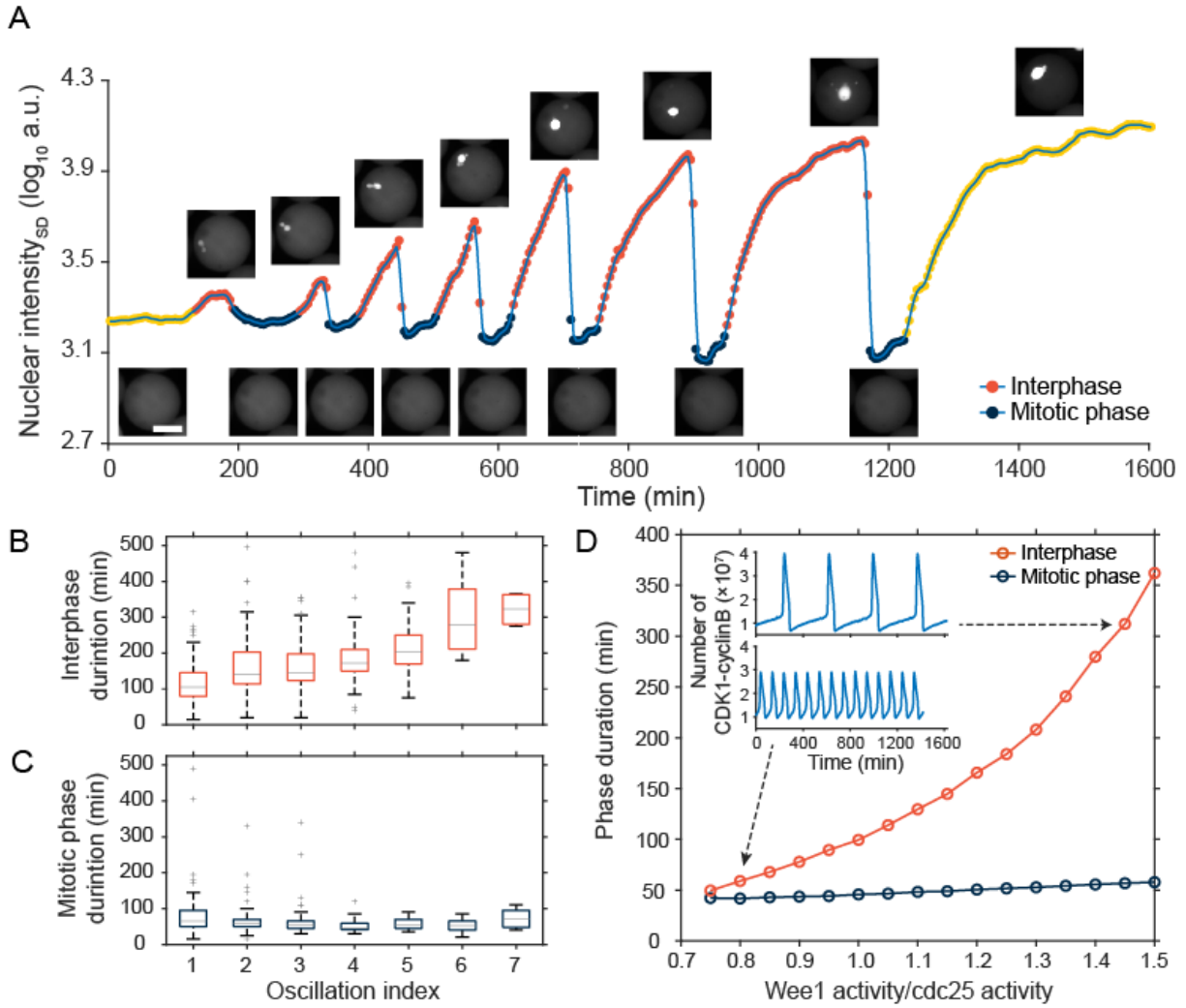


Figure 24 Pulsatile waveform of the cell cycle oscillations

(A) Cell cycle oscillations in droplets containing *Xenopus* extract, sperm DNA and NLS-GFP. Images above and beneath of the curve show a representative droplet oscillating between interphase (red dots) and mitotic phase (blue dots). Yellow dots indicate pre- and post-oscillation periods. X-axis, time after imaging (around 15min after activation); y-axis, the standard deviation of NLS-GFP intensity inside one droplet, logarithm scale. Scale bar: 50 μm . Periods of interphase (B) and mitotic phase (C) versus cycling number. (D) Theoretical modeling of the periods of oscillations at the interphase and mitotic phase, consistent with our experimental observations.

3.8. Conclusion

In this Chapter, I present the development of a novel artificial cell system that enables highly robust and tunable mitotic oscillations. Taking advantage of the microfluidics system as

well as automatic image processing, this system enables measurements at high throughput, high sensitivity, and high-spatiotemporal resolution, and opens exciting possibilities for systematic studying oscillator properties. We showed that the cycling *Xenopus* extract can reliably recapitulate various cell cycle events and is amenable to external regulations. Although the work described here is focused on cell cycles, it may have general implications in the design principles of biological oscillators given that common topologies are shared among biological oscillators

Our energy depletion model has suggested an interesting mechanism to modulate oscillations with a single control parameter that depends on the energy-tunable balance of two positive feedback loops. The rapid, synchronous cleavages of early embryo require high energy consumption (Zotin and Zotina, 1967), it is possible that the mid-blastula transition which triggers prolonged cell cycle is sensed by an energy-dependent “checkpoint”. Our results also showed a significant difference between interphase and mitotic phase during the slowing. This suggests that while interphase is sensitive to the energy level, the mitotic phase is isolated and functions in a pulsatile pattern.

Investigation of tunability and robustness in real biological oscillator will provide valuable data to verify and guide theoretical studies. Importantly, such exploration is critical to understand the control mechanisms of biological oscillators. In addition, by dissecting the cell cycle circuit *in vivo*, it will be the first time to systematically analyze the mechanism of changing tunability in the cell cycle. This study provides an optimized scheme for cell cycle period control, which may help inspire novel treatment strategies for diseases caused by cell cycle malfunction like cancer. Furthermore, as the frequency range in the cell cycle is changing drastically from embryo to adult, a study on frequency range may provide useful information on organism development and cell differentiation.

Chapter 4 Discussions

Biological oscillators are widespread in living organisms and play important roles in various biological functions including cell proliferation and circadian rhythm. In my Ph.D. study, I have comprehensively investigated the design principles of biological oscillators from both theoretical and experimental perspectives.

I first performed a systematic network search using numerical simulations to theoretically examine the role of network structures on oscillator functions, including robustness and tunability. Robustness and tunability are critical features that differentiate biological oscillators from physical or simple biochemical oscillators. These properties allow biological oscillators to stably function in a noisy environment and adapt to external changes. My theoretical study identified a novel local structure, incoherent or coherent inputs, that directly promotes or weakens oscillator robustness. This discovery has two major significance. First, it provides an intuitive understanding of how natural evolution can gradually select highly robust oscillators. Second, it provides a useful and easily adaptable method for designing robust synthetic oscillators or manipulates known biological oscillators. I further studied tunability using similar pipelines. I verified that positive feedbacks could increase the frequency tunability of biological oscillators and showed that the role of positive feedbacks is additive. In addition, we found that the oscillator waveform is associated with its network circuit, suggesting a potential correlation between oscillator tuning pattern and their waveform shape.

I also performed an experimental study to verify results from computational analysis and to guide further theoretical investigations. We first developed an artificial mitotic cycle system by encapsulating reaction mixtures containing cycling *Xenopus* egg cytoplasm in cell-scale micro-emulsions. We showed that we can successfully recapitulate various cell cycle activities in a cell-sized compartment. Using this system, we collected the evidence that incoherent input increases the oscillator robustness. In this experiment, we also find that baseline and amplitude of cell cycle oscillation keeps increasing over time, different with previous computational models. To explain this phenomenon, we proposed an energy-dependent model and showed computationally that the new model can explain the observed experimental result. This result suggesting that energy level may play an important role in determining the progression of the cell cycle. To investigate the role of positive feedbacks on oscillator tunability, we further developed an artificial mitotic cycle system using microfluidic devices to allow for reliable high-throughput analysis. Using this system, we collected experimental evidence supporting positive feedbacks increasing the oscillator tunability. In the meantime, and we also showed that the cell cycle is a pulsatile oscillator with consistent mitotic phase and variable interphase, in accordance with a previous study (Araujo et al., 2016).

My graduate study has shown that coordinated computational and experimental efforts has its unique advantage in advancing our understanding of biological systems. While the initial question about robustness and tunability are purely theoretical, experimental system is needed to support our computational results in real biological oscillators. During experimental verification, we found phenomena like increased baselines, which again requires a theoretical explanation. This continuous pursue of questions cannot be achieved without an integrated multidisciplinary approach. In addition, my work will also provide valuable data to verify and guide further studies

on oscillator properties and help understand the control mechanisms of the biological oscillator. Such knowledge may help inspire novel treatment strategies for diseases caused by oscillator malfunctions.

In my research on oscillator tunability, I have shown that the frequency tuning and amplitude tuning are two distinct strategies of oscillator regulation. These two different tuning patterns have been observed in many signaling pathways and their differences are considered critical for reliable oscillator function under different environment (Micali et al., 2015). In part 3.8, I have shown that adding wee1 inhibitor decreased cyclinB frequency tunability in droplets. However, our current experimental design also has its limitations. First, we only used wee1 inhibitor as the tool to perturb positive feedbacks, but since there are more positive feedback loops in our system, more drugs to disrupt different molecular circuits is necessary. In addition, since drugs are subjects to diffusion in droplets, and mRNAs takes time to be translated, it would be ideal to identify non-diffusible alternatives of drugs and find tuning parameters that can take effects immediately. In the future, I plan to further my experimental exploration by using more tuning method, like temperature, and test more network structure perturbing methods like new drugs or antibodies. The final goal is not only systematically to verify the role of positive feedbacks on oscillator tunability, but also to explore how different perturbing factors may affect oscillator tuning patterns.

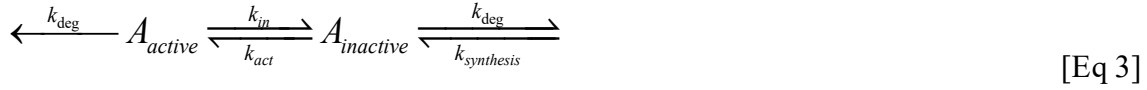
In addition to the role of positive feedbacks on increasing tunability, we also showed that frequency tunability is associated with non-sinusoidal oscillations which introduced the topic of waveform control of biological oscillators. The oscillator waveform represents a higher level of details in biological oscillations. With the recent progress in genetic tools, biological sensors and imaging techniques, more details of biological oscillator have been discovered and investigated.

The waveform of biological oscillator have been suggested to play critical roles in maintaining oscillator functions in different biological systems, including neural system (Cole and Voytek, 2017), signaling pathways (Zhang et al., 2017) and circadian rhythms (Jo et al., 2018). However, waveform is very difficult to manipulate and record experimentally, and our theoretical understanding on waveform regulation is also limited. These difficulties and limitations have prevented us from further exploration of oscillator waveform regulation which has a great significance in determining functions of biological oscillator. With recent development of biological technologies however, these questions are more within reach. Computational approach on waveform regulation requires detailed analysis of oscillator time series which is very computational expensive. My oscillator enumeration pipeline could be an ideal system to further our understanding of oscillator waveforms. In the future, I plan to record time series of one full cycle in each oscillation and quantify their shape using Fourier coefficients, then I can compute the similarity between different oscillators and identify the network motifs that are responsible for waveform difference. Besides network enumeration pipeline, our experimental system using *Xenopus* egg extract is a useful platform to study waveform tuning, since it allows for real-time droplets imaging and tracking. Together it will not only help understanding biological oscillators but also further our understanding on the regulation of the real biological system.

Appendix

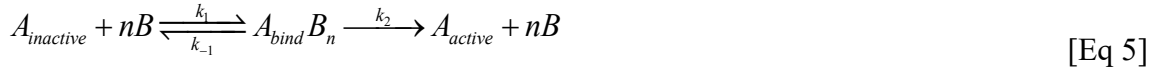
1. Derivation of the enzymatic reaction models

The model we used (i.e., Eq 1) can be derived from the simple mass action kinetics with a few assumptions, as follows. Consider a node A, and when there is no input from outside, the equations are as below:



$$\left. \frac{dA_{active}}{dt} \right|_{basal} = k_{act} A_{inactive} - (k_{deg} + k_{in}) A_{active} \quad [\text{Eq 4}]$$

If protein B activate A through binding, then



Assume that the binding and unbinding of proteins are fast, we have

$$\frac{dAB}{dt} = k_1 [A_{inactive}] [B]^n - (k_{-1} + k_2) [A_{bind} B_n] = 0 \quad [\text{Eq 6}]$$

Assume that the binding between proteins are independent, we have

$$[A_{bind} B_n] = [A_{total}] - [A_{active}] - [A_{inactive}] \quad [\text{Eq 7}]$$

Then the interaction term can be represented by

$$\left. \frac{dA_{active}}{dt} \right|_{interaction} = k_2 [A_{bind} B_n] = k_2 ([A_{total}] - [A_{active}]) \frac{[B]^n}{K + [B]^n} \quad [\text{Eq 8}]$$

where $K = \frac{k_{-1} + k_2}{k_1}$ and the reaction rate of A is:

$$\frac{dA}{dt} = -k_{1,basal}A + k_{2,basal}(1-A) + k_2(1-A) \frac{[B]^n}{K + [B]^n} \quad [\text{Eq 9}]$$

2. Models for real-world biological oscillators

The models we used to investigate the role of incoherent inputs in real-world biological oscillators are adopted from published work (Batchelor et al., 2011; Tsai et al., 2014a).

Cell cycle model:

$$\begin{aligned} \frac{d[cdk1_a]}{dt} &= k_{synth} - k_{dest}[apc_a][cdk1_a] + \frac{1}{\sqrt{r}}k_{cdk1on} \left(1 + p \frac{[cdk1_a]^{ncdk25}}{[cdk1_a]^{ncdk25} + ec50_{cdk25}^{ncdk25}} \right) [cdk1_i] \\ &\quad - \sqrt{r}k_{cdk1off} \left(1 + p \frac{ec50_{wee1}^{mwee1}}{[cdk1_a]^{mwee1} + ec50_{wee1}^{mwee1}} \right) [cdk1_a] \\ \frac{d[cdk1_i]}{dt} &= -k_{dest}[apc_a][cdk1_i] - \frac{1}{\sqrt{r}}k_{cdk1on} \left(1 + p \frac{[cdk1_a]^{ncdk25}}{[cdk1_a]^{ncdk25} + ec50_{cdk25}^{ncdk25}} \right) [cdk1_i] \\ &\quad + \sqrt{r}k_{cdk1off} \left(1 + p \frac{ec50_{wee1}^{mwee1}}{[cdk1_a]^{mwee1} + ec50_{wee1}^{mwee1}} \right) [cdk1_a] \\ \frac{d[plx_a]}{dt} &= k_{plxon} \frac{[cdk1_a]^{nplx}}{[cdk1_a]^{nplx} + ec50_{plx}^{nplx}} (plx_{tot} - [plx_a]) - k_{plxoff}[plx_a] \\ \frac{d[apc_a]}{dt} &= k_{apcon} \frac{[plx_a]^{napc}}{[plx_a]^{napc} + ec50_{apc}^{napc}} (1 - [apc_a]) - k_{apc} [apc_a] \end{aligned}$$

p53-ATR model:

$$\begin{aligned}
\frac{d[p53_{inactive}]}{dt} &= \beta_p - \alpha_{mpi}[Mdm2][p53_{inactive}] - \beta_{sp}[p53_{inactive}] \left(\frac{[ATR_{active}]^{n_s}}{[ATR_{active}]^{n_s} + T_s^{n_s}} \right) \\
&+ \alpha_{wpa}[Wip1][p53_{active}] - \alpha_{pi}[p53_{inactive}] \\
\frac{d[p53_{active}]}{dt} &= \beta_{sp}[p53_{inactive}] \left(\frac{[ATR_{active}]^{n_s}}{[ATR_{active}]^{n_s} + T_s^{n_s}} \right) - \alpha_{wpa}[Wip1][p53_{active}] - \alpha_{mpa}[Mdm2][p53_{active}] \\
\frac{d[Mdm2]}{dt} &= \beta_m[p53_{active}(t - \tau_m)] + \beta_{mi} - \alpha_{sm2}[ATR_{active}][Mdm2] - \alpha_m[Mdm2] \\
\frac{d[Wip1]}{dt} &= \beta_w[p53_{active}(t - \tau_w)] - \alpha_w[Wip1] \\
\frac{d[ATR_{active}]}{dt} &= \beta_{s2}[\theta(t) - \theta(t - t_\tau)] - \alpha_s[ATR_{active}]
\end{aligned}$$

p53-ATM model:

$$\begin{aligned}
\frac{d[p53_{inactive}]}{dt} &= \beta_p - \alpha_{mpi}[Mdm2][p53_{inactive}] - \beta_{sp}[p53_{inactive}] \left(\frac{[ATM - P]^{n_s}}{[ATM - P]^{n_s} + T_s^{n_s}} \right) \\
&+ \alpha_{wpa}[Wip1][p53_{active}] - \alpha_{pi}[p53_{inactive}] \\
\frac{d[p53_{active}]}{dt} &= \beta_{sp}[p53_{inactive}] \left(\frac{[ATM - P]^{n_s}}{[ATM - P]^{n_s} + T_s^{n_s}} \right) - \alpha_{wpa}[Wip1][p53_{active}] - \alpha_{mpa}[Mdm2][p53_{active}] \\
\frac{d[Mdm2]}{dt} &= \beta_m[p53_{active}(t - \tau_m)] + \beta_{mi} - \alpha_{sm}[ATM - P][Mdm2] - \alpha_m[Mdm2] \\
\frac{d[Wip1]}{dt} &= \beta_w[p53_{active}(t - \tau_w)] - \alpha_w[Wip1] \\
\frac{d[ATM - P]}{dt} &= \beta_s[\theta(t) - \theta(t - t_\tau)] - \alpha_s[ATM - P] - \alpha_{ws}[ATM - P] \frac{[Wip1]^{n_w}}{[Wip1]^{n_w} + T^{n_w}}
\end{aligned}$$

3. A stochastic model of the embryonic cell cycle including energy effect

To explore how energy consumption could affect the oscillations, we took ATP into account for phosphorylation and dephosphorylation of Wee1 (Tuck et al., 2013), such that:



In our model, we assumed Wee1 is in equilibrium with the activity of Cdk1 due to fast reactions between Cdk1 and Wee1. Using the reaction coefficients for Wee1 phosphorylation as k_{1Wee1}

and that for Wee1-Pi dephosphorylation as k_{2Wee1} , along with the steady-state approximation, we have:

$$k_{1Wee1}[Wee1][ATP] = k_{2Wee1}[Wee1 - Pi][ADP] = k_{2Wee1}([Wee1_{tot}] - [Wee1])(1 - [ATP]) \quad [\text{Eq 11}]$$

All above modifications for Wee1 reactions also applied to Cdc25. After normalizing [ATP] and [ADP] by $[ATP] + [ADP]$, we have the updated reaction rates summarized in Table A3. Here the $[wee1]_0$ and $[cdc25-Pi]_0$ represent the steady-state concentration of active Wee1 and Cdc25 when ATP is not considered in reaction. The ratios of the steady-state to total concentrations of Wee1 and Cdc25 can be calculated as a function of active CDK1 using the parameters from previous work (Novak and Tyson, 1993a)

TableA 1 Parameter ranges in the cell cycle model, related to STAR Methods: Models for real-world biological oscillators.

	Parameter	Nominal value (Tsai et al., 2014)	Parameter range for random parameter simulations with linear range
0	k_{synth}	1.5	0-10
1	k_{dest}	0.4	0-1
2	r	1	1
3	k_{cdc25}	0.0354	0-1
4	k_{wee1}	0.0354	0-1
5	$p1$	5	0-50
6	$p2$	5	0-50
7	$ec50_{cdc25}$	30 nM	0-200 nM
8	n_{cdc25}	11	1-15

9	$ec50_{wee1}$	35 nM	0-200nM
10	n_{wee1}	3.5	1-10
11	k_{plxon}	1.5	0-10
12	k_{plxoff}	0.15	0-1
13	$ec50_{plx}$	60 nM	0-200 nM
14	n_{plx}	5	2-6
15	k_{apcon}	1.5	0-10
16	$k_{apc off}$	0.125	0-1
17	$ec50_{apc}$	0.5	0-1
18	n_{apc}	4	2-6

TableA 2 Reaction rates and stoichiometry of the cell cycle two-ODE model

Reaction	Rate	Stoichiometry
Active Cdk1 Synthesis	$\rho_1 = k_{sy}$	$\langle Cdk1_a \rangle = \langle Cdk1_a \rangle + 1$
Active Cdk1 to Inactive Cdk1	$\rho_2 = \sqrt{r} \left(a_{Wee1} + \frac{b_{Wee1} EC50_{Wee1}^{n_{Wee1}}}{\langle Cdk1_a \rangle^{n_{Wee1}} + EC50_{Wee1}^{n_{Wee1}}} \right) \langle Cdk1_a \rangle$	$\langle Cdk1_a \rangle = \langle Cdk1_a \rangle - 1$ $\langle Cdk1_i \rangle = \langle Cdk1_i \rangle + 1$
Inactive Cdk1 to Active Cdk1	$\rho_3 = \frac{1}{\sqrt{r}} \left(a_{Cdc25} + \frac{b_{Cdc25} \langle Cdk1_a \rangle^{n_{Cdc25}}}{\langle Cdk1_a \rangle^{n_{Cdc25}} + EC50_{Cdc25}^{n_{Cdc25}}} \right) \langle Cdk1_i \rangle$	$\langle Cdk1_a \rangle = \langle Cdk1_a \rangle + 1$ $\langle Cdk1_i \rangle = \langle Cdk1_i \rangle - 1$

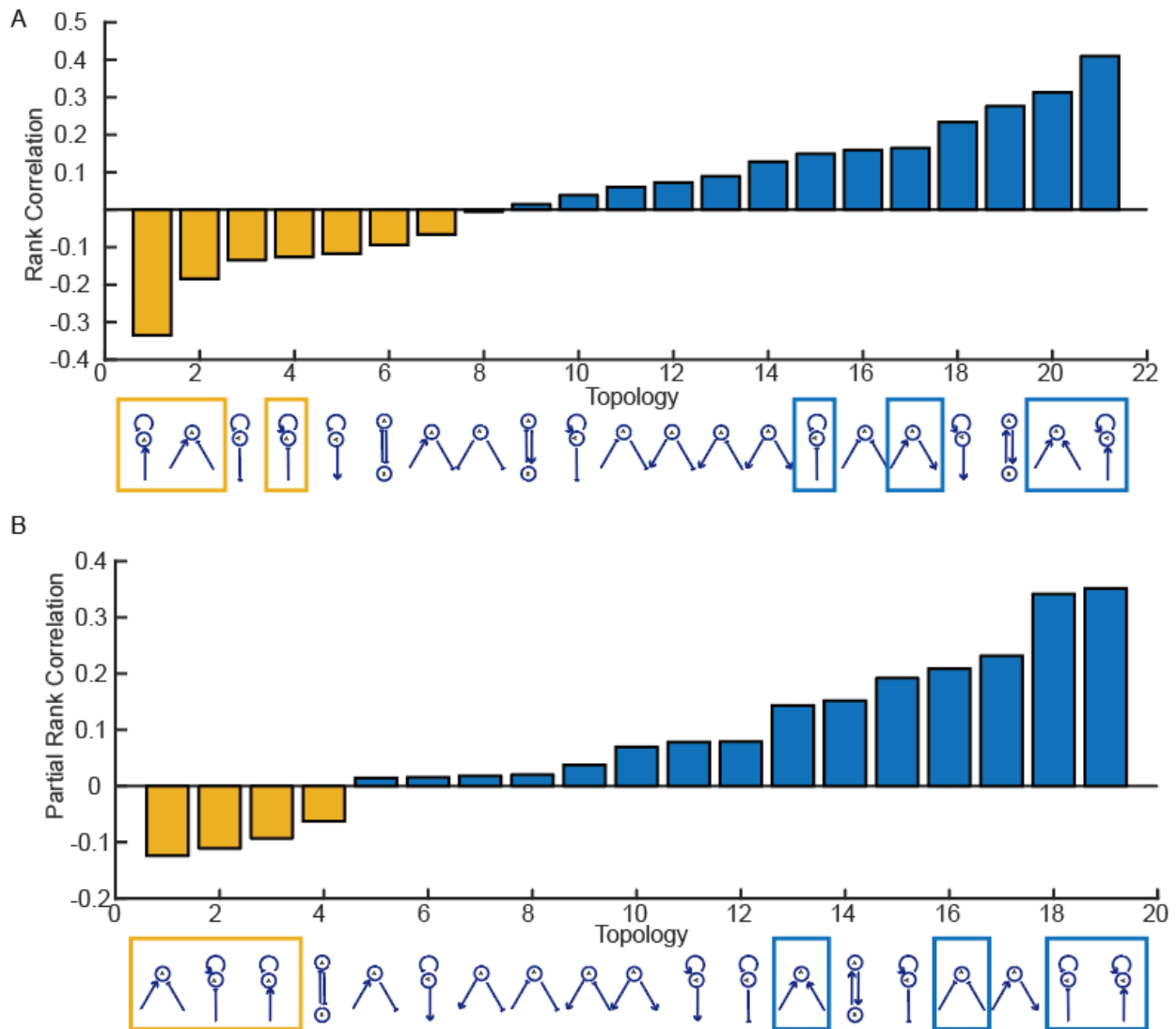
Active Cdk1 Degradation	$\rho_4 = \left(a_{deg} + \frac{b_{deg} \langle Cdk1_a \rangle^{n_{deg}}}{\langle Cdk1_a \rangle^{n_{deg}} + EC50_{deg}^{n_{deg}}} \right) \langle Cdk1_a \rangle$	$\langle Cdk1_a \rangle = \langle Cdk1_a \rangle - 1$
Inactive Cdk1 Degradation	$\rho_5 = \left(a_{deg} + \frac{b_{deg} \langle Cdk1_a \rangle^{n_{deg}}}{\langle Cdk1_a \rangle^{n_{deg}} + EC50_{deg}^{n_{deg}}} \right) \langle Cdk1_i \rangle$	$\langle Cdk1_i \rangle = \langle Cdk1_i \rangle - 1$

TableA 3 Reaction rates in the model considering ATP

Reaction	Rate
Active Cdk1 Synthesis	$\rho_1 = k_{sy}$
Active Cdk1 to Inactive Cdk1	$\rho_2 = 2[ATP] \langle Cdk1_a \rangle \left(a_{Wee1} + \frac{b_{Wee1} EC50_{Wee1}^{n_{Wee1}}}{\langle Cdk1_a \rangle^{n_{Wee1}} + EC50_{Wee1}^{n_{Wee1}}} \right) \left(\frac{1 - [ATP]}{[ATP] \left(1 - \frac{2[Wee1_0]}{[Wee1_{tot}]} \right) + \frac{[Wee1_0]}{[Wee1_{tot}]}} \right)$
Inactive Cdk1 to Active Cdk1	$\rho_3 = \langle Cdk1_i \rangle \left(a_{Cdc25} + \frac{b_{Cdc25} \langle Cdk1_a \rangle^{n_{Cdc25}}}{\langle Cdk1_a \rangle^{n_{Cdc25}} + EC50_{Cdc25}^{n_{Cdc25}}} \right) \left(\frac{[ATP]}{1 - \frac{[Cdc25 - Pi_0]}{[Cdc25_{tot}]} + \left(2 \frac{[Cdc25 - Pi_0]}{[Cdc25_{tot}]} - 1 \right) [ATP]} \right)$
Active Cdk1 Degradation	$\rho_4 = \left(a_{deg} + \frac{b_{deg} \langle Cdk1_a \rangle^{n_{deg}}}{\langle Cdk1_a \rangle^{n_{deg}} + EC50_{deg}^{n_{deg}}} \right) \langle Cdk1_a \rangle$

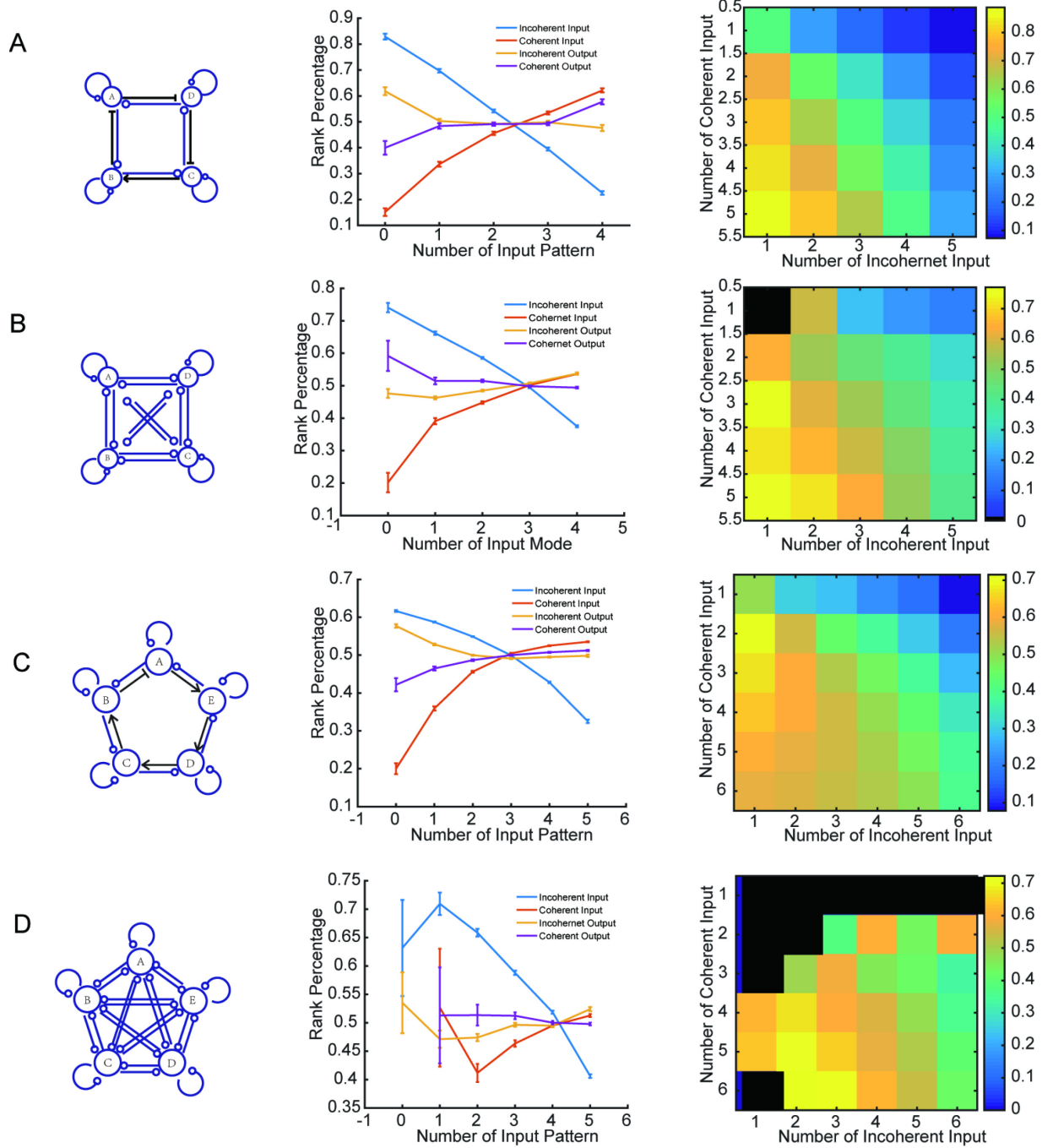
Inactive Cdk1
Degradation

$$\rho_5 = \left(a_{deg} + \frac{b_{deg} \langle Cdk1_a \rangle^{n_{deg}}}{\langle Cdk1_a \rangle^{n_{deg}} + EC50_{deg}^{n_{deg}}} \right) \langle Cdk1_i \rangle$$



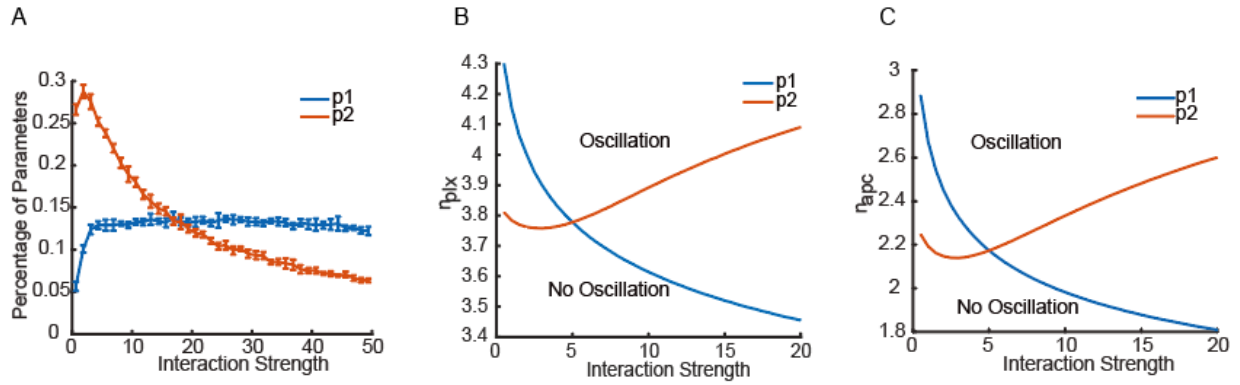
FigureA 1 Incoherent inputs improve the robustness of biological oscillators in network enumeration.

(A) Spearman's rank correlation between the changes in the rank percentage of the Q value of a topology and a two-edge modification. B. Partial rank correlation between the change in the rank percentage of the Q value of a topology and a two-edge modification (controlling other two-edge modifications). Note that two motifs with the lowest rank correlation are dropped to avoid linear correlation of inputs.



FigureA 2 Role of some network motifs in oscillators with more than 3 nodes.

The left panels show network topologies (as in Figures 7D-G). The middle panels show the relationship between the mean rank percentage of the Q values and the number of nodes with different input logic. The right panels show the mean rank percentage of the Q values as a function of the number of coherent inputs and the number of incoherent inputs the topologies contain.



FigureA 3 .Supplemental analysis on cell cycle model

(A) Percentage of parameters that yield sustained oscillations changes with increasing interaction strength of Cdc25 (p1) or Wee1 (p2). The parameter ranges of simulation are shown in Table S2. It shows that strong cdc25 can benefit robust oscillations. (B, C) Hopf bifurcation diagram of nplx (B) and nabc (C) with Cdc25 interaction strength and Wee1 interaction strength.

Bibliography

- Ainsworth, M., Lee, S., Cunningham, M.O., Traub, R.D., Kopell, N.J., and Whittington, M.A. (2012). Rates and rhythms: a synergistic view of frequency and temporal coding in neuronal networks. *Neuron* 75, 572-583.
- Ananthasubramaniam, B., and Herzog, H. (2014). Positive feedback promotes oscillations in negative feedback loops. *PLoS One* 9, e104761.
- Antoch, M.P., Song, E.J., Chang, A.M., Vitaterna, M.H., Zhao, Y., Wilsbacher, L.D., Sangoram, A.M., King, D.P., Pinto, L.H., and Takahashi, J.S. (1997). Functional identification of the mouse circadian Clock gene by transgenic BAC rescue. *Cell* 89, 655-667.
- Araujo, A.R., Gelens, L., Sheriff, R.S., and Santos, S.D. (2016). Positive Feedback Keeps Duration of Mitosis Temporally Insulated from Upstream Cell-Cycle Events. *Mol Cell* 64, 362-375.
- Atkinson, M.R., Savageau, M.A., Myers, J.T., and Ninfa, A.J. (2003). Development of genetic circuitry exhibiting toggle switch or oscillatory behavior in *Escherichia coli*. *Cell* 113, 597-607.
- Barkai, N., and Leibler, S. (2000). Circadian clocks limited by noise. *Nature* 403, 267-268.
- Batchelor, E., Loewer, A., Mock, C., and Lahav, G. (2011). Stimulus-dependent dynamics of p53 in single cells. *Mol Syst Biol* 7, 488.
- Bell-Pedersen, D., Cassone, V.M., Earnest, D.J., Golden, S.S., Hardin, P.E., Thomas, T.L., and Zoran, M.J. (2005). Circadian rhythms from multiple oscillators: lessons from diverse organisms. *Nat Rev Genet* 6, 544-556.
- Benazeraf, B., and Pourquie, O. (2013). Formation and segmentation of the vertebrate body axis. *Annu Rev Cell Dev Biol* 29, 1-26.
- Bieler, J., Cannavo, R., Gustafson, K., Gobet, C., Gatfield, D., and Naef, F. (2014). Robust synchronization of coupled circadian and cell cycle oscillators in single mammalian cells. *Mol Syst Biol* 10, 739.
- Brown, H., DiFrancesco, D., and Noble, S. (1979). Cardiac pacemaker oscillation and its modulation by autonomic transmitters. *J Exp Biol* 81, 175-204.
- Buchthal, F., Guld, C., and Rosenfalck, P. (1954). Action Potential Parameters in Normal Human Muscle and Their Dependence on Physical Variables. *Acta Physiol Scand* 32, 200-218.

- Butzin, N.C., Hochendoner, P., Ogle, C.T., Hill, P., and Mather, W.H. (2016). Marching along to an Offbeat Drum: Entrainment of Synthetic Gene Oscillators by a Noisy Stimulus. *ACS Synth Biol* 5, 146-153.
- Cai, L., Dalal, C.K., and Elowitz, M.B. (2008). Frequency-modulated nuclear localization bursts coordinate gene regulation. *Nature* 455, 485-490.
- Castillo-Hair, S.M., Villota, E.R., and Coronado, A.M. (2015). Design principles for robust oscillatory behavior. *Syst Synth Biol* 9, 125-133.
- Chance, B., Schoener, B., and Elsaesser, S. (1965). Metabolic Control Phenomena Involved in Damped Sinusoidal Oscillations of Reduced Diphosphopyridine Nucleotide in a Cell-Free Extract of *Saccharomyces Carlsbergensis*. *J Biol Chem* 240, 3170-3181.
- Chang, J.B., and Ferrell Jr, J.E. (2013). Mitotic trigger waves and the spatial coordination of the *Xenopus* cell cycle. *Nature* 500, 603-607.
- Chen, A.H., Lubkowitz, D., Yeong, V., Chang, R.L., and Silver, P.A. (2015a). Transplantability of a circadian clock to a noncircadian organism. *Sci Adv* 1.
- Chen, Y., Kim, J.K., Hirning, A.J., Josic, K., and Bennett, M.R. (2015b). Emergent genetic oscillations in a synthetic microbial consortium. *Science* 349, 986-989.
- Cole, S.R., and Voytek, B. (2017). Brain Oscillations and the Importance of Waveform Shape. *Trends Cogn Sci* 21, 137-149.
- Cross, F.R., Buchler, N.E., and Skotheim, J.M. (2011). Evolution of networks and sequences in eukaryotic cell cycle control. *Philos Trans R Soc Lond B Biol Sci* 366, 3532-3544.
- Crosthwaite, S.K., Dunlap, J.C., and Loros, J.J. (1997). *Neurospora wc-1* and *wc-2*: transcription, photoresponses, and the origins of circadian rhythmicity. *Science* 276, 763-769.
- Damiati, S., Mhanna, R., Kodzius, R., and Ehmoser, E.K. (2018). Cell-Free Approaches in Synthetic Biology Utilizing Microfluidics. *Genes (Basel)* 9.
- Danino, T., Mondragon-Palomino, O., Tsimring, L., and Hasty, J. (2010). A synchronized quorum of genetic clocks. *Nature* 463, 326-330.
- Dies, M., Galera-Laporta, L., and Garcia-Ojalvo, J. (2016). Mutual regulation causes co-entrainment between a synthetic oscillator and the bacterial cell cycle. *Integr Biol (Camb)* 8, 533-541.
- Din, M.O., Danino, T., Prindle, A., Skalak, M., Selimkhanov, J., Allen, K., Julio, E., Atolia, E., Tsimring, L.S., Bhatia, S.N., *et al.* (2016). Synchronized cycles of bacterial lysis for in vivo delivery. *Nature* 536, 81-85.
- Du, W., Li, L., Nichols, K.P., and Ismagilov, R.F. (2009). SlipChip. *Lab Chip* 9, 2286-2292.

- Dunlap, J.C. (1999). Molecular bases for circadian clocks. *Cell* 96, 271-290.
- Elowitz, M.B., and Leibler, S. (2000). A synthetic oscillatory network of transcriptional regulators. *Nature* 403, 335-338.
- Feillet, C., van der Horst, G.T., Levi, F., Rand, D.A., and Delaunay, F. (2015). Coupling between the Circadian Clock and Cell Cycle Oscillators: Implication for Healthy Cells and Malignant Growth. *Front Neurol* 6, 96.
- Ferrell, J.E., Jr. (2008). Feedback regulation of opposing enzymes generates robust, all-or-none bistable responses. *Curr Biol* 18, R244-245.
- Ferrell, J.E., Jr., Tsai, T.Y., and Yang, Q. (2011). Modeling the cell cycle: why do certain circuits oscillate? *Cell* 144, 874-885.
- Fitzhugh, R. (1961). Impulses and Physiological States in Theoretical Models of Nerve Membrane. *Biophysical Journal* 1, 445-&.
- Forger, D.B. (2017). *Biological clocks, rhythms, and oscillations : the theory of biological timekeeping* (Cambridge, Massachusetts: The MIT Press).
- Friesen, W.O., and Block, G.D. (1984). What is a biological oscillator? *Am J Physiol* 246, R847-853.
- Fung, E., Wong, W.W., Suen, J.K., Bulter, T., Lee, S.G., and Liao, J.C. (2005). A synthetic gene-metabolic oscillator. *Nature* 435, 118-122.
- Gallego, M., and Virshup, D.M. (2007). Post-translational modifications regulate the ticking of the circadian clock. *Nat Rev Mol Cell Biol* 8, 139-148.
- Gautier, J., Norbury, C., Lohka, M., Nurse, P., and Maller, J. (1988). Purified maturation-promoting factor contains the product of a *Xenopus* homolog of the fission yeast cell cycle control gene *cdc2+*. *Cell* 54, 433-439.
- Gelens, L., Anderson, G.A., and Ferrell, J.E., Jr. (2014). Spatial trigger waves: positive feedback gets you a long way. *Mol Biol Cell* 25, 3486-3493.
- Genot, A.J., Baccouche, A., Sieskind, R., Aubert-Kato, N., Bredeche, N., Bartolo, J.F., Taly, V., Fujii, T., and Rondelez, Y. (2016). High-resolution mapping of bifurcations in nonlinear biochemical circuits. *Nat Chem* 8, 760-767.
- Gerard, C., Gonze, D., and Goldbeter, A. (2012). Effect of positive feedback loops on the robustness of oscillations in the network of cyclin-dependent kinases driving the mammalian cell cycle. *FEBS J* 279, 3411-3431.
- Gerisch, G. (1968). Cell aggregation and differentiation in *Dictyostelium*. *Curr Top Dev Biol* 3, 157-197.

- Gerisch, G., Fromm, H., Huesgen, A., and Wick, U. (1975). Control of cell-contact sites by cyclic AMP pulses in differentiating Dictyostelium cells. *Nature* 255, 547-549.
- Ghosh, A., and Chance, B. (1964). Oscillations of Glycolytic Intermediates in Yeast Cells. *Biochem Biophys Res Commun* 16, 174-&.
- Goldbeter, A. (2002). Computational approaches to cellular rhythms. *Nature* 420, 238-245.
- Golden, S.S., and Canales, S.R. (2003). Cyanobacterial circadian clocks--timing is everything. *Nat Rev Microbiol* 1, 191-199.
- Good, M.C., Vahey, M.D., Skandarajah, A., Fletcher, D.A., and Heald, R. (2013). Cytoplasmic volume modulates spindle size during embryogenesis. *Science* 342, 856-860.
- Goodwin, B.C. (1965). Oscillatory behavior in enzymatic control processes. *Adv Enzyme Regul* 3, 425-438.
- Goodwin, B.C., and Cohen, M.H. (1969). A phase-shift model for the spatial and temporal organization of developing systems. *J Theor Biol* 25, 49-107.
- Guan, Y., Li, Z., Wang, S., Barnes, P.M., Liu, X., Xu, H., Jin, M., Liu, A.P., and Yang, Q. (2018). A robust and tunable mitotic oscillator in artificial cells. *Elife* 7.
- Hamblen, M.J., White, N.E., Emery, P.T.J., Kaiser, K., and Hall, J.C. (1998). Molecular and behavioral analysis of four period mutants in *Drosophila melanogaster* encompassing extreme short, novel long, and unorthodox arrhythmic types. *Genetics* 149, 165-178.
- Han, J.D., Bertin, N., Hao, T., Goldberg, D.S., Berriz, G.F., Zhang, L.V., Dupuy, D., Walhout, A.J., Cusick, M.E., Roth, F.P., *et al.* (2004). Evidence for dynamically organized modularity in the yeast protein-protein interaction network. *Nature* 430, 88-93.
- Hartwell, L.H. (1971). Genetic control of the cell division cycle in yeast. II. Genes controlling DNA replication and its initiation. *J Mol Biol* 59, 183-194.
- Hartwell, L.H., Culotti, J., Pringle, J.R., and Reid, B.J. (1974). Genetic control of the cell division cycle in yeast. *Science* 183, 46-51.
- Hartwell, L.H., Culotti, J., and Reid, B. (1970). Genetic control of the cell-division cycle in yeast. I. Detection of mutants. *Proc Natl Acad Sci U S A* 66, 352-359.
- Hartwell, L.H., and Kastan, M.B. (1994). Cell cycle control and cancer. *Science* 266, 1821-1828.
- Hartwell, L.H., Mortimer, R.K., Culotti, J., and Culotti, M. (1973). Genetic Control of the Cell Division Cycle in Yeast: V. Genetic Analysis of cdc Mutants. *Genetics* 74, 267-286.
- Higgins, J. (1964). A Chemical Mechanism for Oscillation of Glycolytic Intermediates in Yeast Cells. *Proc Natl Acad Sci U S A* 51, 989-994.

- Ho, K.K., Lee, J.W., Durand, G., Majumder, S., and Liu, A.P. (2017). Protein aggregation with poly(vinyl) alcohol surfactant reduces double emulsion-encapsulated mammalian cell-free expression. *PLoS One* *12*, e0174689.
- Hodgkin, A.L., and Huxley, A.F. (1952a). The components of membrane conductance in the giant axon of *Loligo*. *J Physiol* *116*, 473-496.
- Hodgkin, A.L., and Huxley, A.F. (1952b). Currents carried by sodium and potassium ions through the membrane of the giant axon of *Loligo*. *J Physiol* *116*, 449-472.
- Hodgkin, A.L., and Huxley, A.F. (1952c). The dual effect of membrane potential on sodium conductance in the giant axon of *Loligo*. *J Physiol* *116*, 497-506.
- Hodgkin, A.L., and Huxley, A.F. (1952d). A quantitative description of membrane current and its application to conduction and excitation in nerve. *J Physiol* *117*, 500-544.
- Hodgkin, A.L., Huxley, A.F., and Katz, B. (1952). Measurement of current-voltage relations in the membrane of the giant axon of *Loligo*. *J Physiol* *116*, 424-448.
- Hodgkin, A.L., and Katz, B. (1949). The effect of temperature on the electrical activity of the giant axon of the squid. *J Physiol* *109*, 240-249.
- Huh, S., Ker, D.F., Bise, R., Chen, M., and Kanade, T. (2011). Automated mitosis detection of stem cell populations in phase-contrast microscopy images. *IEEE Trans Med Imaging* *30*, 586-596.
- Hussain, F., Gupta, C., Hirning, A.J., Ott, W., Matthews, K.S., Josic, K., and Bennett, M.R. (2014). Engineered temperature compensation in a synthetic genetic clock. *Proc Natl Acad Sci U S A* *111*, 972-977.
- Isomura, A., and Kageyama, R. (2014). Ultradian oscillations and pulses: coordinating cellular responses and cell fate decisions. *Development* *141*, 3627-3636.
- Jacob, F., Perrin, D., Sanchez, C., and Monod, J. (1960). [Operon: a group of genes with the expression coordinated by an operator]. *C R Hebd Seances Acad Sci* *250*, 1727-1729.
- Jo, H.H., Kim, Y.J., Kim, J.K., Foo, M., Somers, D.E., and Kim, P.J. (2018). Waveforms of molecular oscillations reveal circadian timekeeping mechanisms. *Commun Biol* *1*, 207.
- Kastan, M.B., and Bartek, J. (2004). Cell-cycle checkpoints and cancer. *Nature* *432*, 316-323.
- Kim, S.Y., and Ferrell, J.E., Jr. (2007). Substrate competition as a source of ultrasensitivity in the inactivation of Wee1. *Cell* *128*, 1133-1145.
- Kitano, H. (2007). Towards a theory of biological robustness. *Mol Syst Biol* *3*, 137.
- Kumagai, A., and Dunphy, W.G. (1992). Regulation of the *cdc25* protein during the cell cycle in *Xenopus* extracts. *Cell* *70*, 139-151.

- Lee, J.H., and Paull, T.T. (2005). ATM activation by DNA double-strand breaks through the Mre11-Rad50-Nbs1 complex. *Science* 308, 551-554.
- Levine, J.H., Lin, Y., and Elowitz, M.B. (2013). Functional roles of pulsing in genetic circuits. *Science* 342, 1193-1200.
- Li, Z., Liu, S., and Yang, Q. (2017). Incoherent Inputs Enhance the Robustness of Biological Oscillators. *Cell Syst* 5, 72-81 e74.
- Li, Z., and Yang, Q. (2018). Systems and synthetic biology approaches in understanding biological oscillators. *Quant Biol* 6, 1-14.
- Liu, Y., Tsinoremas, N.F., Johnson, C.H., Lebedeva, N.V., Golden, S.S., Ishiura, M., and Kondo, T. (1995). Circadian orchestration of gene expression in cyanobacteria. *Genes Dev* 9, 1469-1478.
- Lockhart, R., Taylor, J., Tibshirani, R.J., and Tibshirani, R. (2014). A Significance Test for the Lasso. *Ann Stat* 42, 413-468.
- Lohka, M.J., Hayes, M.K., and Maller, J.L. (1988). Purification of maturation-promoting factor, an intracellular regulator of early mitotic events. *Proc Natl Acad Sci U S A* 85, 3009-3013.
- Lomnitz, J.G., and Savageau, M.A. (2014). Strategy revealing phenotypic differences among synthetic oscillator designs. *ACS Synth Biol* 3, 686-701.
- Ma, W., Lai, L., Ouyang, Q., and Tang, C. (2006). Robustness and modular design of the *Drosophila* segment polarity network. *Mol Syst Biol* 2, 70.
- Ma, W., Trusina, A., El-Samad, H., Lim, W.A., and Tang, C. (2009). Defining network topologies that can achieve biochemical adaptation. *Cell* 138, 760-773.
- Maeda, K., and Kurata, H. (2018). Long negative feedback loop enhances period tunability of biological oscillators. *J Theor Biol* 440, 21-31.
- Marguet, P., Tanouchi, Y., Spitz, E., Smith, C., and You, L. (2010). Oscillations by minimal bacterial suicide circuits reveal hidden facets of host-circuit physiology. *PLoS One* 5, e11909.
- Masui, Y., and Markert, C.L. (1971). Cytoplasmic control of nuclear behavior during meiotic maturation of frog oocytes. *J Exp Zool* 177, 129-145.
- McDonald, E.R., 3rd, and El-Deiry, W.S. (2000). Cell cycle control as a basis for cancer drug development (Review). *Int J Oncol* 16, 871-886.
- Micali, G., Aquino, G., Richards, D.M., and Endres, R.G. (2015). Accurate encoding and decoding by single cells: amplitude versus frequency modulation. *PLoS Comput Biol* 11, e1004222.
- Milo, R., Itzkovitz, S., Kashtan, N., Levitt, R., Shen-Orr, S., Ayzenshtat, I., Sheffer, M., and Alon, U. (2004). Superfamilies of evolved and designed networks. *Science* 303, 1538-1542.

- Milo, R., Shen-Orr, S., Itzkovitz, S., Kashtan, N., Chklovskii, D., and Alon, U. (2002). Network motifs: simple building blocks of complex networks. *Science* 298, 824-827.
- Mondragon-Palomino, O., Danino, T., Selimkhanov, J., Tsimring, L., and Hasty, J. (2011). Entrainment of a population of synthetic genetic oscillators. *Science* 333, 1315-1319.
- Moore, R., Ooi, H.K., Kang, T., Bleris, L., and Ma, L. (2015). MiR-192-Mediated Positive Feedback Loop Controls the Robustness of Stress-Induced p53 Oscillations in Breast Cancer Cells. *PLoS Comput Biol* 11, e1004653.
- Morris, C., and Lecar, H. (1981). Voltage Oscillations in the Barnacle Giant Muscle-Fiber. *Biophysical Journal* 35, 193-213.
- Mueller, P.R., Coleman, T.R., and Dunphy, W.G. (1995). Cell cycle regulation of a *Xenopus* Wee1-like kinase. *Mol Biol Cell* 6, 119-134.
- Murray, A.W. (1991). Cell cycle extracts. *Methods in cell biology* 36, 581-605.
- Murray, A.W., and Kirschner, M.W. (1989). Cyclin synthesis drives the early embryonic cell cycle. *Nature* 339, 275-280.
- Nelson, D.E., Ihekwaba, A.E., Elliott, M., Johnson, J.R., Gibney, C.A., Foreman, B.E., Nelson, G., See, V., Horton, C.A., Spiller, D.G., *et al.* (2004). Oscillations in NF-kappaB signaling control the dynamics of gene expression. *Science* 306, 704-708.
- Nguyen, L.K. (2012). Regulation of oscillation dynamics in biochemical systems with dual negative feedback loops. *J R Soc Interface* 9, 1998-2010.
- Novak, B., and Bentrup, F.W. (1972). An electrophysiological study of regeneration in *Acetabularia mediterranea*. *Planta* 108, 227-244.
- Novak, B., and Tyson, J.J. (1993a). Modeling the Cell Division Cycle: M-phase Trigger, Oscillations, and Size Control. *Journal of Theoretical Biology* 165, 101-134.
- Novak, B., and Tyson, J.J. (1993b). Numerical analysis of a comprehensive model of M-phase control in *Xenopus* oocyte extracts and intact embryos. *Journal of cell science* 106 (Pt 4), 1153-1168.
- Novak, B., and Tyson, J.J. (2008). Design principles of biochemical oscillators. *Nat Rev Mol Cell Biol* 9, 981-991.
- Oates, A.C., Morelli, L.G., and Ares, S. (2012). Patterning embryos with oscillations: structure, function and dynamics of the vertebrate segmentation clock. *Development* 139, 625-639.
- Olsen, L.F., and Degn, H. (1978). Oscillatory kinetics of the peroxidase-oxidase reaction in an open system. Experimental and theoretical studies. *Biochim Biophys Acta* 523, 321-334.

- Paydarfar, D., and Eldridge, F.L. (1987). Phase resetting and dysrhythmic responses of the respiratory oscillator. *Am J Physiol* 252, R55-62.
- Peshkin, L., Wuhr, M., Pearl, E., Haas, W., Freeman, R.M., Jr., Gerhart, J.C., Klein, A.M., Horb, M., Gygi, S.P., and Kirschner, M.W. (2015). On the Relationship of Protein and mRNA Dynamics in Vertebrate Embryonic Development. *Dev Cell* 35, 383-394.
- Pomerening, J.R., Kim, S.Y., and Ferrell, J.E., Jr. (2005). Systems-level dissection of the cell-cycle oscillator: bypassing positive feedback produces damped oscillations. *Cell* 122, 565-578.
- Pomerening, J.R., Sontag, E.D., and Ferrell, J.E., Jr. (2003). Building a cell cycle oscillator: hysteresis and bistability in the activation of Cdc2. *Nat Cell Biol* 5, 346-351.
- Potvin-Trottier, L., Lord, N.D., Vinnicombe, G., and Paulsson, J. (2016). Synchronous long-term oscillations in a synthetic gene circuit. *Nature advance online publication*.
- Prigogine, I., Lefever, R., Goldbeter, A., and Herschkowitz-Kaufman, M. (1969). Symmetry breaking instabilities in biological systems. *Nature* 223, 913-916.
- Prindle, A., Samayoa, P., Razinkov, I., Danino, T., Tsimring, L.S., and Hasty, J. (2011). A sensing array of radically coupled genetic 'biopixels'. *Nature* 481, 39-44.
- Purvis, J.E., Karhohs, K.W., Mock, C., Batchelor, E., Loewer, A., and Lahav, G. (2012). p53 Dynamics Control Cell Fate. *Science* 336, 1440-1444.
- Pye, K., and Chance, B. (1966). Sustained sinusoidal oscillations of reduced pyridine nucleotide in a cell-free extract of *Saccharomyces carlsbergensis*. *Proc Natl Acad Sci U S A* 55, 888-894.
- Rust, M.J., Markson, J.S., Lane, W.S., Fisher, D.S., and O'Shea, E.K. (2007). Ordered phosphorylation governs oscillation of a three-protein circadian clock. *Science* 318, 809-812.
- Salazar, C., Politi, A.Z., and Hofer, T. (2008). Decoding of calcium oscillations by phosphorylation cycles: analytic results. *Biophys J* 94, 1203-1215.
- Sanchez, T., Chen, D.T., DeCamp, S.J., Heymann, M., and Dogic, Z. (2012). Spontaneous motion in hierarchically assembled active matter. *Nature* 491, 431-434.
- Scott, S.R., and Hasty, J. (2016). Quorum Sensing Communication Modules for Microbial Consortia. *ACS Synth Biol* 5, 969-977.
- Shah, N.A., and Sarkar, C.A. (2011). Robust network topologies for generating switch-like cellular responses. *PLoS Comput Biol* 7, e1002085.
- Shreeram, S., Demidov, O.N., Hee, W.K., Yamaguchi, H., Onishi, N., Kek, C., Timofeev, O.N., Dudgeon, C., Fornace, A.J., Anderson, C.W., *et al.* (2006). Wip1 phosphatase modulates ATM-dependent signaling pathways. *Mol Cell* 23, 757-764.

- Smith, L.D., and Ecker, R.E. (1971). The interaction of steroids with *Rana pipiens* Oocytes in the induction of maturation. *Dev Biol* 25, 232-247.
- Stricker, J., Cookson, S., Bennett, M.R., Mather, W.H., Tsimring, L.S., and Hasty, J. (2008). A fast, robust and tunable synthetic gene oscillator. *Nature* 456, 516-519.
- Sudakin, V., Ganoth, D., Dahan, A., Heller, H., Hershko, J., Luca, F.C., Ruderman, J.V., and Hershko, A. (1995). The cyclosome, a large complex containing cyclin-selective ubiquitin ligase activity, targets cyclins for destruction at the end of mitosis. *Mol Biol Cell* 6, 185-197.
- Thron, C.D. (1996). A model for a bistable biochemical trigger of mitosis. *Biophys Chem* 57, 239-251.
- Tigges, M., Denervaud, N., Greber, D., Stelling, J., and Fussenegger, M. (2010). A synthetic low-frequency mammalian oscillator. *Nucleic Acids Res* 38, 2702-2711.
- Tigges, M., Marquez-Lago, T.T., Stelling, J., and Fussenegger, M. (2009). A tunable synthetic mammalian oscillator. *Nature* 457, 309-312.
- Toettcher, J.E., Mock, C., Batchelor, E., Loewer, A., and Lahav, G. (2010). A synthetic-natural hybrid oscillator in human cells. *Proc Natl Acad Sci U S A* 107, 17047-17052.
- Tomazou, M., Barahona, M., Polizzi, K.M., and Stan, G.B. (2018). Computational Re-design of Synthetic Genetic Oscillators for Independent Amplitude and Frequency Modulation. *Cell Syst* 6, 508-520 e505.
- Tomida, T., Takekawa, M., and Saito, H. (2015). Oscillation of p38 activity controls efficient pro-inflammatory gene expression. *Nat Commun* 6, 8350.
- Tsai, T.Y., Choi, Y.S., Ma, W., Pomerening, J.R., Tang, C., and Ferrell, J.E., Jr. (2008). Robust, tunable biological oscillations from interlinked positive and negative feedback loops. *Science* 321, 126-129.
- Tsai, T.Y., Theriot, J.A., and Ferrell, J.E., Jr. (2014a). Changes in oscillatory dynamics in the cell cycle of early *Xenopus laevis* embryos. *PLoS Biol* 12, e1001788.
- Tsai, T.Y.C., Theriot, J.A., and Ferrell, J.E., Jr. (2014b). Changes in Oscillatory Dynamics in the Cell Cycle of Early *Xenopus laevis* Embryos. *PLoS Biol* 12, e1001788.
- Tuck, C., Zhang, T., Potapova, T., Malumbres, M., and Novak, B. (2013). Robust mitotic entry is ensured by a latching switch. *Biology open* 2, 924-931.
- Wagner, A. (2005). Circuit topology and the evolution of robustness in two-gene circadian oscillators. *Proc Natl Acad Sci U S A* 102, 11775-11780.
- Weitz, M., Kim, J., Kapsner, K., Winfree, E., Franco, E., and Simmel, F.C. (2014). Diversity in the dynamical behaviour of a compartmentalized programmable biochemical oscillator. *Nat Chem* 6, 295-302.

Woods, M.L., Leon, M., Perez-Carrasco, R., and Barnes, C.P. (2016). A Statistical Approach Reveals Designs for the Most Robust Stochastic Gene Oscillators. *ACS Synth Biol*.

Yang, Q., and Ferrell, J.E. (2013a). The Cdk1-APC/C cell cycle oscillator circuit functions as a time-delayed, ultrasensitive switch. *Nat Cell Biol* *15*, 519-525.

Yang, Q., and Ferrell, J.E., Jr. (2013b). The Cdk1-APC/C cell cycle oscillator circuit functions as a time-delayed, ultrasensitive switch. *Nat Cell Biol* *15*, 519-525.

Yang, Q., Pando, B.F., Dong, G., Golden, S.S., and van Oudenaarden, A. (2010). Circadian gating of the cell cycle revealed in single cyanobacterial cells. *Science* *327*, 1522-1526.

Zhang, Z.B., Wang, Q.Y., Ke, Y.X., Liu, S.Y., Ju, J.Q., Lim, W.A., Tang, C., and Wei, P. (2017). Design of Tunable Oscillatory Dynamics in a Synthetic NF-kappaB Signaling Circuit. *Cell Syst* *5*, 460-470 e465.

Zotin, A.I., and Zotina, R.S. (1967). Thermodynamic aspects of developmental biology. *J Theor Biol* *17*, 57-75.